Tracking number: OE 12.09
Award No: DE-OE0000072
Identification Number: DE-0000072
CFDA No. 81.122

Final Report

Development of Toroidal Core Transformers

By

Francisco de Leon
Associate Professor
Department of Electrical and Computer Engineering
New York University
Six Metrotech Center
Brooklyn, NY 11201
Tel (718) 260 3961
fdeleon@poly.edu
fdeleon@nyu.edu
http://www.poly.edu/power

August 2014

Acknowledgment: This material is based upon work supported by the Department of Energy under Award Number DE-OE0000072.

Executive Summary

The original objective of this project was to design, build and test a few prototypes of single-phase dry-type distribution transformers of 25 kVA, 2.4 kV primary to 120 V transformers using cores made of a continuous steel strip shaped like a doughnut (toroid). At different points during the development of the project, the scope was enhanced to include the more practical case of a 25 kVA transformer for a 13.8 kV primary system voltage. Later, the scope was further expanded to design and build a 50 kVA unit to transformer voltage from 7.62 kV to 2x120 V. This is a common transformer used by Con Edison of New York and they are willing to test it in the field.

The project officially started in September 2009 and ended in May 2014. The progress was reported periodically to DOE in eighteen quarterly reports. A Continuation Application was submitted to DOE in June 2010. In May 2011 we have requested a non-cost extension of the project. In December 2011, the Statement of Project Objectives (SOPO) was updated to reflect the real conditions and situation of the project as of 2011. A second Continuation Application was made and funding was approved in 2013 by DOE and the end date was extended to May 2014.

The technical challenges that were overcome in this project include: the development of the technology to pass the impulse tests, derive a model for the thermal performance, produce a sound mechanical design, and estimate the inrush current. However, the greatest challenge that we faced during the development of the project was the complications of procuring the necessary parts and materials to build the transformers. The actual manufacturing process is relatively fast, but getting all parts together is a very lengthy process.

The main products of this project are two prototypes of toroidal distribution transformers of 7.62 kV (to be used in a 13.8 kV system) to 2x120 V secondary (standard utilization voltage); one is rated at 25 kVA and the other at 50 kVA. The 25 kVA transformer passed the impulse test in KEMA high-voltage laboratories. Additional products include: nine papers published in the IEEE Transactions on Power Delivery, one patent has been filed, three PhD students were

supported from beginning to graduation, five postdoctoral fellows, and three MSc students were partially supported.

The electrical characteristics of our dry-type toroidal transformers are similar to those of the oil-immersed pole mounted transformers currently in use by many utilities, but toroids have higher efficiency. The no-load losses of the 50 kVA prototype are only 45 W. A standard transformer has no-load losses between 90 and 240 W. Thus, even the finest transformer built today with standard technology has double the amount of no-load losses than the prototype toroidal transformer.

When the manufacturing process is prepared for mass production, the cost of a dry-type toroidal transformer would be similar to the price of an oil-filed standard design. However, because of the greatly reduced losses, the total ownership cost of a toroidal transformer could be about half of a traditional design.

We got a grant from Power Bridge NY in the amount of $149,985 from June 2014 to May 2015 to continue developing the transformer with commercialization objectives. We are considering the possibility to incorporate a company to manufacture the transformers and have contacted investors.

The current status of the real life testing is as follows: after several months of silence, Con Edison has re-started conversations and has shown willingness to test the transformer. Other companies, PSE&G and National Grid have recently also shown interest and we will present our product to them soon.

Contents

1. Introduction

The U.S. Environmental Protection Agency estimates losses of 60 to 80 billion kWh attributable to distribution transformer inefficiencies, which rob U.S. business and American consumers of approximately $4 billion per year. The American Council for an Energy Efficiency Economy has identified (in 2006) distribution transformers as the second devices with the largest potential to save energy (only after residential furnaces and boilers).

Currently, there are two basic arrangements for the iron-cores used to build distribution transformers: (1) The Core-Type, cores are assembled by stacking laminations and the transformer is completed by sliding pre-made windings; (2) Shell-Type, a continuously wound core is cut and wrapped around the windings a few laminations at a time. As a consequence, both arrangements of the finished core are left with air gaps that increase the magnetizing current and the no-load loss. Figure 1.1 illustrates the internal construction of both types.

Core type Shell type

Figure 1.1. Arrangement of core and windings (active element) of core-type and shell-type distribution transformers.

The alternative construction proposed in this project, currently used in low-voltage and low-power applications, is to use a core made of a continuous steel strip that is wound into a doughnut shape (toroid) and then wrapped entirely in coils (see Figure 1.2). This gapless construction allows for smaller, more efficient, lighter, and cooler transformers with reduced electromagnetic interference and lower acoustic noise. The main technical advantage is that the no-load loss is substantially reduced. There are also savings to be found in the load losses because the windings have fewer (and shorter) turns. These advantages have a greater impact for transformers that operate in lightly loaded (suburban and rural) areas because the no-load loss is very small. Since toroidal transformers can be made smaller than standard transformers, it is possible to replace oil immersed overhead transformers with dry toroidal units, reducing the potential for violent faults in addition to the environmental benefits of avoiding the use of oil.

Figure 1.2. Arrangement of core and windings (active element) of the new toroidal distribution transformers.

Toroidal transformers are not currently in use in distribution systems. Given the lack of experience with toroidal design at medium and high voltages, efforts have been made to develop the technology to pass the impulse tests, study the thermal performance and produce a sound mechanical design. All the design has been done at the School of Engineering of New York

University, by graduate students (M.S. and Ph.D.) and post-doctoral fellows under the guidance of Prof. Francisco de Leon.

The development of toroidal core transformers for medium-voltage applications was a project supported by the US Department of Energy under Grant DEOE0000072. The underlying idea is to benefit from the virtues of the toroidal construction to manufacture, test and install toroidal transformers suitable for power distribution applications. At this time (August 2014) we have built two working prototypes, one of 25 kVA and another one of 50 kVA. The 25 kVA transformer has been successfully tested and passed the impulse tests at Kema high-voltage laboratory. The electrical characteristics of the toroidal dry-type transformers are similar to those of oil-immersed pole mounted transformers currently in use by many utilities, but with higher efficiency. The performance of toroidal transformers is not typical; for example the 50 kVA transformer has no-load losses of only 45 W. A standard transformer has no-load losses between 90 and 240 W. Thus, even the finest transformer built today with standard technology has double the amount of no-load loss than the prototype toroidal transformer.

The 50 kVA transformer was designed and built according to the Con Edison purchase requirements. It is intended to be installed on an overhead system to allow for the observation of the unit under real life operation.

It is estimated that, in the mass production phase, the cost of a dry-type toroidal transformer will be very close to that of a standard oil-immersed transformer. However, because of the higher efficiency, the operating cost will be almost half. Its dry-type construction inherently makes it environmental friendly and it is not subjected to explosions. There are 100 million pole mounted transformers in the world. There are 40 million in the US alone with a life expectancy is 40 years. Therefore, about one million every year are substituted even with no growth.

2. Project Development

2.1 Original Objective

The objective of this project is to design, build and test a few prototypes of single-phase dry-type distribution transformers using cores made of a continuous steel strip shaped like a doughnut (toroid). The scope is to minimally build a toroidal transformer with the following specifications: 25 kVA, 2.4 kV primary to 120 V secondary, 95 kV BIL, operating at 60 Hz, with a minimum efficiency of 98.91 %.

2.2 Enhanced Objective

During the development of the project, the scope was enhanced to include more practical distribution transformer applications. The medium voltage of 2.4 kV is a legacy voltage level. Modern distribution systems use higher voltage, for example 13.2 kV or 25 kV. Therefore, a 25 kVA transformer for a 13.2 kV primary system voltage was proposed as the new objective.

Later, the scope was further expanded to design and build a 50 kVA unit to transform voltage from 7.62 kV to 2x120 V. The reason is that although 25 kVA transformers are still in use, the local utilities (Con Edison and Long Island Power Authority) substitute their 25 kVA for 37.5 kVA or 50 kVA. The 50 kVA was preferred because this is a very common transformer for Con Edison and they are willing to test it in the field.

Although toroidal distribution transformers will be dry-type, their efficiency will be even better than the efficiency of the corresponding oil-filled transformers. Then for a 25 kVA transformer the minimum efficiency will be 98.91% and for the 50 kVA the minimum efficiency will be 99.08%.

2.3 Design Challenges

Since there is no industry experience designing and building distribution transformers in toroidal cores, the initial challenge was to design the transformer from top to bottom. All electromagnetic and mechanical design processes necessary to produce a working transformer had to be analyzed. In this section all aspects of toroidal transformer distribution design are reported. Next chapter describes the construction challenges.

2.3.1 Electromagnetic Design

A design program was developed in Matlab to provide preliminary design parameters from the transformer specifications. The input data are the power, frequency, winding voltages, basic insulation level (BIL), and magnetic flux density. Using Faraday's law and the dimensions of the components (core, wires and insulation) the number of turns and the general dimensions of the transformer are estimated. Designs were eventually validated using finite elements simulations.

We realized that there were no formulae available to estimate the leakage inductance; therefore we needed to derive such formulae. The leakage inductance is a very important performance parameter of a distribution transformer since it determines the voltage drop and the short-circuit currents. Three different techniques were proposed to control the leakage inductance: (1) add spaces between the windings; (2) insert a second core between primary and secondary; (3) leave unwound sectors around the core. The details have been published in the following two papers:

I. Hernández, F. de León, and P. Gómez, "*Design Formulas for the Leakage Inductance of Toroidal Distribution Transformers*", IEEE Transactions on Power Delivery, Vol. 26, No. 4, October 2011, pp. 2197-2204.

F. de León, S. Purushothaman, and L. Qaseer, "*Leakage Inductance Design of Toroidal Transformers by Sector Winding*", IEEE Transactions on Power Electronics, Vol. 29, No. 1, January 2014, pp. 473-480.

The design program directly provides the drawing model of the toroidal transformer ready to be simulated in COMSOL Multiphysics. Then we can perform all magnetic, thermal, and mechanical calculations necessary to verify the design.

2.3.2 Insulation Design

The design of the insulation was the most important concern that we had at the beginning. The reason is that there is no experience in the industry. After substantial numerical experimentation (finite elements simulations) and based on the experience the team members had with large power transformer, an electrostatic shielding was proposed to control the impulse response of toroidal transformers. An important difficulty is the fact that the turns touch in the internal part and are far in the outside. This produces a highly nonlinear distribution of the impulse stresses. The first and second turns see a tremendous stress. The results of the study are published in the following paper:

> **P. Gómez, F. de León, and I. Hernández, "*Impulse Response Analysis of Toroidal Core Distribution Transformers for Dielectric Design*", IEEE Transactions on Power Delivery, Vol. 26, No. 2, April 2011, pp. 1231-1238.**

The solution to the impulse response problem came in the form of an electrostatic shield. This is standard in the field of large power transformers. However, we proposed a novel solution, only applicable to the toroidal geometry, which is to make the magnetic core to double as the electrostatic shield by electrically connecting it to the high voltage terminal; see Figure 2.1. This is a patented solution that in addition of controlling the impulse distribution, allows for the use of very thin insulation between layers, therefore providing an excellent thermal performance. The following patent has been filed:

F. de Leon, "Electrostatic Shielding for Transformers", United States Patent Application, Serial No. 61/857,581; Provisional patent filed on July 23, 2013; Utility patent application filed on July 23, 2014.

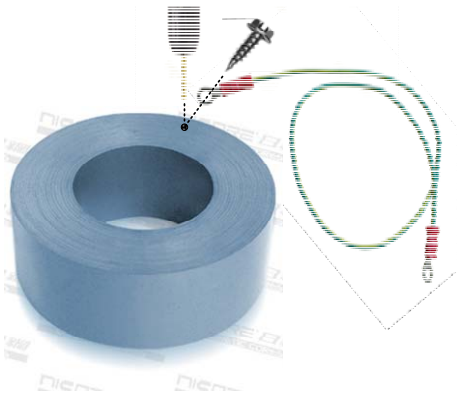

Figure 2.1. Toroidal transformer winding and core showing the connection of the core to the high voltage terminal.

2.3.3 Thermal Design

One of the most important challenges to overcome was the thermal design. Since a dry-type transformer design was sought and air is substantially less efficient than oil at removing heat, it was important to minimize losses. Additionally, since there is no need to cut the core to set the windings on it, we can take full advantage of the excellent properties amorphous materials to produce an extremely efficient transformer. As a result of extensive finite elements simulations, we realized that the thermal performance will greatly improve when we set the high voltage winding inside and the low-voltage winding outside (the opposite to current technology). This construction prevents heat from the low-voltage winding to be trapped in the multi-layer insulation necessary for the high-voltage winding. Moreover, this construction allows setting the

common ground between windings in the middle. All the details, including a model and experimental validation, can be found in the following paper:

> **S. Purushothaman and F. de León, "*Heat Transfer Model for Toroidal Transformers*", IEEE Transactions on Power Delivery, Vol. 27, No. 2, April 2012, pp. 813-820.**

2.3.4 Mechanical Design

The mechanical design includes two major parts: the short circuit stresses and the mechanical integrity of the tank. Because of its closed construction, it is expected that the mechanical strength of toroidal transformers to be better than that of traditional designs. A set of finite elements simulations where performed to corroborate the above hypothesis. Figure 2.4 show an arrow plot of the mechanical forces in a toroidal transformer during a high current short-circuit. Different to traditional designs, the stresses are almost only in the direction tending to elongate or contract the conductors and negligible compression/expansion forces are exerted on insulation. Therefore, no modifications to the design are necessary to deal with short-circuit stresses.

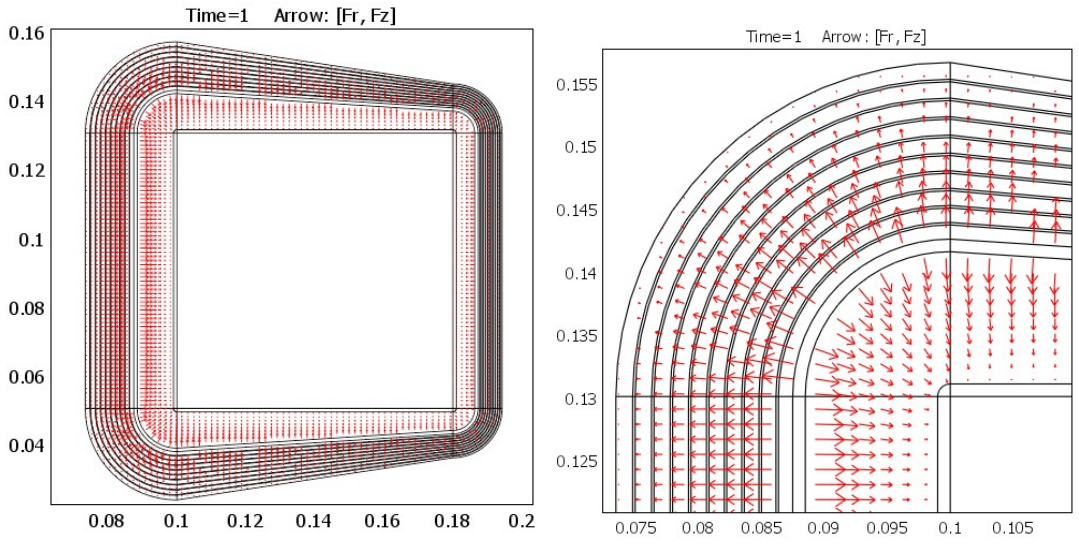

Figure 2.4. Arrow plot of force density for a toroidal transformer under short circuit.

The solution that we proposed for the design of the tank was to use exactly the same tanks that utilities use. In fact, we have gotten several tanks from Con Edison. In this way, we are sure that tanks comply with the specification and all clamping ironwork is at the right location for ease of installation.

2.3.5 Inrush Currents

The sole disadvantage that toroidal transformers have over traditional designs is the larger inrush currents. This is caused by the lack of gaps in the core, which is precisely the feature that gives toroidal transformers their technical advantage over traditional constructions. Inrush currents are produced by the saturation of the core during the energization of the transformer. Since our prototypes have not yet been installed in a real application, we do not have experimental evidence that the larger inrush would be a problem. However, we have continued the research in this area and have published/submitted a number of papers offering solutions to reduce the inrush currents. At this time none of the solution has been implemented because they will inevitably reduce the efficiency of the transformer. The details of this research have been reported in the following papers:

F. de León, A. Farazmand, and P. Joseph, "*Comparing the T and π Equivalent Circuits for the Calculation of Transformer Inrush Currents*", IEEE Transactions on Power Delivery, Vol. 27, No. 4, October 2012, pp. 2390-2398.

S. Jazebi, A. Farazmand, B. Murali, and F. de León, "*A Comparative Study on pi and T Equivalent Circuits for the Analysis of Transformer Ferroresonance*", IEEE Transactions on Power Delivery, Vol. 28, No. 1, January 2013, pp. 526-528.

A. Farazmand, F. de León, K. Zhang, and S. Jazebi, "Analysis, "*Modeling and Simulation of the Phase-Hop Condition in Transformers: The Largest Inrush Currents*", IEEE Transaction on Power Delivery, Vol. 29, No. 4, August 2014, pp. 1918-1926.

S. Jazebi and F. de León, "*Experimentally Validated Reversible Multi-Winding Transformer Model for the Accurate Calculation of Low-Frequency Transients*", accepted for publication in the IEEE Transactions on Power Delivery (early access available).

3. Construction of Prototypes

In this section, after describing the design process, the manufacturing steps are illustrated. As mentioned above, a design program was developed to consider all features described above. IN fact, the program goes through an exhaustive optimization process that complies with all specifications and gives the lowest cost.

3.1 Design Specifications

It is required that the design complies with the DOE final rule on efficiency requirements as presented in Table 3.1. Although the toroidal transformers developed here are dry-type, the transformers are designed to substitute oil-immersed transformers with similar electrical characteristics. Therefore, the design is carried out with the higher efficiency of oil-immersed transformers.

The hottest-spot temperature rise above ambient temperature1 shall not exceed the values given in Table 2.2 [2]. Note that higher winding average temperature rises may apply if the manufacturer provides thermal design test data sustaining that the temperature limits of the insulation are not exceeded [2]. Also temperature of external parts accessible to operators (tank) shall not exceed the temperature rises over ambient temperature at maximum rated load shown in Table 3.2. Hence, for the toroidal pole-mounted transformer, the tank temperature shall not exceed 80°C. The design program computes the temperature of the different parts of the transformer with the electrical model presented in [3].

[1] Based on an average daily ambient temperature of 30°C, with a maximum ambient temperature of 40°C

Table 3.1. Energy efficiency standards for single-phase low-voltage distribution transformers [7]

kVA	Dry-Type (%)	Oil-immersed (%)
15	97.7	98.76
25	98.0	98.91
37.5	98.2	99.01
50	98.3	99.08
75	98.5	99.17
100	98.6	99.23
167	98.7	99.25

Table 3.2. Limits of temperature rise for continuously rated dry-type transformer windings [2]

Insulation temperature class (°C)	Winding hottest-spot temperature rise (°C)	Average winding-temperature rise by resistance (°C)
130	90	75
150	110	90
180	140	115
200	160	130
220	180	150

Table 3.3. Allowable temperature rise of external parts over ambient [2]

Readily accessible	65°C
Not readily accessible	80°C
Note: Not readily accessible is considered to apply to equipment parts located at heights greater than 2.0 m above floor level or otherwise located to make accidental contact unlikely	

3.2 Insulation

A toroidal winding machine is loaded with insulation paper. The insulation used in the toroidal transformer is 6 mil DMD-F composite paper with thermal class F, 155° C. The same insulation material is used to insulate the HV windings of all neighboring layers. The last insulation layer covers the entire HV winding. This layer insulates the HV winding from the LV windings. Note that the LV windings are made with insulated welding cable. Therefore, due to the low continuous operating voltage, there is no need to insulate between layers of the LV.

3.3 Core and Electrostatic Shielding

The material of the core is amorphous iron. The purpose for using amorphous cores is to reduce the energy losses. As the result, the transformer could be designed smaller, lighter and cooler. The nominal flux density is 1.4 [Tesla] for the transformer design.

The core is electrically connected to the high voltage (HV) terminal to use less insulation between the core and the winding. Therefore, the inner winding is the HV and the low voltage (LV) winding is wound on top of the HV winding. This technique creates an electrostatic shield between the core and the HV winding. The function of the electrostatic shield is to produce a more uniform distribution of the electrical stresses that the inter-turn and inter-layer insulation undergo during the impulse test [4], [5].

For this purpose the core is drilled (perpendicular to laminations). An insulated wire (with the same gauge as the HV winding) is screwed to the core with a cable lug; see Figure 3.1. The core connection is then held in place with adhesive tape to the insulation to avoid the replacement of the wire; see Figure 3.1(b).

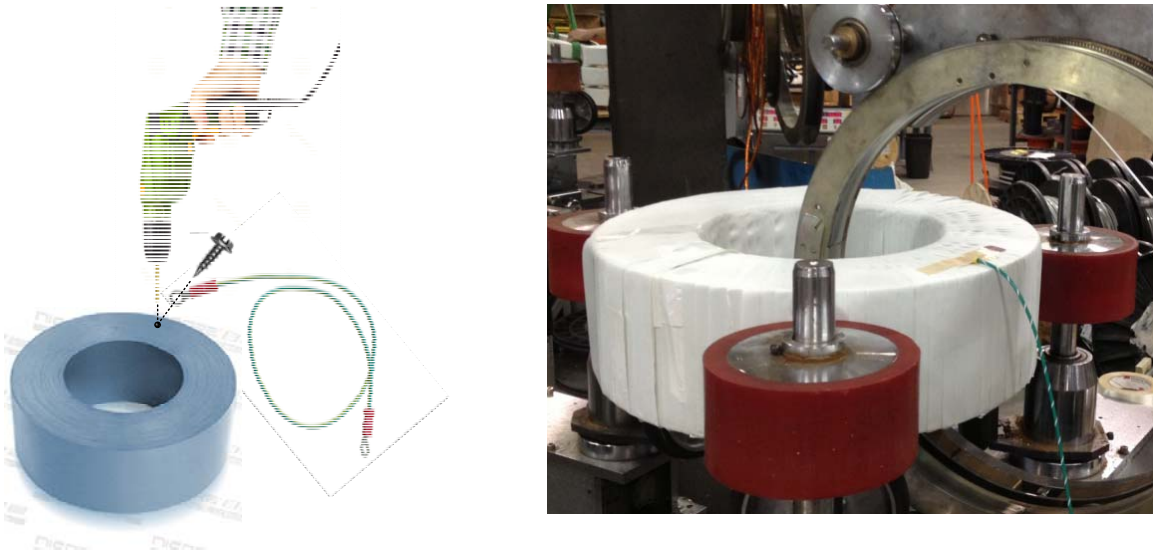

(a) (b)

Figure 3.1. (a) Connection of the core to the HV after drilling the core perpendicular to laminations; (b) the insulated core and the electrical connection.

3.4 High-Voltage Winding

The transformer contains a single high voltage winding which is wound on 340° of the core. Note that, 20° are left unwound to pass two wires; the high voltage winding and the electrostatic shield lead to the core. For the high voltage winding, magnet wire with the electrical characteristics presented in [6] and in the Appendix are used.

3.5 Low-Voltage Winding

The low voltage winding is manufactured with welding cables [7]. On the low-voltage side, the transformer has two windings and series/parallel connection capabilities. Therefore, it can supply 120/240 V loads. The two low-voltage windings are similar and each of them is wound on 160° of the core. This method completely avoids the use of additional insulation between the

two low-voltage windings. Also, this approach increases the impedance between the two LV windings which limits the short circuit current [8], [9].

The low voltage winding strategy is shown in Figure 3.2. Note that, on each side, there is a 20° gap between the two windings to avoid the impulse test failure. It is necessary that the LV windings are wound in a way that the terminals are geometrically located at 180° from the HV winding. However, the other HV lead (connection to the neutral) is geometrically in phase with the LV leads.

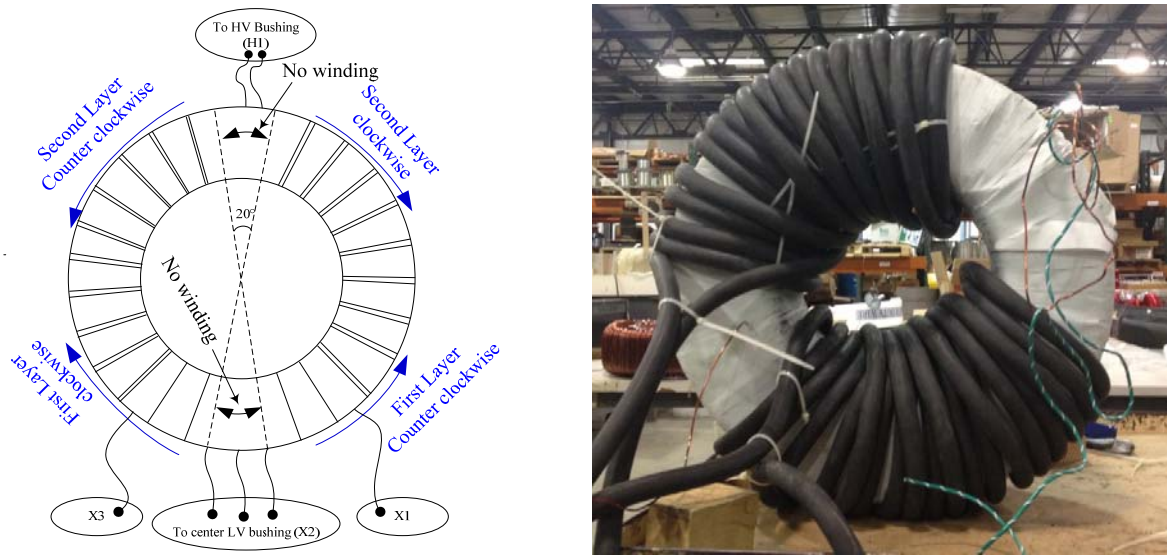

(a) (b)

Figure 3.2. Low voltage winding strategy with two layers.

Both windings start with the first turn located near the HV winding connection to the neutral. In order to get the additive polarity, one of the LV windings is wounded clockwise and the other is wounded counter clockwise. The first turn of the second layer starts on top of the last turn of the first layer. This procedure is followed until the last layer is completed. Note that, to establish

proper connections to the LV bushings, the last layers of the two windings are wound in a way that the end leads locate close to the start leads.

3.6 Selection of Bushings and Surge Arresters

The surge arrester was selected from Ultrasil Polymer-Housed evolution (10 kA) surge arresters manufactured by cooper power systems [10] and with respect to the recommended arrester rating per IEEE Std. C62.22 standard [11]. For example, for the 13.2 Y/7.62 and solidly grounded neutral, the voltage rating of the surge arrester is selected 15 kV rms, where MCOV=12.7 kV rms. The part number is URT1507-0A1C-1D1C.

Transformer mounting bracket is used to install the surge arrester as shown in Figure 3.3(a) and Figure 3.4(c). The bracket dimensions are shown in Figure 3.3(b). A surge arrester bracket is provided adjacent to the HV bushing. This bracket allows mounting of a surge arrester with enough space from the transformer tank to prevent the tank from interfering with the operation of the surge arrester. Bushings should comply with the requirements of IEEE C57.19.00 and IEEE C57.19.01 [12], [13].

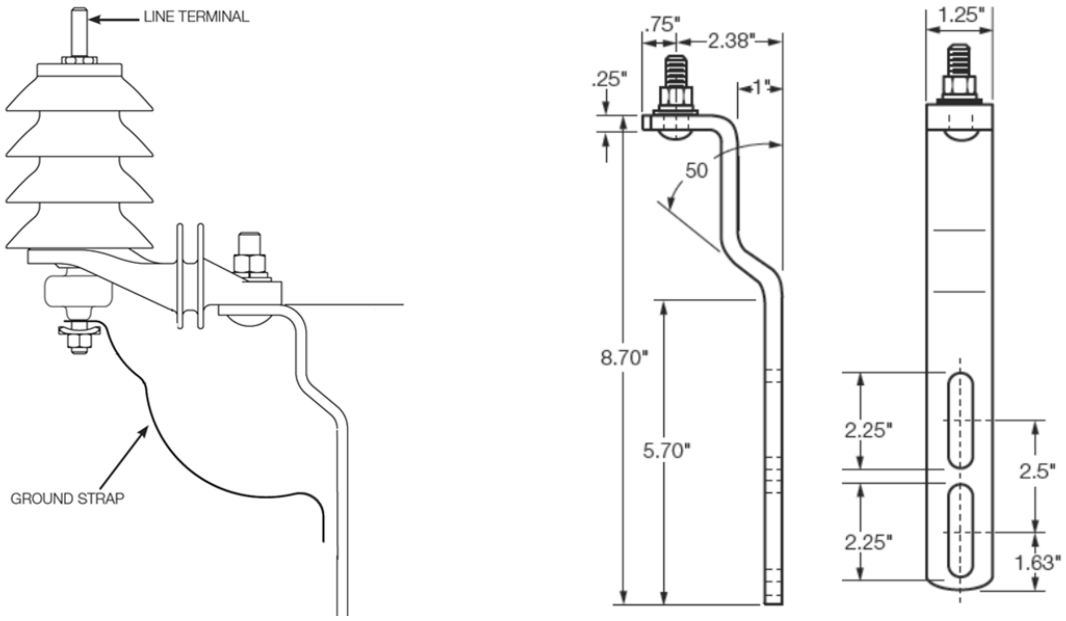

(a) (b)

Figure 3. 3. Evolution surge arrester with isolator, insulated hanger and transformer mounting bracket.

3.7 Transformer Tank

Transformer tanks need to be sealed and need to be rigid. The structure of the tank is shown in Figure 3.4. One earth terminal is located on the primary side of the tank, vertically below the center LV bushing (X2). The other earth connection (tank ground connection) is through a mounting nut welded to the lower part of the tank vertically below the HV bushing. The transformer needs welded lifting lugs and hanger brackets for direct-to-pole mounting. The lead (cover) needs to be electrically connected to the tank; see Figure 3.4(c).

The interior and exterior surfaces of the tank shall either be abrasive blast-cleaned or be pickled, rinsed and dried to avoid corrosion. Before being coated, both surfaces shall be free from rust, grease, oil and moisture. Electrostatically applied polyester powder paint system could be used for superior corrosion protection.

Figure 3.4. Different parts and accessories of the tank.

3.8 Installation of the Active Element in the Tank

To shield the LV winding from the bottom of the tank, alumina plates are utilized. The thermal resistivity of alumina is very low while the electrical resistivity of this material is very

high. Therefore, it is suitable for this application. First, six 2"×2"×0.412" plates are placed at the bottom part of the tank with the arrangement presented in Figure 3.5. Then, the active part of the transformer is moved with the crane into the tank and placed on top of the alumina plates. Then, the transformer tank is filled with the epoxy resin (see Figure 3.6). Note that, to increase the heat transfer efficiency and reduce the weight of the epoxy, a PVC pipe with the same diameter as the ID of the active part could be utilized.

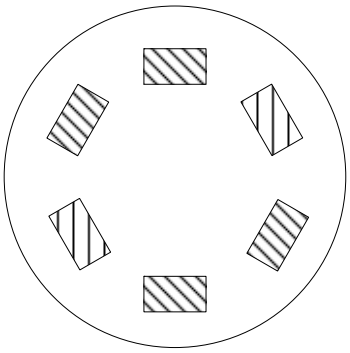

Figure 3.5. Arrangements of ceramic plates at the bottom of the tank.

Figure 3.6. Filling the tank with the epoxy resin.

3.9 Connections

Closed ring (O-type) cable lugs are used for the connection of the low voltage cables to the low voltage bushings. One end of a cable lug is crimped to the cable and the connection end of the lug is fastened to the bushing terminal by means of a nut (see Fig. 3.7).

The IEEE standards [14], applicable to single-phase distribution transformers 200 kVA and smaller, having high voltage windings rated 8660 volts or less requires transformers with additive polarity. All other single-phase transformers must have subtractive polarity. Therefore, to have the additive polarity, windings are connected according to IEEE standard with series connection [15]. The connection diagram is presented together with the nameplate in Figure. 3.8.

Figure 3.7. Connection of the LV leads to the bushing terminals.

3.10 Nameplate Information

The name plate information and connection diagram are provided according to IEEE Standards [2], [15]. The nameplate of a 50 kVA transformer is shown in Fig3.8 as an example. The nameplate information is engraved and filled black on a stainless still plate with 0.03" thickness. The plate is 6"×3-3/8" with round corners. Four corner holes (1/16") are needed for mounting.

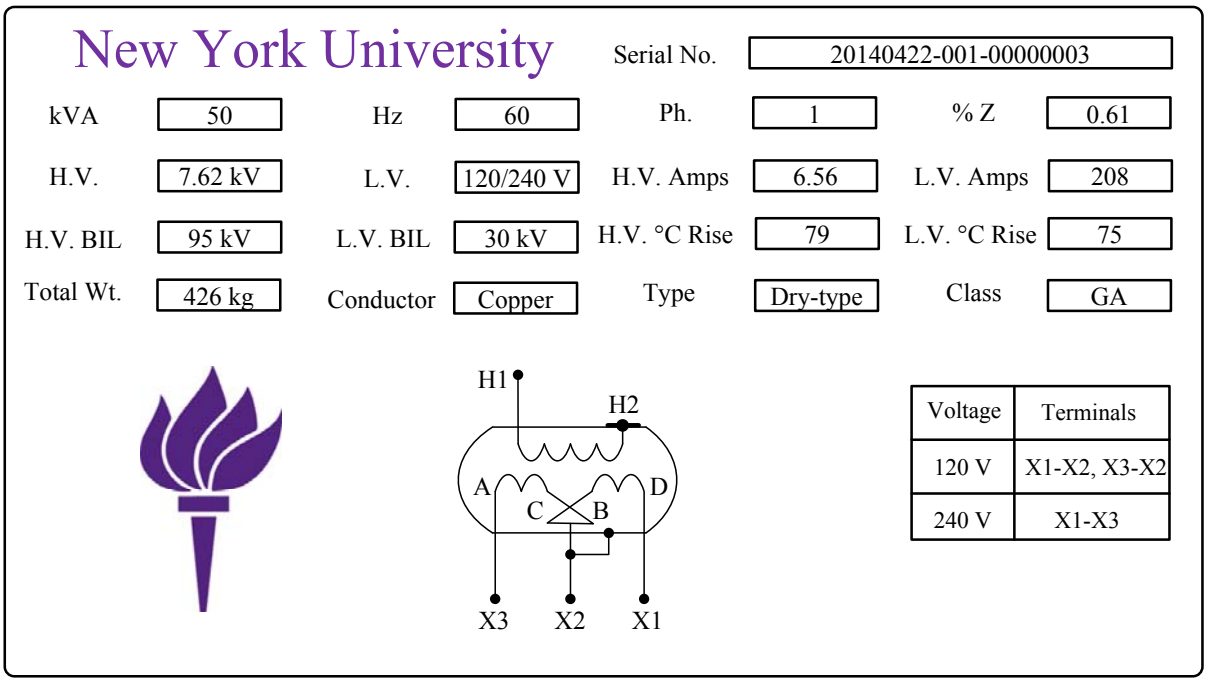

(a)

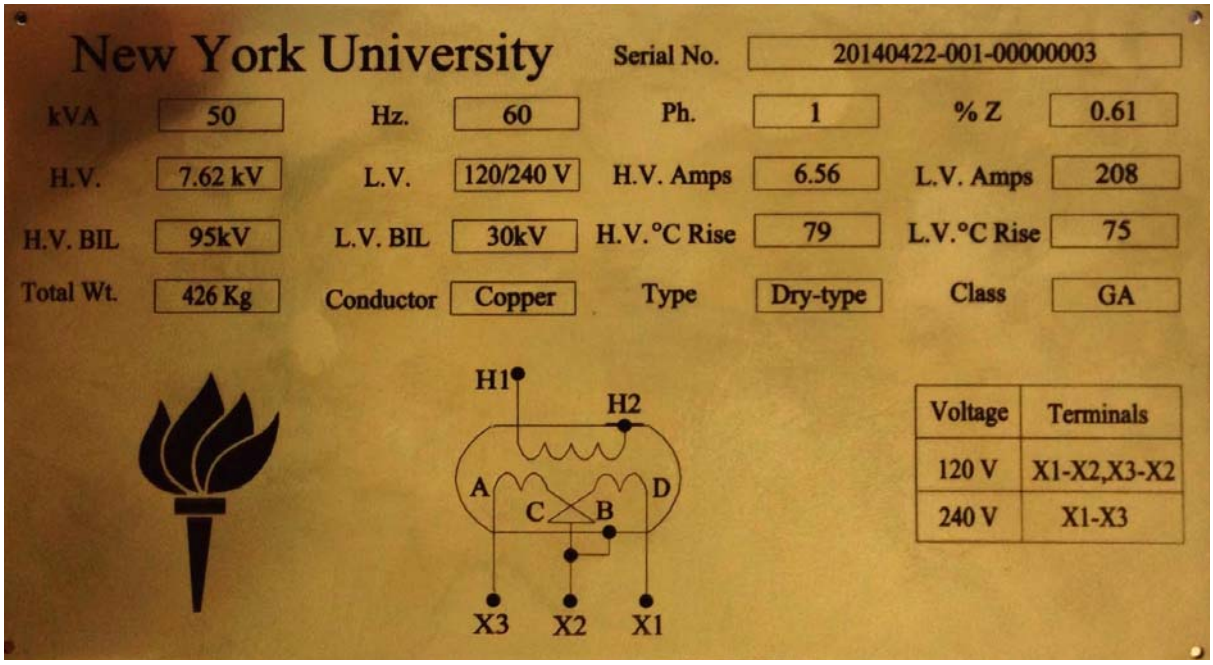

(b)

Figure 3.8. Nameplate for the 50 kVA prototype transformer; (a) designed (b) picture.

3.11 Serial Number

The serial number of the product consists of three parts with 8, 3, and 8 digits. The first part indicates the manufacturing date (YYYY/MM/DD), the second part indicates the product type identification number, and the third part indicates the product number for the specific type. Figure 3.9 illustrates the meaning of the different digits in the serial number.

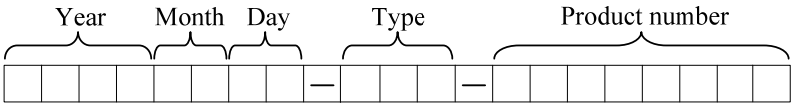

Figure 3.9. Serial number generation.

4. Value Propositions

Nowadays, the standard technology is the oil-immersed transformers. This is so because oil has a better thermal conductivity and insulation properties than air. Therefore, transformers with oil are built with higher efficiency than dry-type transformers. These transformers have several disadvantages. During an overload, the windings produce heat and break down the oil into nitrogen, hydrogen, and oxygen. This also happens in faulty transformers and may produce serious explosions. The oil is usually mineral oil, and may also include fire resistance substances such as PCBs and silicone which are toxic for human.

Today dry-type transformers are expensive. Utilities such as Con Edison should pay 7 times the price of oil-immersed transformers for a dry-type transformer with similar specifications. The insulating material (air/paper) is not usually a good thermal conductor. Therefore dry-type transformers are not as efficient as oil-immersed transformers.

The designed and manufactured transformers object of this project are made with toroidal cores with continuous still strips that are wound like a donut. The core does not have any air-gaps, therefore iron core losses decrease to minimum. Also, because of the special geometry, the resistance of the windings is reduced. This factors makes it very high efficient.

The final product is an ultra-high efficiency dry-type transformer. The efficiency satisfies standards even with 150% overloads. The toroidal geometry makes the transformer smaller and lighter. This transformer has almost the same price as standard transformers. However, the operational costs are almost half of the oil-immersed transformers over the life time. This is shown with comparison of the Capex and Opex in Figure 4.1. For example, for a typical medium sized utility such as Orange and Rockland, with approximately 40,000 oil-filled transformers, if only 10% of the current transformers are replaced, this utility will save $24M/20 years, which means average savings of $1.2M/year in losses.

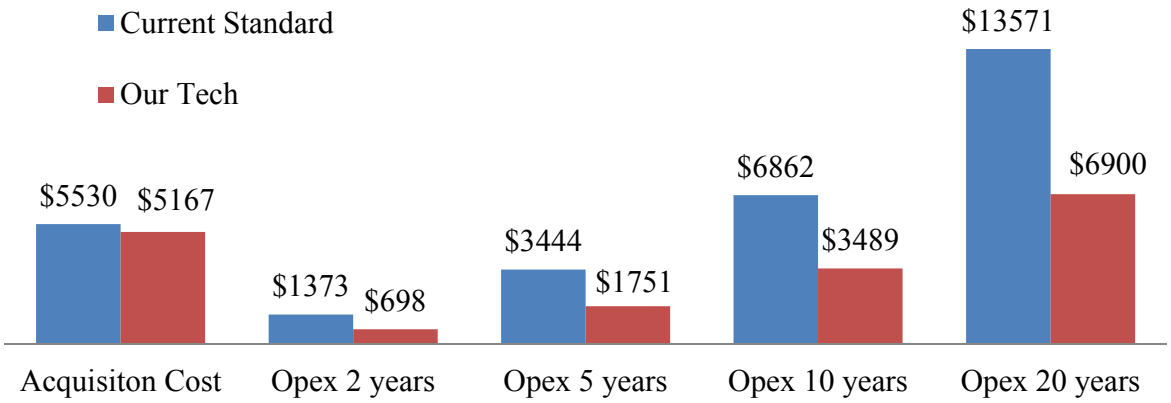

Figure 4.1. Capital and operational costs comparison between the standard transformers and the toroidal transformer.

5. Products

The list of tangible products of this project is given in this section. We have produced two full-size prototypes, published nine papers, applied for one patent, graduated three PhD students and three MSc students, and supported five postdoctoral fellows. We obtained a grant from Power Bridge NY in the amount of $149,985 from June 2014 to May 2015 to continue developing the transformer with commercialization objectives.

5.1 Prototypes

25 kVA toroidal transformer

50 kVA toroidal transformer

5.2 Papers

The following nine papers have been published in the IEEE Transactions:

1) P. Gómez, F. de León, and I. Hernández, "*Impulse Response Analysis of Toroidal Core Distribution Transformers for Dielectric Design*", IEEE Transactions on Power Delivery, Vol. 26, No. 2, April 2011, pp. 1231-1238.

2) I. Hernández, F. de León, and P. Gómez, "*Design Formulas for the Leakage Inductance of Toroidal Distribution Transformers*", IEEE Transactions on Power Delivery, Vol. 26, No. 4, October 2011, pp. 2197-2204.

3) S. Purushothaman and F. de León, "*Heat Transfer Model for Toroidal Transformers"*, IEEE Transactions on Power Delivery, Vol. 27, No. 2, April 2012, pp. 813-820.

4) F. de León, A. Farazmand, and P. Joseph, "*Comparing the T and π Equivalent Circuits for the Calculation of Transformer Inrush Currents*", IEEE Transactions on Power Delivery, Vol. 27, No. 4, October 2012, pp. 2390-2398.

5) S. Jazebi, A. Farazmand, B. Murali, and F. de León, "*A Comparative Study on pi and T Equivalent Circuits for the Analysis of Transformer Ferroresonance*", IEEE Transactions on Power Delivery, Vol. 28, No. 1, January 2013, pp. 526-528.

6) F. de León, S. Purushothaman, and L. Qaseer, "*Leakage Inductance Design of Toroidal Transformers by Sector Winding*", IEEE Transactions on Power Electronics, Vol. 29, No. 1, January 2014, pp. 473-480.

7) F. de León, S. Jazebi, and A. Farazmand, "*Accurate Measurement of the Air-Core Inductance of Iron-Core Transformers with a Non-Ideal Low-Power Rectifier*", IEEE Transaction on Power Delivery, Vol. 29, No. 1, February 2014, pp. 294-296.

8) A. Farazmand, F. de León, K. Zhang, and S. Jazebi, "Analysis, "*Modeling and Simulation of the Phase-Hop Condition in Transformers: The Largest Inrush Currents*", IEEE Transaction on Power Delivery, Vol. 29, No. 4, August 2014, pp. 1918-1926.

9) S. Jazebi and F. de León, "*Experimentally Validated Reversible Multi-Winding Transformer Model for the Accurate Calculation of Low-Frequency Transients*", accepted for publication in the IEEE Transactions on Power Delivery (available in early access).

5.3 Patent

F. de Leon, "Electrostatic Shielding for Transformers", United States Patent Application, Serial No. 61/857,581; Provisional patent filed on July 23, 2013; Utility patent application filed on July 23, 2014.

5.4 List of Students Supported from the Grant

M.Sc. Students:

Githanjali Venkataramani
Matthew Terracciano
Noel Augustine

Ph.D. Students:

Sujit Purushothaman
Ashkan Farazmand
Saeed Jazebi

Post Doctors:

Pablo Gomez
Layth Qaseer
Ashkan Farazmand
Ivan Hernandez
Saeed Jazebi

6. Conclusions

The research performed for this project has demonstrated that it is possible to design and build utility-grade distribution transformers in toroidal cores. The gapless construction of toroidal transformers brings important advantages over the traditional designs. It has been shown that the higher efficiency of the toroidal construction makes possible to substitute oil-filled transformers by dry-type transformers for pole mounted applications.

The technical challenges that were overcome in this project include: the development of the technology to pass the impulse tests, derive a model for the thermal performance, produce a sound mechanical design, and estimate the inrush current. However, the greatest challenges that we faced during the development of the project were the complications of procuring the necessary parts and materials to build the transformers. The actual manufacturing process is relatively fast, but getting all parts together is a very lengthy process.

The following key technologies were developed in the course of this project: (1) to take full advantage of the gapless core construction, an amorphous material was selected for the core. These cores produce very little losses yielding an improved transformer thermal behavior; (2) the magnetic core is electrically connected to the high-voltage terminal to produce an electrostatic shield. Because of this, the insulation layers can be made very thin, which again improves the heat dissipation characteristics of the transformer; (3) the high-voltage winding is wound inside and thus the low-voltage winding is outside. Thus, very little heat is trapped in the multi-layer insulation system needed for the high-voltage winding. With exception of technology (3), these technologies are not currently used in standard transformers. In fact, technologies (1) and (2) are not applicable in standard designs.

The main products of this project are two prototypes of toroidal distribution transformers of 7.62 kV (to be used in a 13.2 kV system) to 2x120 V secondary (standard utilization voltage); one is rated at 25 kVA and the other at 50 kVA. The 25 kVA transformer passed the impulse test in KEMA high-voltage laboratories. Additional products include: nine papers published in the

IEEE Transactions on Power Delivery, one patent has been filed, three PhD students were supported from beginning to graduation, five postdoctoral fellows, and three MSc students were partially supported.

When the manufacturing process is prepared for mass production, the cost of a dry-type toroidal transformer would be similar to the price of an oil-filed standard design. However, because of the greatly reduced losses, the total ownership cost of a toroidal transformer could be about half of a traditional design.

We obtained a grant from Power Bridge NY in the amount of $149,985 from June 2014 to May 2015 to continue developing the transformer with commercialization objectives.

7. References

[1] *Energy Conservation Program for Commercial Equipment: Distribution Transformers Energy Conservation Standards*, Department of Energy Final Rule, 10 CFR Part 431.

[2] *IEEE Standard General Requirements for Dry-Type Distribution and Power Transformers, Including Those with Solid-Cast and/or Resin Encapsulated Windings*, IEEE Std. C57.12.01, May 2006.

[3] S. Purushothaman and F. de León, "Heat Transfer Model for Toroidal Transformers", *Transactions on Power Delivery*, vol. 27, no. 2, April 2012, pp. 813-820.

[4] P. Gómez, F. de León, and I. Hernández, "Impulse Response Analysis of Toroidal Core Distribution Transformers for Dielectric Design", *IEEE Transactions on Power Delivery*, vol. 26, no. 2, April 2011, pp. 1231-1238.

[5] F. de Leon, "Electrostatic Shielding for Transformers", U.S. Patents, 2013.

[6] Machinery's Handbook, 21st Edition, 1982, Industrial Press Inc.

[7] Industrial and Mining Grade Cables, TFcables.

[8] F. de León, S. Purushothaman, and L. Qaseer, "Leakage Inductance Design of Toroidal Transformers by Sector Winding", *IEEE Transactions on Power Electronics*, vol. 29, no. 1, January 2014, pp. 473-480.

[9] Hernández, F. de León, and P. Gómez, "Design Formulas for the Leakage Inductance of Toroidal Distribution Transformers", *IEEE Transactions on Power Delivery*, vol. 26, no. 4, October 2011, pp. 2197-2204.

[10] UltraSIL polymer-housed Evolution (10 kA) IEEE surge arresters for MV systems to 36 kV, Technical Data 235-99, Cooper Power Systems.

[11] *IEEE Guide for the Application of Metal-Oxide Surge Arresters for Alternating-Current Systems*, IEEE Std. C62.22, July 2009.

[12] *IEEE Standard General Requirements and Test Procedure for Power Apparatus Bushings*, C57.19.00, Jun 2005.

[13] *Characteristics and dimensions for outdoor apparatus bushings*, IEEE C57.19.01, Jan 2000.

[14] *IEEE Standard for Overhead-Type Distribution Transformers 500 kVA and Smaller: High Voltage, 34 500 V and Below; Low Voltage, 7970/13 800Y V and Below*, IEEE Std. C57.12.20, Sep. 2011.

[15] *IEEE Standard for Standard Terminal Markings and Connections for Distribution and Power Transformers*, IEEE Std. C57.12.70, Feb. 2012.

8. Appendices

The manuscript versions of the nine papers published as part of this US Department of Energy award DE-OE0000072 follow as an appendix to this report.

Impulse Response Analysis of Toroidal Core Distribution Transformers for Dielectric Design

Pablo Gómez, *Member, IEEE,* Francisco de León, *Senior Member, IEEE*, Iván A. Hernández, *Student Member, IEEE*

***Abstract*—Toroidal transformers are currently used only in low voltage applications. There is no published experience for toroidal transformer design at distribution level voltages. This paper explores the lightning impulse response of toroidal distribution transformers in order to obtain a dielectric design able to withstand standardized impulse tests. Three-dimensional finite element simulations are performed to determine the capacitance matrix on a turn-to-turn basis. Then, a lumped parameter RLC model is applied to predict the transient response of the winding, as well as to obtain the potential distribution along the winding and corresponding dielectric stresses. The model computes the impulse potential distribution and the dynamic (inter-turn and inter-layer) dielectric stresses. Different insulation design strategies are proposed by means of electrostatic shielding and variation of the inter-layer insulation.**

***Index Terms*— Distribution Transformers, Electrostatic Analysis, Finite Element Method, Impulse Test, Insulation Design, Toroidal Transformers, Transient Analysis.**

I. Introduction

THERE are two basic arrangements for the iron-cores used at present to build distribution transformers: (1) Core-type, where the cores are assembled by stacking laminations and sliding pre-made coils; and (2) Shell-type, where a continuously wound core is cut and wrapped around the coils a few laminations at a time [1], [2]. In both arrangements the finished core has air gaps that increase the magnetizing current and the no-load losses.

An alternative construction, currently used for low voltage applications and explored in this paper for distribution level voltages, is to use a core made of a continuous steel strip shaped like a doughnut (toroid) with the coils wound around [3]; see Fig. 1. This gapless construction allows for the construction of smaller, more efficient, lighter, and cooler transformers [4], [5]. The no-load losses are substantially reduced. There are also savings in the load losses because the windings have fewer turns since these transformers can be designed with a larger flux density. Therefore, there are savings in raw materials (iron and copper) for the same losses than a standard design and even the tank is smaller.

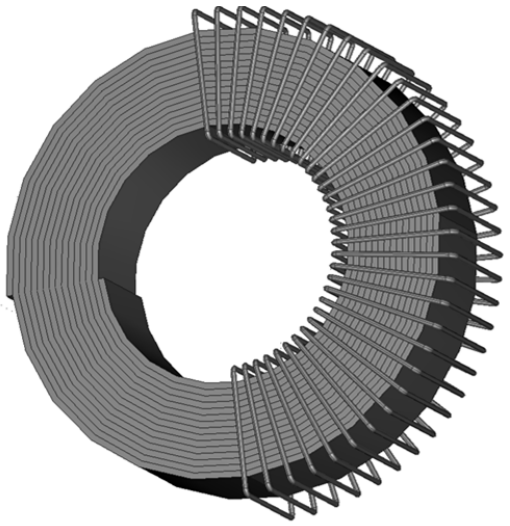

Fig. 1. Toroidal transformer (only a few turns of one winding are shown)

This work is part of a project supported by the US Department of Energy aimed to benefit from the toroidal construction virtues to construct and install toroidal transformers suitable for power distribution application. Given the lack of experience with this type of design at medium and high voltages, studies including electromagnetic, thermal and mechanical analysis are required to understand its particular physical behavior. This paper is part of a series describing such studies via computational design, optimization and verification, building prototypes, performance verification and observation of prototypes installed on a utility distribution system.

This paper is focused on analyzing the lightning impulse response of a toroidal distribution transformer in order to obtain a dielectric design able to withstand standardized impulse tests. This is done by means of three-dimensional finite element simulations, as well as electromagnetic transient simulations considering a lumped parameter RLC (turn-by-turn) model of the transformer winding. Such computational tools, which have been extensively used for electromagnetic transient analysis of conventional transformer arrangements (see for instance [6]-[11]), are applied in this paper for toroidal distribution transformers for the first time.

This work is supported by the U.S. Department of Energy under Grant DEOE0000072

P. Gómez is with the Electrical Engineering Department of SEPI-ESIME Zacatenco, Instituto Politécnico Nacional (IPN), U. P. "Adolfo López Mateos", Edificio Z-4 Primer piso C. P. 07738, Mexico, D. F. MEX (e-mail: pgomezz@ipn.mx).

F. de León is with the Department of Electrical & Computer Engineering, Polytechnic Institute of New York University, Six MetroTech Center, Brooklyn, NY 11201, New York, USA (e-mail: fdeleon@poly.edu).

I. Hernandez is with CINVESTAV Guadalajara, 45015 Jalisco, México (email: ihernand@gdl.cinvestav.mx

Another contribution of this paper is the application of electrostatic shielding in the design of the insulation system of toroidal transformers. Two insulation design strategies are proposed in the paper and their effectiveness in reducing the transient voltage and dielectric stress in the winding is demonstrated. The first one is the addition of an electrostatic shield uniformly spaced with respect to the winding. The second one is the use of an electrostatic shield that has a varying distance to the winding, by means of a gradual increase of insulation thickness between winding and shield (without affecting the winding positions). The two strategies are equally successful to properly distribute the impulse surge. The selection between them depends on manufacturer efficiencies and preferences

The dynamic performance of the toroidal transformer insulation system for lightning impulse is studied by means of two examples, one transformer of 25 kVA and another one of 50 kVA. Both transformers have the same ratings in terms of voltage ratio (13.8/0.120 kV) and BIL (95 kV).

II. Electrostatic Analysis

Given the complex geometry of the windings in a toroidal transformer, a 3D arrangement is required for the electrostatic analysis, as shown in Fig. 2. In this paper the internal (low-voltage winding, which is grounded) is represented by a solid toroidal shape since its detailed representation is not needed. Note that the transformer core is not visible. For the purposes of this paper each turn of the high-voltage winding is modeled as a closed loop, then the mutual capacitances can be obtained from the energy method.

Assuming that the high voltage winding has N layers and n turns per layer, the following capacitive values need to be computed:

- $C_{s,o}$ Self capacitance of any turn at the outer layer (N)
- $C_{s,i}$ Self capacitance of any turn at the inner layer (1)
- $C_{s,m}$ Self capacitance of any turn at any interior layer (2, … N-1)
- $C_{it,o}$ Mutual capacitance between any two adjacent turns at the outer layer (N)
- $C_{it,i}$ Mutual capacitance between any two adjacent turns at the inner layer (i)
- $C_{it,m}$ Mutual capacitance between any two adjacent turns at any interior layer (2, … N-1)
- $C_{iL,o}$ Mutual capacitance between the i-th turn at the outer layer and the i-th turn at the following interior layer
- $C_{iL,m}$ Mutual capacitance between the i-th turns of any 2 interior layers

These elements are computed by means of FEM simulations using the electrostatic energy method [12]. Self capacitances are computed from the electrostatic energy W_i obtained when applying a voltage V_i to the i^{th} turn of the winding:

$$W_i = \frac{1}{2} C_{ii} V_i^2 \qquad (1)$$

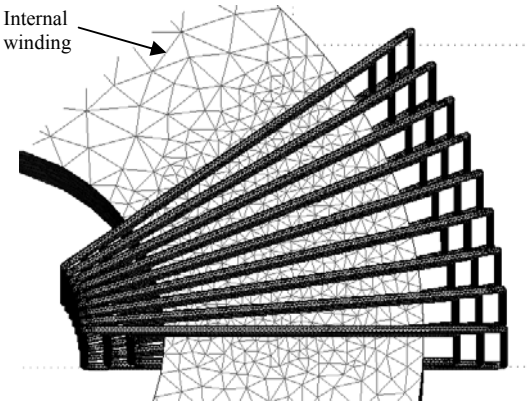

Fig.2. Geometry and meshing for FEM simulations (distances between layers were exaggerated for illustration purposes)

Mutual capacitance C_{ij} is computed from the electrostatic energy W_{ij} obtained when applying voltage at both turns i and j:

$$W_{ij} = \frac{1}{2} C_{ij} V_i V_j - \frac{1}{2}\left(C_{ii} V_i + C_{jj} V_j\right) \qquad (2)$$

Self capacitances must be calculated first from (1), in order to obtain the mutual elements from (2). Mutual capacitances between non-adjacent turns or layers are not considered since FEM simulations have shown that, for the arrangements under study, their values are at least one order of magnitude smaller than the values between adjacent turns. Transient simulations in which capacitive values for all turns (including non-adjacent) were included confirmed that they have no effect on the results for the geometrical configuration under analysis.

An important issue when finding the solution of such a detailed geometry lies in the finite element meshing. Considering the thin insulation between turns produces very narrow regions. This is particularly true at the internal part of the winding. Therefore, a very large number of elements (in the order of millions) is required to obtain an accurate solution.

Taking advantage of the toroidal symmetry to speed up the simulations and consume less memory, the geometry can be simplified by considering only a section of the actual number of turns and layers. For the example shown in Fig.2, three layers and nine turns per layer are found sufficient to approximate the capacitance values of a real arrangement of 11 layers with 214 turns per layer. This has been validated by initial simulations in which the results from the complete geometry are compared to those of the simplified one.

Each electrostatic simulation for the calculation of the capacitive matrix takes about 12 minutes in a powerful computer (two Xeon multi-core processors running at 2.27 GHz with 72 GB RAM).

It can be observed in Fig. 2 that, in contrast to shell or core type transformers, the distance between turns in a toroidal configuration is not constant. While the distance between turns at the internal part of the toroid is kept at the minimum required to avoid dielectric breakdown, the distance at the

external part is several times larger resulting in small capacitive coupling between turns (series capacitance). Thus, the well-known distribution constant $\alpha = \sqrt{C_{ground} / C_{series}}$ is several times larger for toroidal transformers than that for conventional constructions. This particularity of toroidal transformers produces highly non-uniform initial potential distribution (at the wave front), giving rise to large dielectric stresses as well as increased transient overvoltages. This makes necessary the use of electrostatic shielding.

III. Transient Analysis

Fast and very fast front transients in transformers are commonly analyzed using internal models, which can take into account the distribution of the incident surge along the windings. These models are described either by distributed parameters, using the transmission line theory [13], [14], or as a ladder connection of lumped parameter segments [6], [15]. The latter models can be solved by network analysis or by integrating the corresponding state-space equations.

Additionally, an admittance matrix model (black box model) based on terminal measurements has been presented in [16] and [17]. This model can be implemented in time domain simulation programs by means of a rational approximation procedure.

For the size of a distribution toroidal transformer and the frequency range involved in the lightning waveform, a turn of the transformer can be considered as electrically short. Therefore, a lumped parameter model considering a winding turn as the basic element is chosen in the present work.

This Section describes the lumped parameter model used in this paper to obtain the transient response of the winding. It is based in [6], and considers a lossy and frequency dependent multilayer winding.

After computing the winding capacitance matrix **C**, the geometric inductance matrix is obtained as

$$\mathbf{L} = \mu_0 \, \varepsilon \, \mathbf{C}^{-1} \tag{3}$$

In (3), ε is the permittivity of the surrounding medium. Conductor losses due to skin and proximity effects can be computed from the following expression [18]:

$$\mathbf{R} = \frac{1}{d}\sqrt{\frac{2\omega}{\sigma_c \mu_c}}\mathbf{L} \tag{4}$$

In (4), d is the distance between layers, ω is the angular frequency, σ_c is the conductivity of the winding conductor and μ_c is its permeability. On the other hand, dielectric losses can be included in the form of a shunt conductance matrix given by

$$\mathbf{G} = (\omega \tan\delta)\mathbf{C} \tag{5}$$

where $\tan\delta$ is the loss tangent of the winding insulation. From matrices **R**, **L** and **C** and **G** a nodal system can be defined to describe the winding (Fig. 3):

$$\mathbf{I}(\omega) = \mathbf{Y}(\omega)\mathbf{V}(\omega) \tag{6}$$

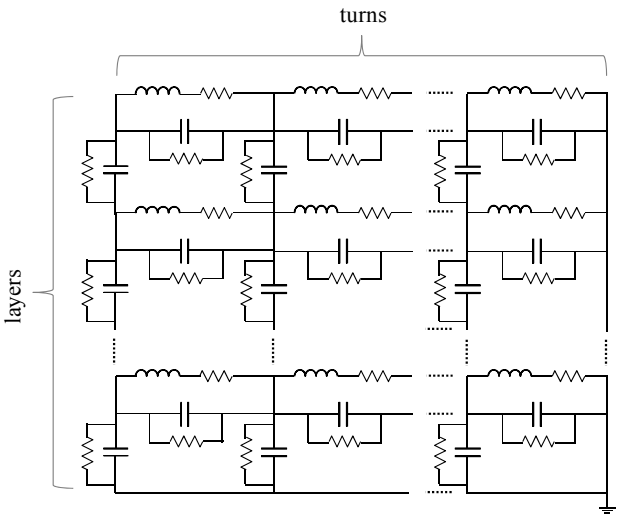

Fig.3. Circuital representation of the winding. Mutual inductances between turns and between layers, as well as ground capacitances of outer layers, are omitted in the figure for the sake of simplicity.

$\mathbf{V}(\omega)$ and $\mathbf{I}(\omega)$ correspond to the vectors of nodal voltages and currents; $\mathbf{Y}(\omega)$ is the nodal admittance matrix, which is defined as follows

$$\mathbf{Y}(\omega) = \mathbf{G} + j\omega\mathbf{C} + \mathbf{\Gamma} + \mathbf{G}_{con} \tag{7}$$

Matrix $\mathbf{G}_{con}$ contains the conductance elements required for the topological connection of layers, as well as the source and ground connections (if needed); $\mathbf{\Gamma}$ is the nodal matrix of inverse impedance, computed from $\mathbf{Z} = \mathbf{R} + j\omega\mathbf{L}$ and the incidence matrix **K** (since **Z** is a branch matrix):

$$\mathbf{\Gamma} = \mathbf{K}\,\mathbf{Z}^{-1}\,\mathbf{K}^{t} \tag{8}$$

where

$$\mathbf{K} = \begin{bmatrix} 1 & 0 & 0 & \cdots & 0 & 0 \\ -1 & 1 & 0 & \cdots & 0 & 0 \\ 0 & -1 & 1 & \cdots & 0 & 0 \\ \vdots & \vdots & \vdots & \ddots & \vdots & \vdots \\ 0 & 0 & 0 & \cdots & 1 & 0 \\ 0 & 0 & 0 & \cdots & -1 & 1 \end{bmatrix} \tag{9}$$

Finally, the time domain response of the winding is obtained by solving (6) for **V** and applying the inverse numerical Laplace transform [19], [20].

Maximum dielectric stresses (DS) between turns and between layers can be obtained from the elements of the nodal voltages vector **V** and the minimum distance between corresponding turns as:

$$\max(DS_{ij}) = \frac{|V_i - V_j|}{\min(d_{ij})} \tag{10}$$

IV. Electrostatic Shielding

There are three essential methods to improve the impulse response of power transformers: electrostatic shielding, addition of dummy strands, and interleaving of turns [1]. The latter method is in general preferred for transformers working at high-voltage transmission levels. However, for a toroidal transformer working at distribution level voltage with a large turns ratio (e.g. 13.8/0.120kV), the winding arrangement (by layers) and the small cross sectional area of the winding conductors makes it cumbersome and ineffective to attempt any interleaving or addition of dummy strands.

Hence, electrostatic shielding is chosen for toroidal distribution transformers. Its basic idea is to improve the initial potential distribution by compensating the current drained by the ground capacitances with currents injected to the series capacitances [20]. This is illustrated in Fig. 4. The shield is connected to the winding terminal and therefore it needs to be isolated from the turns and the tank along its length. Also, the shield should not form a closed path; a gap between the shield ends is necessary.

An electrostatic shield, inverted C-shaped, is proposed for the toroidal transformer constructed by means of a thin conductor material covered by an insulation layer and partially wrapped around the winding. The internal part of the winding remains unshielded (unwrapped) since the turns are close enough to each other in this region; see Fig. 5. Additionally, note that the size (and therefore the cost) of the toroidal transformer is very much dependent of the minimum internal diameter needed for the winding machine. Therefore, not shielding the center is convenient.

The distance between the shield and the winding is of particular importance. The shield has to be close enough to the winding to be effective and far enough from the winding to avoid dielectric breakdown. This is analyzed for the test case presented the next Section.

V. Test Cases

Two toroidal transformers with rating of 25 and 50 kVA are considered. Voltage ratio and BIL rating are the same for both: 13.8/0.120 kV and 95 kV. The main geometrical data of the high-voltage windings of these two transformers is listed in Table I. The following assumptions are made for simulation purposes:

a) The number of turns is considered equal for all layers; in an actual transformer each outer layer has fewer turns than the previous one.
b) Due to the previous assumption, turns from each layer are considered completely aligned, as shown in Fig 2.
c) The minimum distance between turns is given by the typical thickness of the varnish film for the corresponding conductor diameter [22].
d) The distance between layers is initially assumed to be 1 mm (plus the conductor varnish).

The set of capacitive values obtained from FEM for both transformers is listed on the Appendix. An alternating direction of the winding between layers is proposed, i.e., if the 1st layer is wound in the clockwise direction, then the 2nd layer is wound in the counterclockwise direction and so forth. This winding strategy yields reduced dielectric stresses when compared with continuous (same direction) windings.

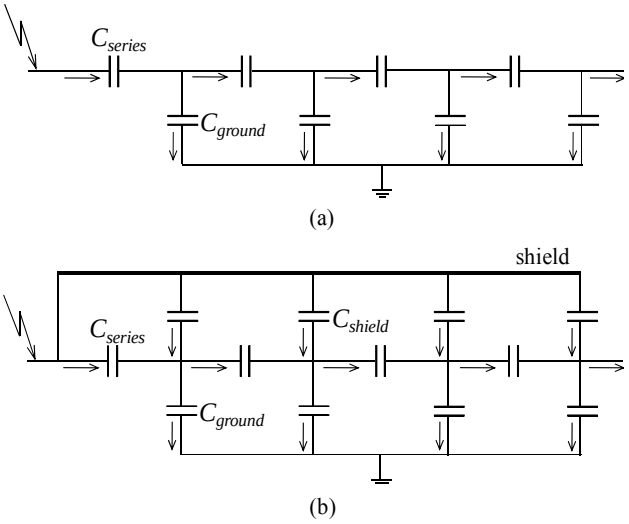

Fig. 4. Initial current distribution along the winding: (a) original, (b) with electrostatic shield.

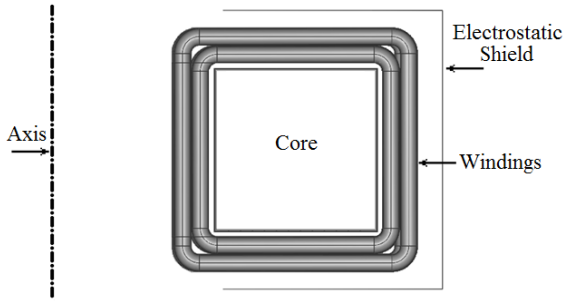

Fig. 5. Axisymmetric view of the toroidal transformer with an inverted C-shape electrostatic shield.

The transient response of the transformers is analyzed by means of the injection of a standard 1.2/50μs lightning impulse (full wave) at the initial terminal of the winding, which is located at the outermost layer of the winding. The lumped parameter model shown in Fig. 3 is constructed and solved as described in Section III.

TABLE I
Main Geometrical Data of the Transformers under Study

Rating [kVA]	25	50
External diameter of the core [mm]	510	600
Internal diameter of the core [mm]	250	250
Conductor gauge [AWG]	11	7
Conductor diameter [mm]	2.3048	3.6648
Distance between layers [mm]	1.0762	1.0940
Distance between windings [mm]	1.0000	1.0000
Distance between winding and core [mm]	1.0000	1.0000
Minimum distance between turns [mm]	0.0762	0.0940
Number of layers	11	12
Number of turns per layer	214	108

The performance of the shield is improved by a configuration equivalent to gradually removing the shield from the winding, which helps to approximate a uniform potential distribution. This is possible by: (a) decreasing the shield surface or (b) increasing the distance between the winding and the shield. However, option (a) implies a constant distance between the shield and the winding, which could result in dielectric breakdown given that the initial potential along the winding drops rapidly while the potential in the shield remains almost constant.

After substantial simulation tests, three alternatives of electrostatic shielding are deemed to be practical: two shields with constant distances of 1 and 2 mm to the outer layer of the winding, as well as a shield with a varying distance to the outer layer, from 0.1mm to 1 mm. The latter shield is included by means of a gradually increasing the insulation thickness between winding and shield.

Fig. 6 shows the initial potential distribution along the windings. As expected, the potential distribution without shield (continuous line) is highly non-uniform for both transformers. Additionally, some spikes can be seen, which are a consequence of the capacitive coupling between layers at the layers' ends. This distribution can be improved by including an electrostatic shield in the transformer design.

The way in which the different shields affect the initial potential distribution is shown in Fig. 6. By producing a more uniform distribution, the voltage drop between consecutive turns along the winding is reduced.

Fig. 7 shows the transient response of the winding at turn 107 for the 25 kVA transformer and at turn 52 for the 50 kVA transformer, corresponding to the regions of maximum voltage stress. One can appreciate that the shield is able to damp the transient oscillations reducing the maximum transient voltages. Additionally, as expected, the closer the shield is to the winding, the larger the mitigation of the overvoltage. However, this distance is limited by the dielectric strength of the insulation between winding and shield. The results for the uniform shield distanced 1 mm to the winding and the varying shield are almost identical for both transformers.

Fig. 8 illustrates the distribution of the maximum voltage obtained along the winding for the whole transient period, hereafter called impulse potential distribution. The voltage distribution along the whole winding of the different shielded transformers is more uniform compared to the unshielded transformers. The performance of the varying shield in the context of mitigating the transient voltage is very similar to that of the uniform shield separated 1 mm from the winding. With these two shielding strategies, the maximum value of transient voltage is reduced by 21.8% for the 25 kVA transformer, and by 11.3% for the 50 kVA transformer, with respect to the unshielded case.

The dielectric performance of the winding is analyzed considering three main variables:

a) Inter-turn dielectric stress
b) Inter-layer dielectric stress
c) Winding-to-shield dielectric stress

Fig. 9 shows the inter-turn stress along the complete winding. It can be seen in the plots how the stress is reduced by applying the different shields. The maximum value of inter-turn stress in the 25kVA and the 50kVA transformers is reduced by 57.2% and 56.1%, respectively, with the uniform shield located 1 mm from the winding. On the other hand, these stresses are reduced by 65.4% and 55.6% with the varying shield. It can also be noticed that, even without any shield, the stress is kept at an acceptable level. The maximum value obtained for both transformers is well below the dielectric strength of any high performance varnish [17]. Therefore, no extra insulation needs to be added between turns.

The inter-layer stress is plotted in Fig. 10. The inter-layer stresses are several times larger than the inter-turn stresses. The potential difference between turns of consecutive layers can be very large, particularly at the layers' ends (corresponding to the peaks in Fig. 9). The stress is especially large between the first two layers for both transformers under analysis. However, the values obtained with or without the shield are below the dielectric strength of a varnish included as reference (56 MV/m) [23].

One can see from Fig. 10 that the shields produce reduced inter-layer stresses when compared to the unshielded case. The reduction (in percent) of the stress at each inter-layer when applying the shields is shown in Table II. It can be noticed that the reduction is slightly larger when applying the varying shield. Furthermore, the shields produce an increase (by a small percentage) in the stress between layers 1 and 2 for the 50kVA transformer. This does not present a problem since the stress is still below the dielectric strength of the varnish considered.

From Figs. 8, 9 and 10, it seems that the best two options are: (a) use a uniform shield spaced 1 mm from the winding or, (b) use a shield with a varying distance to the winding, from 0.1 to 1 mm. Both strategies keep the transient voltage below the BIL, while the inter-turn and inter-layer stresses have acceptable levels.

TABLE II
REDUCTION OF THE INTER-LAYER STRESS WITH APPLICATION OF ELECTROSTATIC SHIELDING

Inter-layer	Dielectric stress reduction (%)			
	Uniform shield		Varying shield	
	25 kVA	50 kVA	25 kVA	50 kVA
1-2	12.0	-3.9*	17.0	-5.1*
2-3, 3-4	22.3	9.2	23.9	11.2
4-5, 5-6	21.5	25.7	25.1	28.4
6-7, 7-8	16.3	16.3	19.3	18.3
8-9, 9-10	13.5	13.7	16.0	15.8
10-11, 11-12	14.6	14.1	17.0	15.9
HV-LV	14.5	10.2	17.4	16.6

*Negative values correspond to increase in stress

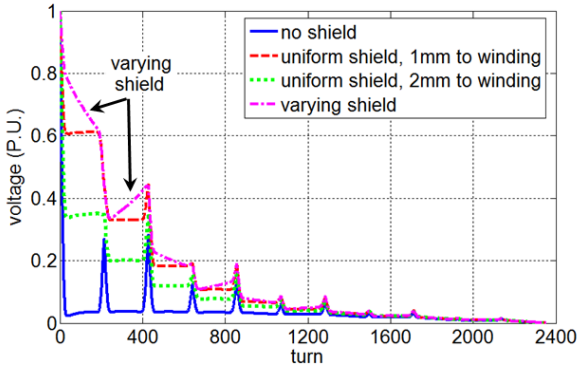

(a)

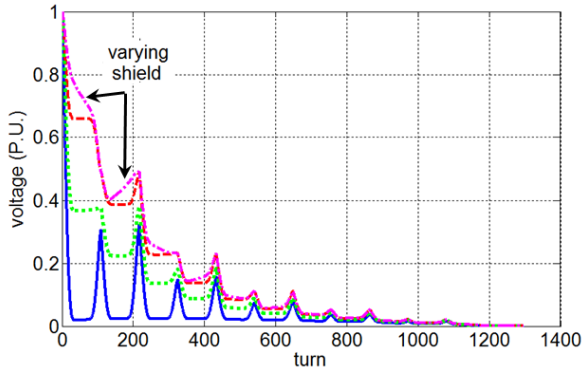

(b)

Fig.6. Initial potential distribution: (a) 25 kVA transformer, (b) 50 kVA transformer

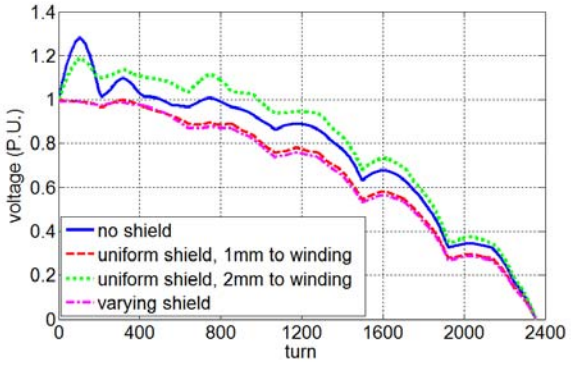

(a)

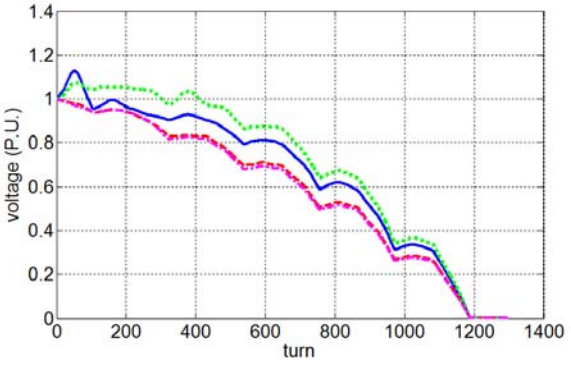

(b)

Fig.8. Impulse potential distribution: (a) 25 kVA transformer, (b) 50 kVA transformer

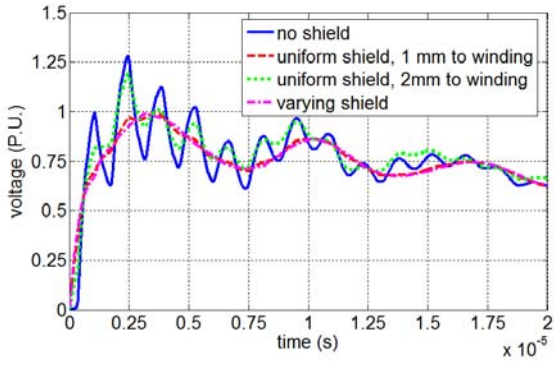

(a)

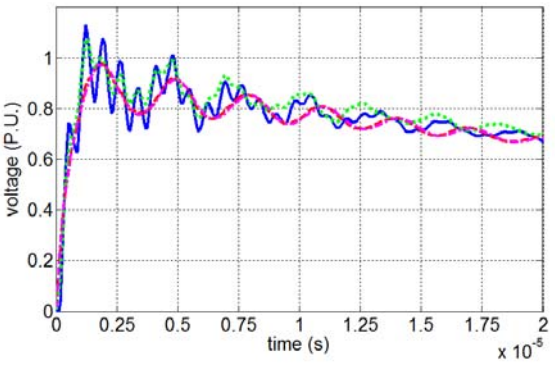

(b)

Fig.7. Transient response at the turn of max. voltage stress: (a) 25 kVA transformer, turn 107, (b) 50 kVA transformer, turn 52

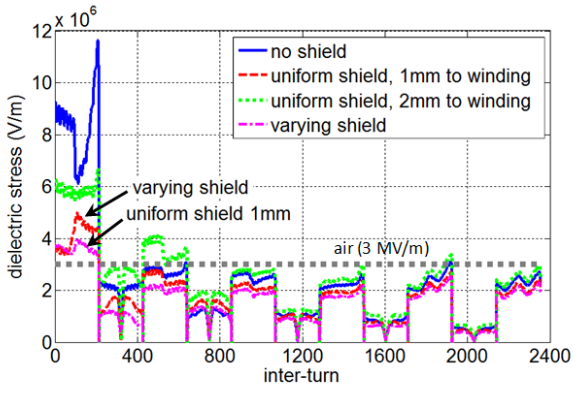

(a)

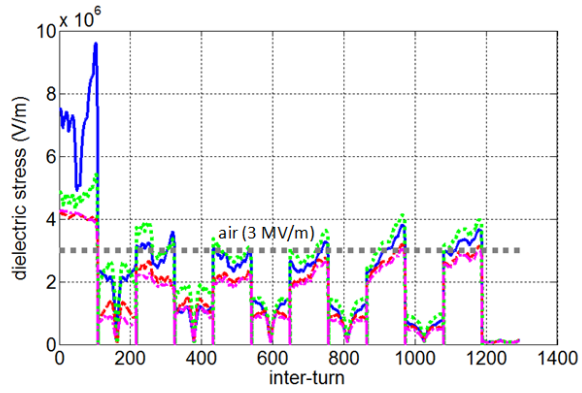

(b)

Fig.9. Inter-turn dielectric stress: (a) 25 kVA transformer, (b) 50 kVA transformer

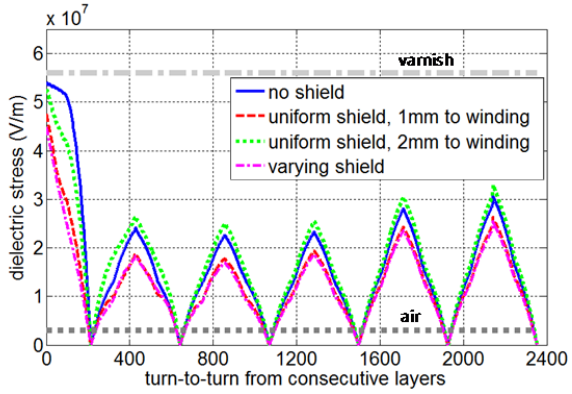

(a)

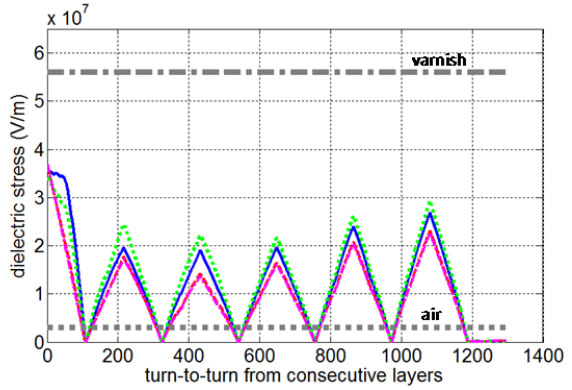

(b)

Fig.10. Inter-layer dielectric stress: (a) 25 kVA transformer, (b) 50 kVA transformer

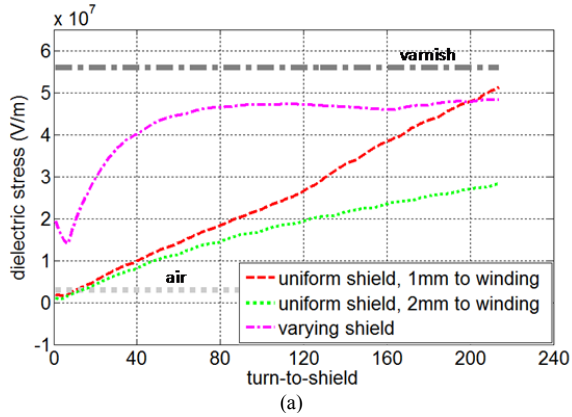

(a)

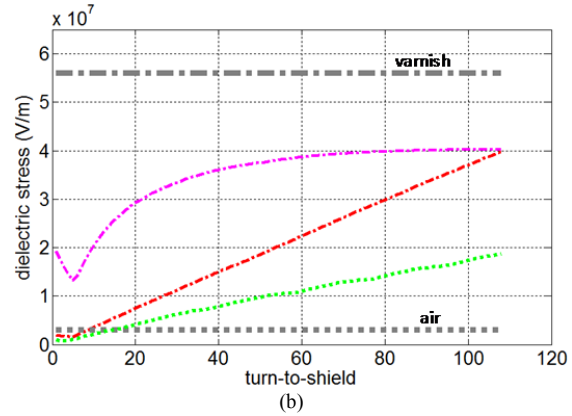

(b)

Fig.11. Winding-to-shield dielectric stress: (a) 25 kVA transformer, (b) 50 kVA transformer

The performance of the shields in terms of the dielectric stress between the shield itself and the winding is shown in Fig. 11. While the uniform shield presents a growing behavior of the stress along the outer layer of the winding, this stress tends to be constant for the varying shield. This means that, if the insulation between the winding and the shield is too thin, there is a possibility of dielectric breakdown at the end of the layer when a uniform shield is applied. However, the manufacturing process to include the varying shield is more complicated. Consequently, the uniform shield placed at the correct distance (1 mm for the cases analyzed) can be a better option. All transient voltages and stresses (between turns, layers and to the shield) are kept at acceptable levels without requiring of the cumbersome manufacturing of a varying distance of shield to the winding.

VI. Conclusions

The dynamic impulse response of a toroidal distribution transformer has been presented in this paper. By means of electrostatic 3D-FEM simulations the turn-by-turn capacitance matrix of the winding has been computed. Transient simulations on a lumped parameter model of the winding are used to design the insulation. In contrast to conventional transformers, the distance between turns in a toroidal core transformer is not constant. The larger distance between turns at the external region of the toroidal core yields a smaller series capacitance compared with traditional designs producing a very non-uniform initial potential distribution. This posses stringent design constraints since the non-uniform potential distribution gives rise to large transient voltages and dielectric stresses. To overcome this issue, three electrostatic shielding configurations have been proposed: two uniform shields with different distance to the winding and a shield with a linearly increasing distance to the winding. From the results of the simulations performed, the following conclusions are obtained:

1. Inter-turn stress is low for the whole winding. A typical insulation film corresponding to its AWG size and a dielectric strength above 12 MV/m is shown to be adequate for the tested cases.
2. Inter-layer stress is the critical factor for this type of transformers. The distance between layers has to be carefully selected to avoid inter-layer breakdown.
3. The inclusion of a shield at 1 mm from the winding or a shield with a varying distance to the winding (from 0.1 to 1 mm) results in lower inter-turn and inter-layer stress, as well as damped transient voltages.
4. When a uniform shield is considered, the distance between shield and winding has to be carefully selected in order to achieve the largest possible reduction in dielectric stress and transient voltage while avoiding dielectric breakdown between shield and winding.
5. Proposed in this paper is a shield with a varying distance to the winding, which prevents dielectric

breakdown between winding and shield.

VII. Appendix

Capacitive Values for the 25 kVA and 50 kVA Transformers without Shielding

Capacitance*	Value (pF)	
	25 kVA	50 kVA
$C_{s,o}$	71.71	104.32
$C_{s,i}$	56.67	84.23
$C_{s,m}$	63.20	88.70
$C_{it,o}$	25.78	35.23
$C_{it,m}$	15.48	16.44
$C_{iL,o}$	13.43	24.76
$C_{iL,m}$	12.74	23.24
$C_{it,i}$	10.45	10.90

*Refer to Section II for the corresponding nomenclature

VIII. References

[1] S. V. Kulkarni and S. A. Khaparde, *Transformer Engineering: design and practice*. CRC Press 2004, pp. 36-38.

[2] M. Heathcote, *J & P Transformer Book*. Newnes, 2007, pp. 13-15.

[3] I. M. Gottlieb, *Practical Transformer Handbook*. Newnes, 1998, pp. 12-15.

[4] G. J. Taggart and J. D. Goff, "Optimizing linear power supply performance with line frequency toroidal transformers," *NorthCon '94*, Seattle, WA , USA, 11-13 Oct. 1994, pp. 67-71.

[5] F. de León, B. Gladstone, and M. van der Veen, "Transformer Based Solutions to Power Quality Problems," *Power Systems World Conference and Exhibit*, Rosemont IL, USA, September 2001, pp 303-314.

[6] P. I. Fergestad and T. Henriksen, "Transient oscillations in multiwinding transformers," *IEEE Trans. Power App. Syst*., vol. PAS-93, pp. 500–509, Mar./Apr. 1974.

[7] Z. Azzouz, A. Foggia, L. Pierrat, and G. Meunier, "3D Finite Element Computation of the High Frequency Parameters of Power Transformer Windings," *IEEE Trans. on Magnetics*, vol. 29, no. 2, pp. 1407-1410, March 1993

[8] E. Bjerkan, H. K. Høidalen, "High Frequency FEM-based Power Transformer Modeling: Investigation of Internal Stresses due to Network-Initiated Overvoltages", *International Conference on Power Systems Transients (IPST'05)*, Montreal, Canada, June 19-23, 2005.

[9] G. Liang, H. Sun, X. Zhang, and X. Cui, "Modeling of transformer windings under very fast transient overvoltages," *IEEE Trans. on Electromagnetic Compatibility*, 48(4), November 2006.

[10] F. D. Torre, A. P. Morando, and G. Todeschini, "Three-Phase Distributed Model of High-Voltage Windings to Study Internal Steep-Fronted Surge Propagation in a Straightforward Transformer," *IEEE Trans. on Power Delivery*, Vol. 23, No. 4, pp. 2050-2057, Oct. 2008.

[11] X. M. Lopez-Fernandez and C. Alvarez-Mariño, "Computation Method for Transients in Power Transformers With Lossy Windings," *IEEE Trans. on Magnetics*, Vol. 45, No. 3, pp. 1863-1866, March 2009.

[12] Comsol Multiphysics, *AC/DC User's Guide*, Comsol AB Group, 2006, pp. 1-156.

[13] Y. Shibuya, S. Fujita, and N. Hosokawa, "Analysis of very fast transient overvoltage in transformer winding", *IEE Proc. Generation Transmission and Distribution*, Vol. 144, No. 5, September 1997.

[14] M. Popov, L. V. Sluis, and G. C. Paap, "Computation of very fast transient overvoltages in transformer windings," *IEEE Trans. Power Delivery*, vol. 18, no. 4, pp. 1268–1274, Oct. 2003.

[15] R.C. Degeneff, W.J. McNutt, W. Neugebauer, J. Panek, M.E. McCallum, C.C. Honey: "Transformer Response to System Switching Voltage", IEEE Transactions on Power Apparatus and Systems, Volume PAS-101, No.6, June 1982, pp. 1457-1470.

[16] B. Gustavsen and A. Semlyen, "Application of vector fitting to the state equation representation of transformers for simulation of electromagnetic transients," *IEEE Trans. Power Delivery*, vol. 13, pp. 834–842, July 1998.

[17] B. Gustavsen, "Wide band modeling of power transformers," *IEEE Trans. Power Delivery*, vol. 19, no. 1, pp. 414–422, January 2004.

[18] K. J. Cornick, B. Filliat, C. Kieny, and W. Muller, "Distribution of very fast transient overvoltages in transformer windings," *CIGRE Report 1992*, pp. 12–204.

[19] P. Gómez and F. A. Uribe, "The numerical Laplace transform: an accurate tool for analyzing electromagnetic transients on power system devices," *Int. Journal of Electrical Power & Energy Systems*, Vol. 31, No. 2-3, pp. 116-123, Feb.-Mar. 2009.

[20] J. Wilcox, "Numerical Laplace Transformation and Inversion," *Int. J. Elect. Enging. Educ*., Vol 15, pp. 247-265, 1978.

[21] P. Chowdhuri, *Electromagnetic Transients in Power Systems*. Research Studies Press Limited/ John Wiley & Sons, Inc, 1996, pp. 348-351.

[22] ANSI/NEMA MW1000-2003 Standard for Magnet Wire.

[23] B. Górnicka and L. Górecki, "Method of assessment of varnishes modified with nanofillers," *Materials Science-Poland*, Vol. 27, No. 4/2, 2009.

IX. Biographies

Pablo Gómez (S'01, M'07) was born in Zapopan, México, in 1978. He received the B.Sc. degree in Mechanical and Electrical Engineering from Universidad Autonoma de Coahuila, Mexico, in 1999 . He received the M.Sc. and Ph.D. degrees in Electrical Engineering from CINVESTAV, Guadalajara, Mexico in 2002 and 2005, respectively. Since 2005, he is a full-time professor with the Electrical Engineering Department of SEPI-ESIME Zacatenco, National Polytechnic Institute, Mexico City, Mexico. from 2008 to 2010, he was on a postdoctoral leave at Polytechnic Institute of New York University, Brooklyn, New York, USA. His research interests are in the modeling and simulation for electromagnetic transient analysis and electromagnetic compatibility.

Francisco de León (S'86–M'92–SM'02) received the B.Sc. and the M.Sc. (Hons.) degrees in electrical engineering from the National Polytechnic Institute, Mexico City, Mexico, in 1983 and 1986, respectively, and the Ph.D. degree from the University of Toronto, Toronto, ON, Canada, in 1992. He has held several academic positions in Mexico and has worked for the Canadian electric industry. Currently, he is an Associate Professor at the Polytechnic Institute of NYU, Brooklyn, NY. His research interests include the analysis of power definitions under nonsinusoidal conditions, the transient and steady-state analyses of power systems, the thermal rating of cables and transformers, and the calculation of electromagnetic fields applied to machine design and modeling.

Iván Hernández (S'06) was born in Salamanca, Guanajuato, Mexico in 1979. He received the B.Sc. in electrical Engineering from the University of Guanajuato (Mexico) in 2002, and the M.Sc. degree in Electrical Engineering from the CINVESTAV Guadalajara (Mexico) in 2005. He is a Ph.D. student in CINVESTAV Guadalajara. From 2008 to 2010 he was a visiting researcher at Polytechnic Institute of New York University. He was an electrical engineer designer for two years in FMS Ingenieria, Guadalajara, Mexico. His research interests are the numerical analysis applied to machine design and software simulation tools applied to electromagnetic fields.

Design Formulas for the Leakage Inductance of Toroidal Distribution Transformers

Iván Hernández, *Student Member, IEEE*, Francisco de León, *Senior Member, IEEE*, and Pablo Gómez, *Member, IEEE*

***Abstract*—In this paper design formulas for the calculation of the leakage inductance of toroidal transformers are presented. The formulas are obtained from the analytical integration of the stored energy. The formulas are sufficiently simple and accurate to be introduced in the loop of a design program avoiding expensive finite element simulations. It is found that toroidal transformers naturally produce the minimum leakage inductance possible for medium-voltage power transformers. To limit the short-circuit currents in power and distribution systems, a larger than the minimum leakage inductance is often required. This paper presents two methodologies to increase the leakage inductance of toroidal distribution transformers: selectively enlarging the inter-winding spacing and inserting a piece of ferromagnetic material in the leakage flux region between the windings. Extensive validation with 2D and 3D finite element simulations is performed. Additionally, experimental verification of both formulas and numerical simulations was carried out comparing the calculations against measurements on prototypes.**

***Index Terms* — Toroidal Transformers, Leakage Inductance, Finite Element Method.**

I. Introduction

FARADAY in 1831 built the first transformer in a toroidal core [1]; see Fig. 1. The first industrial grade transformer, the one of the Ganz factory in Budapest of 1885, was also wound on a toroidal core [2]; see Fig. 2. Currently, however, toroidal transformers are not widely used for transmission and distribution of bulk power. There are two basic arrangements used to build the iron-cores of medium and large transformers [3]-[6]: (1) Core-type where the cores are assembled by stacking laminations and sliding pre-made windings, and; (2) Shell-type where a continuously wound core is cut and wrapped around the windings a few laminations at a time. In both arrangements the finished core has air gaps that increase the magnetizing current and the no-load losses.

Toroidal transformers have found modern applications in the low-voltage low-power of many power supplies for electronic equipment, avionics, and audio systems [7], [8]. A very limited amount of published material exists in the IEEE related to toroidal transformers for power conversion applications; see [9]-[11]. There are no papers published related to mid- or high-voltage toroidal transformer intended for use at utility voltages. Transformers wound on non-gapped toroidal cores using grain oriented silicon steel are more efficient, smaller, cooler, and emit reduced acoustic and electromagnetic noise when compared with standard transformer constructions. To extrapolate these advantages to distribution transformers, an effort is being made now, as part of a US Department of Energy funded project, to produce toroidal transformers suitable for power distribution system applications. Although toroidal transformers have many advantages over the traditional constructions, there are also a few disadvantages that need to be overcome before widespread adoption of toroidal transformers is possible. Most importantly, there is no published experience in the industry designing and building toroidal transformers suitable to operate at medium and high voltage. Unresolved issues with toroidal transformer design and manufacturing include: matching the leakage impedance specification, limiting inrush currents, designing and constructing to withstand short-circuit currents, the study of electromagnetic transients (impulse test), design for cost optimization, and the ability to pass industry standard acceptance tests. This paper is part of a series

Fig. 1. Photo of Faraday's original transformer [1]

Fig. 2. Drawing of the Ganz factory transformer [2]

This work was supported by the U.S. Department of Energy under Grant DEOE0000072.

I. Hernández is with CINVESTAV Guadalajara, 45015 Jalisco, México (email: ihernand@gdl.cinvestav.mx

F. de León is with the Department of Electrical and Computer Engineering of Polytechnic Institute of New York University, Six Metrotech Center, Brooklyn, NY, 11201 (email: fdeleon@poly.edu).

P. Gómez is with the Electrical Engineering Department of SEPI-ESIME Zacatenco, Instituto Politécnico Nacional (IPN), U. P. "Adolfo López Mateos", Edificio Z-4 Primer piso C. P. 07738, Mexico, D. F. MEX (e-mail: pgomezz@ipn.mx).

describing the solutions to those issues via electromagnetic design, design verification, building prototypes, performance verification and observation of prototypes installed on a utility distribution system. In low-voltage, low-power applications the leakage inductance can be minimized using planar transformers or highly interleaved windings. For high-power, medium-voltage transformers, the leakage inductance of toroids is the minimum achievable. The reason for this is the closed concentric geometry. The first winding completely covers the core and subsequent windings cover the internal windings. There are no yokes where the flux could escape to the air. Therefore, the electromagnetic coupling is maximized, while the leakage and stray fields are minimized. The small regulation characteristic that can be obtained with toroidal transformers by minimizing the leakage impedance is desirable for many applications. However, in a power system the transformers' leakage impedance is one of the important components limiting the short-circuit currents. Consequently, a larger than natural leakage inductance may be required for a toroidal transformer.

A contribution of this paper is to propose two methods to increase the leakage inductance of toroidal transformers: (1) Enlarging the spacing between primary and secondary windings, and; (2) Inserting high permeability materials between primary and secondary windings.

Another contribution of this paper is the derivation of equations suitable for implementation in a design program for the calculation of the leakage inductance of toroidal transformers. The final expressions are numerically very efficient and sufficiently accurate for practical design work. Validation against a large number of finite element simulations in 2D and 3D covering distribution transformers of 25, 37.5, 50 and 75 kVA was performed.

II. Distribution of the Leakage Field

Coherent with the standardized method to measure the leakage inductance, for its computation one must simulate the short circuit test. In other words, force $N_1I_1 = N_2I_2$, eliminating the magnetizing current. Fig. 3(a) shows an axisymmetric view of the distribution of the magnetic field strength in a toroidal transformer during a short circuit test. Five distinct sections having different field distribution characteristics can be identified:

1. Vertical internal part of the windings
2. Vertical external part of the windings
3. Top and bottom horizontal parts
4. Internal corners
5. External corners

One can distinguish three sub-regions: two corresponding to the two windings and one for the insulation between them in each of the five regions. Fig. 3(b) shows the magnetic field strength on the vertical part of the windings along the line A-A'. One can see that the magnetic flux in the vertical direction almost follows the trapezoidal distribution characteristic of traditional transformer designs. Additionally, note that the magnetic field strength is independent of the vertical position.

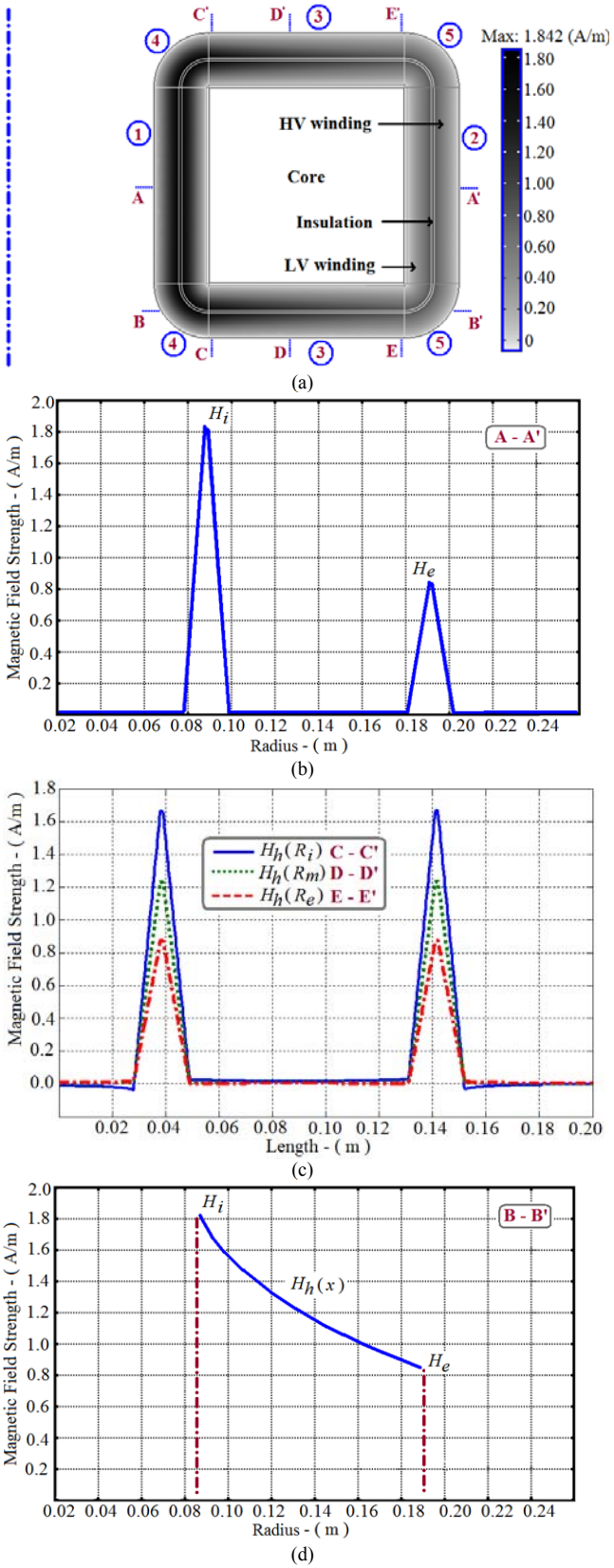

Fig. 3. Distribution of the magnetic field strength in the toroidal transformer: (a) Axisymmetric view; (b) Radial distribution of the magnetic field on the vertical sections; (c) Magnetic field strength on the horizontal sections at three positions; (d) Radial variation of the field at the insulation of the horizontal parts.

The top and bottom sections, regions 3 of Fig. 3(a), have identical magnetic field distributions as shown in Fig. 3(c). Note, however, that while the vertical variation of the field follows the trapezoidal distribution, the field strength reduces in inverse proportion with distance to the axis; see Fig. 3(d).

The leakage inductance of the toroidal transformer can be obtained through closed form volumetric integration of the distribution of the magnetic energy stored as follows:

$$L_{leak} = \frac{2W_{stored}}{I^2} = \frac{2}{I^2}\int_V \frac{H \cdot B}{2}\, dV = \frac{\mu_0}{I^2}\int_V |H|^2\, dV \qquad (1)$$

It is noticed that the different components of the leakage inductance can be obtained by analyzing the distribution of the magnetic field strength H at each section. Two main assumptions are made regarding the distribution of the magnetic field strength:

- The radial distribution (around the toroidal circumference) is considered constant (axisymmetric model).
- The distribution of H transversal to the windings is considered as follows: it rises linearly in one winding, varies inversely with x in the insulation between windings and decays linearly in the opposite winding. This type of distribution can be described by the following expression:

$$H = \begin{cases} H_{peak}\left(\dfrac{x}{a}\right), & 0 \le x \le a \\ H(x), & a \le x \le a+g \\ H_{peak}\left(1-\dfrac{x-a-g}{b}\right), & a+g \le x \le a+g+b \end{cases} \qquad (2)$$

where H_{peak} is the maximum value of the magnetic field strength; in this paper H_{peak} is identified in five ways depending on the section being considered: H_i, H_e (internal and external vertical sections of the winding, respectively); $H_{gi}(x)$, $H_{ge}(x)$ correspond to the internal and external spaces between the windings (i.e. insulation); and $H_h(x)$ (horizontal sections of the winding); while a, b and g correspond to the thickness of the high-voltage (HV) winding, low-voltage (LV) winding and inter-winding insulation, respectively (as indicated in Fig. 4).

III. Design Formulas for the Leakage Inductance

From the identification of the five different sections, the total leakage inductance of the winding can be computed as:

$$L_{leak} = L_{leak,1} + L_{leak,2} + 2L_{leak,3} + 2L_{leak,4} + 2L_{leak,5} \qquad (3)$$

where $L_{leak,i}$ correspond to the leakage inductance component of the i-th section of the winding (for i = 1, 2, 3, 4, 5). Expressions for each section are obtained below (using the Cartesian coordinate system).

A. Vertical Parts (Sections 1 and 2)

In sections 1 and 2 (internal and external vertical parts of the winding, respectively), the peak values of H (H_i, H_e, H_{gi}, H_{ge}) are shown in Fig.4. These peaks can be computed from Ampere's Law as follows:

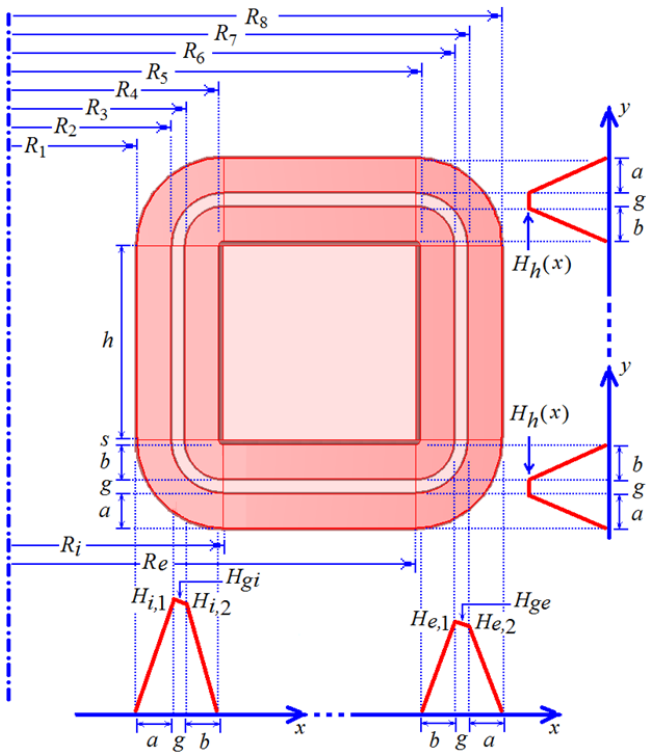

Fig. 4. Main geometrical data of a toroidal distribution transformer.

$$H_{i,1} = \frac{NI}{2\pi R_2}; \quad H_{gi}(x) = \frac{NI}{2\pi(R_2+x)}; \quad H_{i,2} = \frac{NI}{2\pi R_3}; \qquad (4a)$$

$$H_{e,1} = \frac{NI}{2\pi R_6}; \quad H_{ge}(x) = \frac{NI}{2\pi(R_6+x)}; \quad H_{e,2} = \frac{NI}{2\pi R_7}; \qquad (4b)$$

where N is the number of turns of the exciting winding, I is the current; R_2 and R_6 are the internal radii of the insulation for the vertical regions 1 and 2, respectively; and R_3 and R_7 are the internal radii of the external winding for regions 1 and 2. The reduction of the magnetic field strength between the windings, from H_{gi} to H_{ge} as $1/x$ is considered. When the insulation between windings is small, we can assume that H has a trapezoidal distribution. In [12] we have computed that 1 mm of insulation between windings is enough to produce transformers class 95 kV BIL.

Combining (1) and (4), the leakage inductance of section 1 is computed from:

$$L_{leak,1} = \frac{2\pi\mu_0 h}{I^2}\left[R_{m1}\int_0^a \left|H_{i,1}\left(\frac{x}{a}\right)\right|^2 dx + R_{m2}\int_a^{a+g}|H_{gi}|^2\, dx + R_{m3}\int_{a+g}^{a+g+b}\left|H_{i,2}\left(1-\frac{x-a-g}{b}\right)\right|^2 dx\right] \qquad (5)$$

where h is the height of the toroid, R_{m1}, R_{m2} and R_{m3} correspond to mean radii of the HV winding, insulation and LV winding, respectively, and computed in general as:

$$R_{mj} = \left(R_j + R_{j+1}\right)/2 \qquad (6)$$

Substituting (4a) into (5) and performing the integral one gets:

$$L_{leak,1}=\frac{N^2\mu_0 h}{2\pi}\left[\left(\frac{R_{m1}}{R_2^2}\right)\frac{a}{3}+\left(\frac{R_{m2}}{R_2R_3}\right)\frac{g}{2}+\left(\frac{R_{m3}}{R_3^2}\right)\frac{b}{3}\right] \quad (7)$$

The leakage inductance for section 2 is computed in a similar manner as:

$$L_{leak,2}=\frac{N^2\mu_0 h}{2\pi}\left[\left(\frac{R_{m5}}{R_6^2}\right)\frac{a}{3}+\left(\frac{R_{m6}}{R_6R_7}\right)\frac{g}{2}+\left(\frac{R_{m7}}{R_7^2}\right)\frac{b}{3}\right] \quad (8)$$

B. Horizontal Parts (Sections 3)

The top and bottom parts have the same field distribution; see Fig 3(c). The value of H at the inter-winding insulation is computed from Ampere's Law as follows:

$$H_h(x)=\frac{NI}{2\pi x} \quad (9)$$

The radial distance on x-axis can take values from $R_i \le x \le R_e$, where R_i and R_e are the internal and external radii of the toroid, respectively. Thus, the leakage inductance of the horizontal sections is obtained from:

$$L_{leak,3}=\frac{2\pi\,\mu_0\,R_{mh}}{I^2}\left\{\int_{R_i}^{R_e}\left[\int_0^b\left|H_h\left(\frac{y}{b}\right)\right|^2 dx+\int_b^{b+g}\left|H_h\right|^2 dx+\int_{b+g}^{b+g+a}\left|H_h\left(1-\frac{y-b-g}{a}\right)\right|^2 dx\right]dy\right\} \quad (10)$$

R_{mh} is the mean radius of the horizontal sections, given by:

$$R_{mh}=\left(R_i+R_e\right)/2 \quad (11)$$

Substituting (9) in (10), performing the integral, and using (11) we get:

$$L_{leak,3}=\frac{N^2\mu_0\left(R_e^2-R_i^2\right)}{2\pi\,R_eR_i}\left(\frac{b}{3}+g+\frac{a}{3}\right) \quad (12)$$

C. Corners (Sections 4 and 5)

For the corners, the same peak values for the magnetic field defined for the internal H_i and external H_e vertical parts are considered as given by (4a) and (4b). The trapezoidal distribution of H is around the corner, so it was necessary to perform the integral around its periphery denoted by φ (from 0 to $\pi/2$); the leakage inductance for the internal corners is obtained from the following expression:

$$L_{leak,4}=\frac{2\pi\,\mu_0}{I^2}\left\{\int_0^{\pi/2}\left[R_{m1}\int_0^a\left|H_{i,1}\left(\frac{x}{a}\right)\right|^2 xdx+R_{m2}\int_a^{a+g}\left|H_{gi}\right|^2 xdx+R_{m3}\int_{a+g}^{a+g+b}\left|H_{i,2}\left(1-\frac{x-a-g}{b}\right)\right|^2 xdx\right]d\varphi\right\} \quad (13)$$

Solving (13), it follows that:

$$L_{leak,4}=\frac{N^2\mu_0}{4\pi R_2^2}\left(\frac{R_{m1}t_1a}{6}+R_{m2}\,t_2g+\frac{R_{m3}t_3b}{6}\right) \quad (14)$$

where:

$$t_1=3a+4\left(s+b+g\right) \quad (15a)$$

$$t_2=g+2\left(s+b\right) \quad (15b)$$

$$t_3=3b+4s \quad (15c)$$

Similarly, the leakage inductance for the external corners is computed as:

$$L_{leak,5}=\frac{N^2\mu_0}{4\pi R_6^2}\left(\frac{R_{m5}t_3b}{6}+R_{m6}\,t_2g+\frac{R_{m7}t_1a}{6}\right) \quad (16)$$

D. Generalized Expression

One can appreciate that (7), (8), (12), (14) and (16) have a similar form. Therefore, a generalized expression for the calculation of the contribution to the leakage inductance of each section can be obtained as follows:

$$L_{leak,i}=\frac{N^2\mu_0}{2\pi}\eta_i\left(\alpha_i\,a+\phi_i\,g+\beta_i\,b\right) \quad (17)$$

The coefficients for the different sections are given in Table I. The total leakage inductance is computed from (3).

TABLE I
COEFFICIENTS FOR THE DIFFERENT COMPONENTS OF THE LEAKAGE INDUCTANCE FORMULA (17)

	Coefficient			
Section	η_i	α_i	ϕ_i	β_i
1	h	$\frac{R_{m1}}{3R_2^2}$	$\frac{R_{m2}}{2R_2R_3}$	$\frac{R_{m3}}{3R_3^2}$
2	h	$\frac{R_{m7}}{3R_7^2}$	$\frac{R_{m6}}{2R_6R_7}$	$\frac{R_{m5}}{3R_6^2}$
3	$\frac{R_e^2-R_i^2}{R_eR_i}$	$\frac{1}{3}$	1	$\frac{1}{3}$
4	$\frac{1}{2R_2^2}$	$\frac{R_{m1}t_1}{6}$	$R_{m2}\,t_2$	$\frac{R_{m3}t_3}{6}$
5	$\frac{1}{2R_6^2}$	$\frac{R_{m7}t_1}{6}$	$R_{m6}\,t_2$	$\frac{R_{m5}t_3}{6}$

IV. TEST CASES

Table II shows the design parameters of a set of toroidal distribution transformers used to demonstrate the applicability of the methods and the accuracy of the formulas. We have selected the standardized sizes for distribution transformers as per [13]. The leakage inductance reference values have been computed with 3-D finite element simulations using the commercially available software (COMSOL Multiphysics) [14].

The FEM simulations performed solve for the magneto-static formulation. All materials are considered as being isotropic; we used copper windings and electrical steel M4 (0.28 mm) for the main core considering its B-H curve as provided by the manufacturer.

In the simulations the toroid was enclosed by a tank represented by a rectangle in the axisymmetric 2-D case and by a cylinder in the 3-D case. Magnetic insulation was applied to the boundaries of the tank walls. For the 2-D simulations about 40,000 triangular elements were necessary consuming about 2 GB on RAM. For the 3-D simulations about 400,000 tetrahedrons were employed consuming 9 GB on RAM. The

axisymmetric 2-D and 3-D simulation results were almost identical. Therefore, we conclude, as expected from a symmetrical construction, that to compute the leakage inductance 2-D axisymmetric modeling is sufficient.

Table III shows the values of leakage inductances and reactances in percent that can be achieved with toroidal transformers. The inductive values are referred to the HV winding. From Table III one can appreciate that the results are in good agreement, with maximum differences of 3%.

Table IV shows the leakage impedance values recommended by the IEEE Standard 242-1986 [13] for the calculation of short-circuit currents. It can be noticed that the reactance in percent of toroidal transformers may be substantially smaller than that of conventional transformers. Therefore, larger short-circuit currents can be expected. Although small regulation is in general a desirable characteristic for a transformer, for some applications the larger short-circuit currents that occur may not be acceptable. In the next section two methods to increase the leakage inductance are proposed.

TABLE II
DESIGN PARAMETERS FOR SINGLE PHASE TOROIDAL TRANSFORMERS

	25 kVA	37.5 kVA	50 kVA	75 kVA
HV-(kV)	13.80	13.80	13.80	13.80
LV-(kV)	0.12	0.12	0.12	0.12
B_m (T)	1.70	1.70	1.70	1.70
f (Hz)	60.00	60.00	60.00	60.00
Np	4715	4370	4370	3335
R_i (mm)	100.00	101.50	110.50	121.50
R_e (mm)	180.00	185.50	194.50	217.50
h (mm)	80.00	84.00	84.00	96.00
a (mm)	10.24	12.64	17.39	17.90
b (mm)	10.41	10.41	11.68	20.81
g (mm)	1.00	1.00	1.00	1.00
s (mm)	0.50	0.50	0.50	0.50

B_m is the magnetic flux density average in the core, *f* is the operation frequency, *Np* is the number of turns of the HV side.

TABLE III
PARAMETERS COMPUTED FOR SINGLE-PHASE TOROIDAL TRANSFORMERS

	Leakage Inductance (H)		Leakage Reactance (%)		%
	FEM	Formula	FEM	Formula	Diff
25 kVA	0.1050	0.1079	0.5198	0.5339	2.76
37.5 kVA	0.1011	0.1041	0.7508	0.7724	2.99
50 kVA	0.1200	0.1236	1.1879	1.2234	3.01
75 kVA	0.1086	0.1114	1.6121	1.6544	2.86

The computed values were referred to the HV winding.

TABLE IV
IMPEDANCE DATA FOR SINGLE PHASE TRANSFORMERS FROM [13]

kVA 1-phase	Suggested X/R Ratio for Calculation	Normal Range of Percent Impedance (% Z)
25.0	1.1	1.2-6.0
37.5	1.4	1.2-6.5
50.0	1.6	1.2-6.4
75.0	1.8	1.2-6.6

V. METHODOLOGIES FOR INCREASING THE LEAKAGE INDUCTANCE OF TOROIDAL TRANSFORMERS

A. Increasing Inter-Winding Spacing

One can perceive from Tables III and IV that the leakage inductance of a 25 kVA toroidal transformer may be as small as half of what is specified in the standard [12].

From the expressions obtained in Section III, and their analogy with the technology of traditional transformer constructions, it can be inferred that increasing the spacing between windings will increase the leakage inductance. This is a technique known to designers and manufacturers of traditional transformer constructions. It is possible to identify in (7), (8), (12), (14) and (16) the middle term as the inductance corresponding to leakage flux in the insulation (or air). To build toroidal transformers the internal space at the center of the toroid must be large enough for the winding machine to pass. Therefore, only the top, bottom and external regions can be used in practice to increase the leakage path. Furthermore, when considering manufacturing aspects the most suitable region to increase the inter-winding space is the external part (region 2 of Fig, 3(a)). Therefore, in this paper, only the external inter-winding space of the toroidal transformer is used to increase the leakage inductance; see Fig. 5. Taking this into consideration, the leakage inductance for the vertical external component of the winding (region 2), given by (8), is modified as follows:

$$L'_{leak,2}=\frac{N^2\mu_0 h}{2\pi}\left[\begin{array}{l}\left(\frac{R_{m5}}{R_6^2}\right)\frac{b}{3}+\\ \left(\frac{1}{2R_6(R_7+\Delta g)}\right)\left(R_{m6}+\frac{\Delta g}{2}\right)(g+\Delta g)+\\ \left(\frac{R_{m7}+\Delta g}{R_7^2}\right)\frac{a}{3}\end{array}\right] \quad (18)$$

where Δg is the increased space in the inter-winding region. The leakage inductance corresponding to the horizontal components of the winding (regions 3 and 4), given by (12), is also modified, resulting in the following expression:

$$L'_{leak,3}=\frac{N^2\mu_0\left[(R_e+\Delta g)^2-R_i^2\right]}{2\pi(R_e+\Delta g)R_i}\left(\frac{b}{3}+g+\frac{a}{3}\right) \quad (19)$$

Fig. 6(a) shows the variation of the leakage inductance with the inter-winding space for the four transformer ratings under study. One can appreciate that increasing the inter-winding spacing increases the leakage inductance by a relative modest amount. The values have been normalized with respect to the minimum inter-winding space needed for insulation purposes (1 mm).

The results from the formulas of this paper against FEM are compared in Fig. 6(b) for the transformer 25 kVA. One can appreciate a very good match between the formulas and FEM (differences of about 4%).

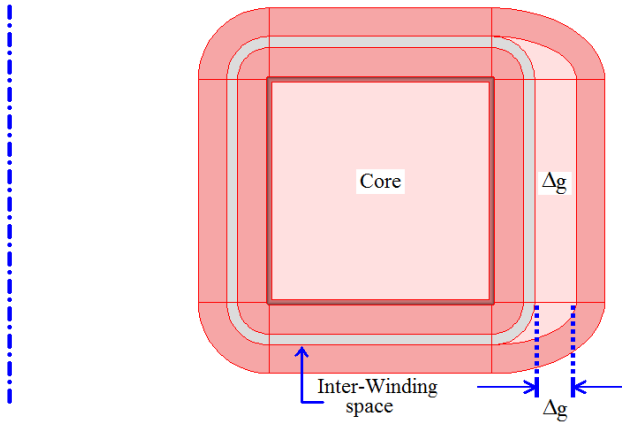

Fig. 5. Enlarging the external vertical inter-winding space to augment the leakage inductance.

As a conclusion of this section one can observe that the technique of increasing inter-winding spacing is effective when relatively small increments of the leakage inductance are needed. However, when large increments are sought, a different technique is necessary. Furthermore, adding larger spaces than required for insulation purposes adds cost and weight to the transformer. The most significant negative consequence is that the external winding has a longer mean length (adding production cost and operation losses).

B. Ferromagnetic Inserts

The second technique proposed in this paper to increase the leakage inductance is to augment the permeability of the material in the leakage region. By inserting a ferromagnetic material between the windings we can dramatically magnify the leakage inductance without a noticeable increase in the transformer size.

The underlying idea is to install a thin core in the inter-winding region on the external face; see Fig. 7. This produces an enlargement of the leakage inductance component corresponding to such region. Equation (8) is modified as:

$$L'_{leak,2}=\frac{N^2\mu_0 h}{2\pi}\left[\begin{array}{l}\left(\frac{R_{m5}}{R_6^2}\right)\frac{R_{m5}\,b}{3}+\\ \left(\frac{1}{2R_6(R_7+g_c)}\right)\left(R_{m6}+\frac{g_c}{2}\right)\left(g+\mu_r g_c\right)+\\ \left(\frac{R_{m7}+g_c}{R_7^2}\right)\frac{a}{3}\end{array}\right] \qquad (20)$$

where g_c is the thickness of the region occupied by the ferromagnetic material and μ_r is its relative permeability. The leakage inductance for the horizontal components of the winding is modified in a similar fashion as (12), yielding:

$$L_{leak,3}=\frac{N^2\mu_0\left[\left(R_e+g_c\right)^2-R_i^2\right]}{2\pi\left(R_e+g_c\right)R_i}\left(\frac{b}{3}+g+\frac{a}{3}\right) \qquad (21)$$

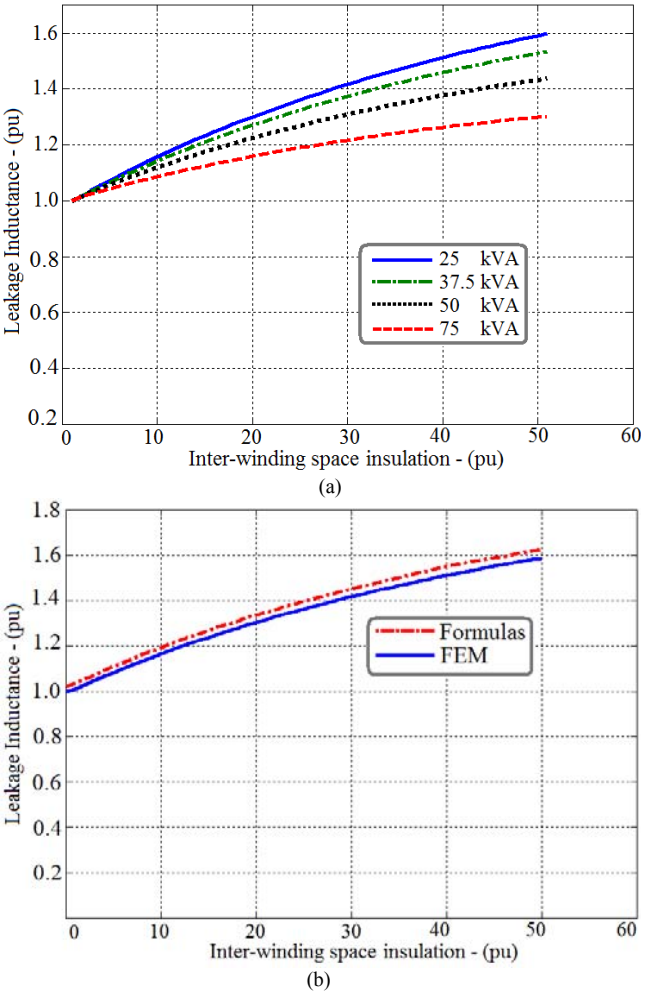

Fig. 6. Variation of the leakage inductance: (a) Calculated for 4 different ratings of toroidal distribution transformers, (b) Comparison of the analytical results with FEM for a 25 kVA toroidal transformer.

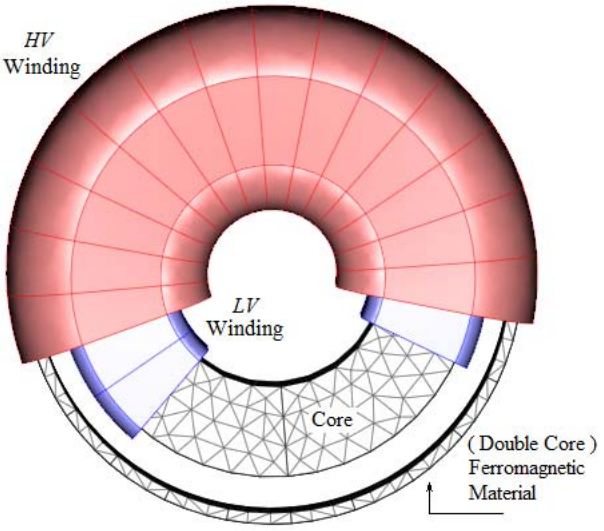

Fig. 7. Illustration of adding ferromagnetic inserts between windings to increase the leakage inductance.

By adding a material with high relative permeability (μ_r) the value of the leakage inductance can be magnified by a large factor. When using this technique care must be taken to avoid saturation of the thin core placed between the windings.

Different ferromagnetic materials [15] were considered for the simulations performed to validate this technique. Fig. 8(a) shows the variation of leakage inductance with thickness for materials with different permeability. The plot is given in per unit (p.u.) normalized to the minimum insulation space and permeability of air μ_0. A comparison between the results of the formulation and FEM is shown in Fig. 8(b). One can notice that the differences are very small.

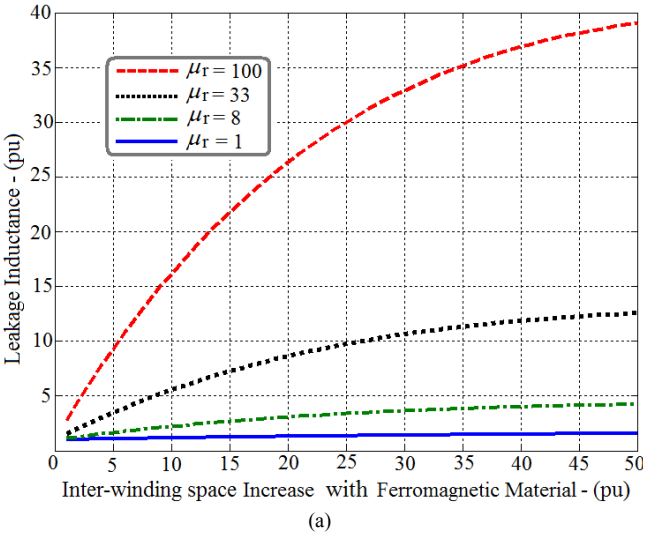

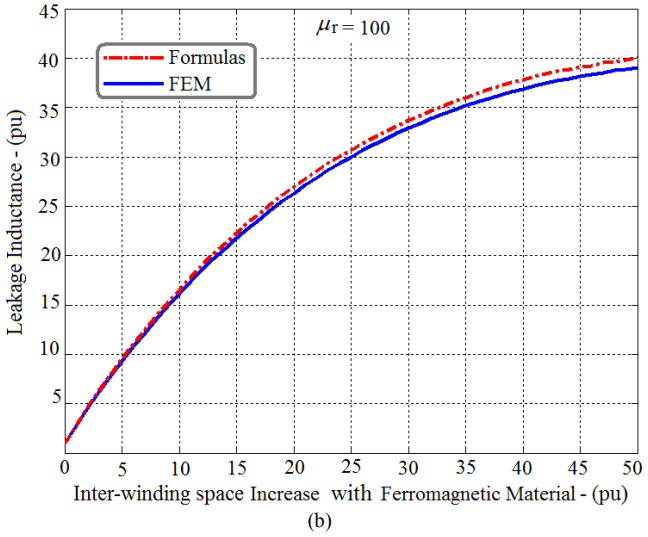

Fig. 8. Increase of the leakage inductance. (a) Inserting 4 different ferromagnetic materials between the windings; (b) Comparison of results between formulas and FEM for the 25 kVA transformer.

VI. Experimental Verification

With the purpose of validating the formulas proposed in this paper and the FEM simulations, a set of prototypes were built with ratings of 150 VA, 300 VA, 1 kVA, 2 kVA, and 4 kVA. The leakage inductance was measured applying two methods: using the standardized short circuit (SC) test and using an RLC meter (7600 Precision LCR meter) available in the lab. This meter uses an *ac* signal of 2 V at 60 Hz and it gives the equivalent series R-L circuit of the transformer directly. In all cases the secondary windings of the transformers are shorted and the primary windings are connected to the source.

Table V shows the comparison of the measurements on the five prototypes against finite elements simulations and the formulas of this paper. One can appreciate that, for most cases, the results are very close between the four different methods (SC, RLC meter, FEM, and formulas). The differences are in general under than 3%. The sole exception is the SC measurement of the 300 VA double-core transformer with 8.47% difference. This transformer was opened and unwound. We found that the external (powder) core was fractured. Therefore, the effective permeability of this core was reduced by the irregular (unintended) air-gap explaining why the measurements gave a slightly smaller leakage inductance when compared with FEM and the formulas.

These experiments not only corroborate the accuracy of the calculation method proposed in the paper, but also confirm the applicability of ferromagnetic inserts to increase the leakage inductance when large leakage is necessary.

TABLE V
LEAKAGE INDUCTANCE MEASURED AND COMPUTED FOR SINGLE-PHASE TOROIDAL TRANSFORMERS

Transformer	Leakage Inductance Measured (mH)		Leakage Inductance Computed (mH)		% Diff SC versus Formula
	SC	RLC	FEM	Formula	
150 VA	0.7200	0.7350	0.6890	0.7095	1.46
1 kVA	0.2150	0.2300	0.2100	0.2092	2.68
2 kVA	0.0493	0.0491	0.0490	0.0503	2.03
4 kVA	0.0209	0.0220	0.0205	0.0205	1.53
*300 VA	13.644	**	15.100	14.800	8.47

* Transformer with double core (as in Fig. 7)
** Not possible to measure with the RLC meter

VII. Conclusions

Formulas suitable for a design program for the calculation of the leakage inductance of toroidal transformers have been developed. From the observation of the distribution of the magnetic flux in the leakage region, precise expressions have been derived for the magnetic field strength. The leakage inductance is obtained by the analytical integration of the total energy stored in the magnetic field. The formulas have been compared against 2D and 3D finite element simulations yielding very good results; differences of under 4%.

Two methodologies to augment the leakage inductance of toroidal transformers have been proposed. We have

investigated increasing the inter-winding spacing and the addition of a ferromagnetic core in the leakage region. Increasing the inter-winding spacing is effective for up to 1.5 p.u. increment of the leakage inductance at the cost of increasing the mean length of the external winding. The addition of a ferromagnetic core between the windings offers an inexpensive alternative to augment the leakage inductance. This technique can be used conveniently to increase the leakage inductance several orders of magnitude.

The accuracy of the formulas and the applicability of the methods to increase the leakage inductance have been corroborated experimentally for a set of prototypes of various sizes.

VIII. Acknowledgements

The authors would like to thank Mr. Ulrik Poulsen of Bridgeport Magnetics for his fast response and expertise building the prototypes. Also, we would like to thank Messrs. Chandira Prabhu and Noel Augustine, M.Sc. students of Polytechnic Institute of New York University, for performing the leakage inductance tests to the prototypes. Additionally, we would like to thank the reviewers for their sharp comments that have added value to the paper.

IX. References

[1] F. A. Furfari and J. W. Coltman, "The Transformer", IEEE Industry Applications Magazine, Jan./Feb. 2002, pp. 11-12.

[2] S. Jeszensky, "History of Transformers", IEEE Power Engineering Review, December 1996, pp. 9-12.

[3] J. H. Harlow, "Electric Power Transformer Engineering", 2nd Ed., New York, CRC Press, 2007.

[4] S. V. Kulkarni, S. A. Khaparde, "Transformer Engineering Design and Practice", New York, Marcel Dekker, Inc., 2004.

[5] R. M. Del Vecchio, B. Poulin, P. T. Feghali, D. M. Shah, R. Ahuja, "Transformer Design Principles - With Application to Core-Form Power Transformers", Canada, Gordon and Breach Science Publishers, 2001.

[6] M. Heathcote, "J & P Transformer Book", 12th Edn, Great Britain, Butterworth-Heinemann Ltd., 1998.

[7] M. van der Veen, "Modern High-end Valve Amplifiers: Based on Toroidal Output Transformers", Elektor Electronics Publishing, 1999.

[8] A. A. Halacsy, "Reactance and Eddy Current Loss in Toroidal Transformatoric Devices-II", *AIEE Transactions on Power App. and Sys.,* vol. 81, No. 3, April 1962, pp. 1017 – 1019.

[9] R. Prieto, J. A. Cobos, V. Bataller, O. Garcia, and J. Uceda, "Study of toroidal transformers by means of 2D approaches", IEEE 28th Annual Power Electronics Specialists Conference, St. Louis, MO, Jun. 22-27, 1997.

[10] R. Prieto, V. Bataller, J. A. Cobos, and J. Uceda, "Influence of the winding strategy in toroidal transformers", Proceedings of the 24th Annual Conference of the IEEE Industrial Electronics Society, 1998, IECON '98, 31 Aug-4 Sep 1998, Vol. 1, pp. 359 – 364.

[11] J. P. Myers, K. A. Weaver, W. R. Wieserman, and U. Poulsen, "O cores - a new approach", Proceedings of the Electrical Insulation Conference and Electrical Manufacturing & Coil Winding Technology Conference, 2003, 23-25 Sept. 2003, pp. 193 – 198.

[12] P. Gómez, F. de León, and I. Hernández, "Impulse Response Analysis of Toroidal Core Distribution Transformers for Dielectric Design", paper accepted for publication in the IEEE Transactions on Power Delivery.

[13] *IEEE Recommended Practice for Protection and Coordination of Industrial and Commercial Power Systems*, IEEE Standard 242-1986, Feb. 1986.

[14] Comsol Multiphysics, *AC/DC User's Guide*, Comsol AB Group, 2006, pp. 1-156.

[15] A. Goldman, *Handbook of Modern Ferromagnetic Materials*, vol. I. Kluwer Academic Publishers Group, 1999, pp. 64-135.

X. Biographies

Iván Hernández (S'06) was born in Salamanca, Guanajuato, Mexico in 1979. He received the B.Sc. in electrical Engineering from the University of Guanajuato (Mexico) in 2002, and the M.Sc. degree in Electrical Engineering from the CINVESTAV Guadalajara (Mexico) in 2005. He is a Ph.D. student in CINVESTAV Guadalajara. From November 2008 to August 2010 he was on a study leave at the Polytechnic Institute of New York University. Previously, he was an electrical engineer designer for two years in FMS Ingeniería, Guadalajara, Mexico. His research interests are the numerical analysis applied to machine design and software simulation tools particularly for electromagnetic fields.

Francisco de León (S'86–M'92–SM'02) was born in Mexico City in 1959. He received the B.Sc. and the M.Sc. degrees in Electrical Engineering from the National Polytechnic Institute (Mexico), in 1983 and 1986 respectively, and obtained his Ph.D. degree from the University of Toronto (Canada) in 1992. He has held several academic positions in Mexico and has worked for the Canadian electric industry. Currently he is an Associate Professor at the Polytechnic Institute of New York University, Brooklyn, NY. His research interests include the analysis of power phenomena under nonsinusoidal conditions, the transient and steady-state analyses of power systems, the thermal rating of cables, and the calculation of electromagnetic fields applied to machine design and modeling.

Pablo Gómez (S'01, M'07) was born in Zapopan, México, in 1978. He received the B.Sc. degree in Mechanical and Electrical Engineering from Universidad Autonoma de Coahuila, Mexico, in 1999. He received the M.Sc. and Ph.D. degrees in Electrical Engineering from CINVESTAV, Guadalajara, Mexico in 2002 and 2005, respectively. Since 2005, he is a full-time professor with the Electrical Engineering Department of SEPI-ESIME Zacatenco, National Polytechnic Institute, Mexico City, Mexico. From 2008 to 2010, he was on a postdoctoral leave at the Polytechnic Institute of New York University, Brooklyn, New York, USA. His research interests are in the modeling and simulation for electromagnetic transient analysis and electromagnetic compatibility.

Heat Transfer Model for Toroidal Transformers

Sujit Purushothaman, *Student Member, IEEE*, and Francisco De León, *Senior Member, IEEE*

***Abstract*—Toroidal transformers provide increased design flexibility, efficiency and compact design when compared to traditional shell or core type transformers. In this paper the steady state thermal analysis for toroidal transformers is conducted using a lumped parameter model which can be applied to small power and distribution grade toroidal transformers as well. Two cases are considered: (1) when the transformer is kept in open air and (2) when it is installed in sealed enclosures. The detailed model includes the effects of number of turns of windings, number of layers, insulation properties and geometric properties of the transformer. The model is capable of finding the hot-spots that are of paramount importance for the designer. The model parameters are calculated from the design (geometrical) information, therefore it is suitable to be included in the design loop of transformer design software. Results are compared with finite element simulations and lab tests on prototypes of various power ratings fitted with thermocouples to record internal temperatures. The model can also be used with varied external media and encapsulation, such as: air, oil, and epoxy.**

***Index Terms*—Toroidal Transformers, Thermal rating, Heat Transfer, Equivalent thermal circuit, Finite element method.**

I. Nomenclature

HV: High voltage
LV: Low voltage
HST: Hottest Spot Temperature
Q_{loss}: Total Ohmic loss in transformer [W]
h: Heat transfer coefficient [W/m^2.K]
k: Thermal conductivity [W/m.K]
Nu: Nusslet number
Gr: Grashoff's number
Pr: Prandtl number
Ra: Rayleigh number

II. Introduction

THE first transformer was built by Faraday in 1831 on a toroidal core [1]. Nowadays, toroidal transformers are mostly being used in power supplies for avionics, audio systems and electronic equipment rated for low voltages and relatively low power [2]-[3]. Transformers used in bulk power transmission are of core type or shell type construction. Over the years considerable research has been done on thermal modeling of oil immersed transformers. Equivalent electrical circuits with non-linear resistors have been used to model the air or oil convection currents [4] in transformers. Many models have also been proposed to determine the top oil temperature (TOT) and the hottest spot temperature (HST) [5], [6]. However, the application of toroidal transformers in power transmission and distribution at medium voltage is stunted. This so not only because its construction could be more expensive than traditional designs, but perhaps due to the lack of previously published research work.

The toroidal construction has many advantages over standard power transformers, for example: The lack of an air-gap in the toroidal core allows for a higher design flux density. The closed geometry (where the second winding completely covers the first) produces a transformer with a smaller leakage inductance than that of traditional designs producing transformers with small regulation. Additionally, the acoustic noise and electromagnetic emissions are smaller. In an effort to forward the advantages of toroidal transformers to distribution systems, the US Department of Energy has funded a project to design and develop toroidal transformers for medium voltage distribution systems. This paper is part of a series of papers describing solutions to problems related to the design and construction of these utility grade transformers. Equations to accurately compute the leakage impedance have been obtained and verified experimentally in [7]. The insulation design based on the propagation of the impulse wave in windings on toroidal core has been presented in [8].

The power rating of a transformer is limited by the temperature of the hot-spots. This paper describes a procedure to setup a thermal model of toroidal transformers. The model can predict accurately the temperature of each winding layer along four directions. This model can be used to study temperature distribution for transformers used in medium voltage distribution systems.

Results from the model are compared with finite element simulations yielding a good match. The proposed model was also validated with a set of prototypes (of various power ratings) especially built with thermocouples placed at strategic locations within the transformer. The model has proven to be sufficiently accurate and efficient for practical implementation in a design program.

III. Geometric Arrangement

Traditional core type or shell type transformers consist of uniform windings around the core. This makes it easy to perform thermal studies using lumped parameter circuits [4-6]. Fig. 1 shows the uneven winding distribution due to the geometry of the toroidal core. The core has unequal surface area on the inside and the outside surface because of the smaller radius (Perimeter = $2\pi r$). Hence the conductor spacing is more on the outside than on the inside. Since the cross sectional area of

This work was supported in part by the U.S. Department of Energy under Grant DEOE0000072.

S. Purushothaman and F. de León and are with Polytechnic Institute of NYU, Brooklyn, NY 11201 (e-mail: sujitp@ieee.org, fdeleon@poly.edu).

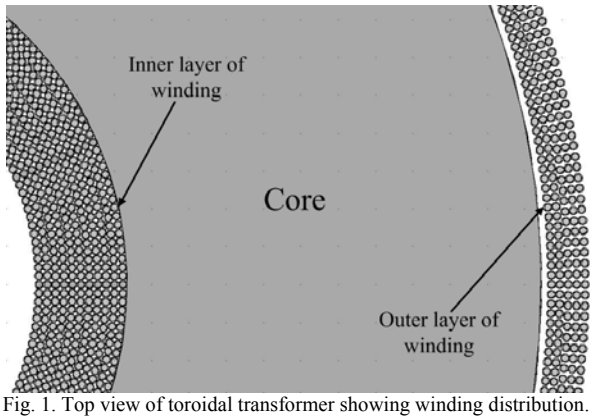

Fig. 1. Top view of toroidal transformer showing winding distribution.

the conductor remains the same everywhere, the conductors' bundle is thicker on the inside and thinner on the outside. This is also applicable to any insulation wrapped between layers. Since a large temperature gradient exists within an insulator, this non-uniform distribution of insulation thickness on the inside and outside is of critical importance to this study.

The unequal surface areas and the non-uniform distribution of windings on toroidal core leads to a complex analysis explained below in Section V.

The transformer under study consists of a toriodal core, covered by a layer of insulation. The LV windings with *n* layers are wound first on the insulated core followed by the *m* layers of the HV windings. The insulation class requirements may cause insulation layers to be added between layers of the HV windings. This reduces thermal performance and hence an accurate thermal modeling is a crucial step in the design a distribution grade toroidal transformer.

IV. Equivalent Thermal Circuit

The thermal-electric analogy for the analysis of heat transfer phenomena is well known and a good explanation can be found in [12], and [14]. The core and both the windings are metallic materials (steel and copper) and hence offer high thermal conductivity, *k*. The windings carry current and produce heat due to Ohmic losses. The eddy current losses and hysteresis losses constitute the core losses. Therefore, in the electrical equivalent circuit the windings and the core are modeled as current sources. The insulation is essentially made of several layers of thin Mylar wound tape, having low electrical and thermal conductivity and so the insulation layers are modeled as thermal resistors in the circuit.

Fig. 2 shows the thermal equivalent circuit super-imposed on the axial slice geometry of a typical toroidal transformer. The uneven distribution of windings causes uneven temperature field around the core. Therefore an equivalent thermal circuit is proposed for each of the four directions; namely, top, outer, bottom and inner directions. The detailed equivalent thermal circuit in the outer direction for the toroidal transformer is as shown in Fig. 3. The circuits for the other three directions are similar with different parameter values. All circuits are connected at the core (center) producing a cross-shaped equivalent circuit.

The heat flow in the inner and outer regions is a cylindrical

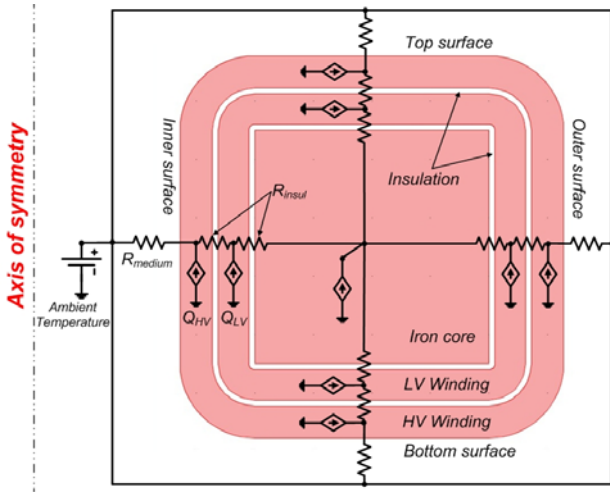

Fig. 2. 2D axial symmetric geometry of toroidal transformer

thermal problem whereas that in the top and bottom regions is Cartesian.

The resistance of the top and bottom insulation layers can be computed as [12]

$$R_{insul} = \frac{t}{k\,A} \tag{1}$$

where *t* is the thickness and *A* is the surface area of the insulation layer. The resistance of the inner and outer insulation (cylindrical) layers can be computed as

$$R_{insul} = \frac{1}{2\,\pi\,k\,H_{insul}} \ln\left(\frac{OD}{ID}\right) \tag{2}$$

where *OD* and *ID* are the outer and inner diameters of the insulation layer respectively. H_{insul} is the height of the layer.

The heat loss in the n^{th} layer, Ql_n is equal to total heat loss in the winding, *Q* times the ratio of the number of turns in the present layer Nl_n to the total number of turns in the winding, *N*.

$$Ql_n = Q\frac{Nl_n}{N} \tag{3}$$

Assuming the heat dissipated in the conductor per unit length to be constant, Ql_n times the ratio of fraction of the length of a turn l_x in the respective direction *x* to the length a turn in the n^{th} layer L_n gives the current sources in each directional circuit.

$$(Ql_n)_x = Ql_n\frac{l_x}{L_n} \tag{4}$$

The temperature of the surrounding medium is modeled as an ideal voltage source since it is assumed that the ambient temperature would not be affected by the presence of the transformer under consideration. The thermal resistance of the surrounding medium is highly dependent on the physical state of the medium (solid (epoxy), liquid (oil) or gas (air)). This resistance can be nonlinear and its computation is complex as described in the next section.

Since the model deals with steady state calculations only, no capacitances are needed in the thermal equivalent circuit. The algorithm for computing the results is given in Appendix II.

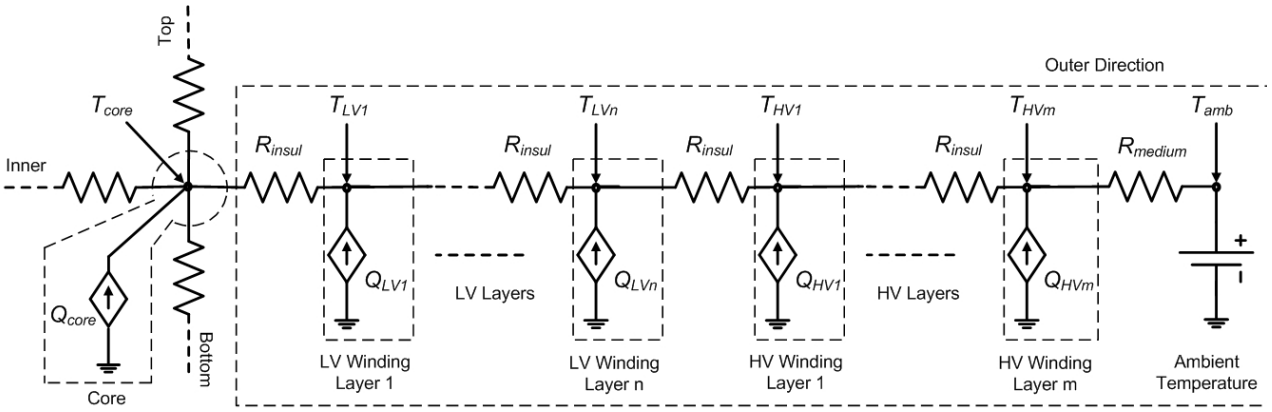

Fig. 3. 2D The detailed thermal circuit in the outer direction for toroidal transformer.

V. Thermal Resistance of Surrounding Medium

Fluid medium (air, oil) dissipate heat by convection and radiation. Convection is the phenomenon of heat transfer by conduction in moving media. Radiation is medium independent and accounts for 20-30% of the total heat flux, hence should not be neglected.

This section explains the computation of heat transfer coefficient h_{conv} for natural convection in the laminar regime. h_{conv} is a function of the geometric arrangement, temperature and properties of convective medium of the surface under consideration. h_{conv} is given by [12], [13]

$$h_{conv} = \frac{Nu\ k}{L} \tag{5}$$

where k is the thermal conductivity of the surrounding medium; L is the characteristic length and Nu is the Nusselt number. In general the relationship between Nu and the Rayleigh number Ra_L is given by (6) and depends on the orientation of the surface under consideration [11]

$$Nu = C\ Ra_L^{\ m} \tag{6}$$

For the top surface [11]

$$\begin{aligned} Ra_L &= 10^4 - 10^7 \quad C = 0.54,\ m = 0.25 \\ Ra_L &= 10^7 - 10^9 \quad C = 0.15,\ m = 0.334 \end{aligned} \tag{7}$$

and L is the ratio of surface area to perimeter. For bottom surface, $C = 0.27$, $m = 0.25$ and L is the length. For vertical faces, L is the length and

$$Nu = 0.671 \times \left(\frac{\Pr \times Ra_L}{\Pr + 0.492 + (0.986 \times \sqrt{\Pr})} \right)^{0.25} \tag{8}$$

The expression for Ra_L is given as follows [12], [13]

$$Ra_L = Gr_L \times \Pr \tag{9}$$

where Gr_L is the Grashoff's number and Pr is the Prandtl number, given by:

$$Gr_L = \frac{g\beta(T_s - T_\infty)L^3}{\nu^2} \tag{10}$$

$$\Pr = \frac{C_p \mu}{k} \tag{11}$$

g = acceleration due to gravity

β = volumetric thermal expansion coefficient

ν = kinematic viscosity

C_p = specific heat capacity at constant pressure

μ = dynamic viscosity.

The convective thermal resistance R_{conv} is given by

$$R_{conv} = \frac{1}{h_{conv}\ A} \tag{12}$$

The radiative heat transfer coefficient h_{rad} is calculated as [12], [13]

$$h_{rad} = \varepsilon\sigma(T_s + T_\infty)(T_s^2 + T_\infty^2) \tag{13}$$

where ε is the emissivity of the surface with area A, dissipating radiative heat flux. T_s and T_∞ are the surface temperature and temperature of the ambient surroundings respectively and σ is the Stefan-Boltzmann constant.

The radiative thermal resistance R_{rad} is given by

$$R_{rad} = \frac{1}{h_{rad}\ A} \tag{14}$$

Since convection and radiation occur simultaneously at the surface, the total thermal resistance of the medium is the parallel combination of R_{conv} and R_{rad}.

In the case of encapsulation of the transformer, the material (epoxy resin) may be treated as a solid insulation medium. Hence R_{conv} would be substituted by (1) and (2) since now the heat transfer is done by conduction.

VI. Finite Element Model

A 2-D axisymmetric model of the prototype was built in COMSOL Multiphysics [10] simulating open air conditions. The model shown in Fig. 4 simulates a toroidal transformer suspended in air to ensure all surfaces contribute to heat dissipation.

The following set of nonlinear equations are solved simultaneously with the finite elements method (FEM): The Navier-Stokes equation [12]

$$\rho\frac{\partial u}{\partial t} + \rho(u \cdot \nabla)u = -\nabla p + \mu\nabla^2 u + \rho g \tag{15}$$

the continuity equation

$$\frac{\partial \rho}{\partial t} + \nabla \cdot (\rho u) = 0 \tag{16}$$

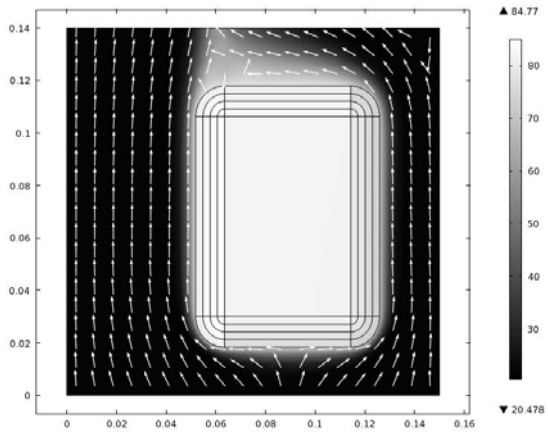

Fig. 4. FEM model of toroidal transformer under test.

and the energy equation

$$\rho C_p \frac{\partial T}{\partial t} + \rho C_p u \cdot \nabla T = \nabla \cdot (k \nabla T) + Q \qquad (17)$$

T is temperature at a point, u is the velocity field, ρ is the density, p is the pressure, and Q is the heat generated.

Fig. 4 shows the FEM surface plot for temperature, T along with an arrow plot showing fluid velocity u. The lower boundary of the model is fixed at 1 atm pressure (p) and temperature (T) at 22^0C. The pressure at the top boundary also fixed at 1 atm pressure. It is also defined as a heat sink. The vertical surface is defined as heat insulation (zero temperature gradient). The vertical surface and transformer surfaces are defined as no-slip (u = 0). Internal boundaries representing inter-layer insulation are defined as thermal resistive boundaries with thickness calculated as described in Section III.

It must be noted that the solution of this highly non-linear problem of natural convection is time consuming even in the most powerful PC computers (dual Intel Xeon processors running at 3.33 GHz with 96 gigabyte RAM) available today (2011). The FEM model has 4099 2nd degree elements and can take a couple of hours for a solution. Such a solution cannot be included in a design program which may take several iterations to obtain the final design. Hence the need for a simple and accurate model is required which can yield the temperature distribution within the transformer without being computationally intensive.

VII. Laboratory Tests

Lab tests were conducted on toroidal core prototypes of various power ratings to verify the proposed model. Fig. 5 presents the test schematic. The prototype (detailed in Appendix I) was suspended in air to simulate the conditions as given in section VI. A Yokogawa PZ-4000 Power Analyzer was used to measure input and output power of the prototype. A National Instruments, NI-USB 9213 Thermocouple measurement unit was used to record temperatures on a computer. The prototype has six thermocouples placed at locations internal to the transformer as per Fig. 6. Cross-sections AA' and BB'

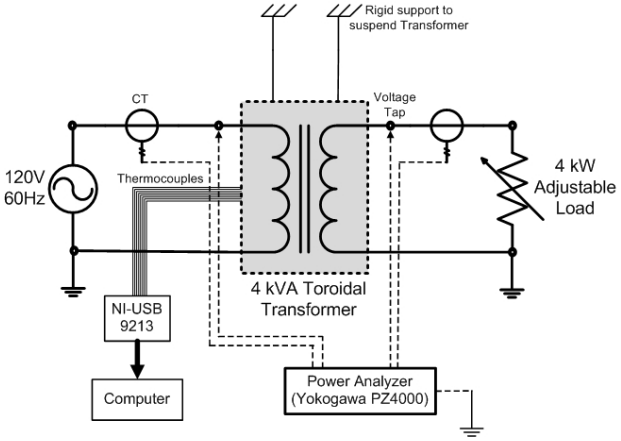

Fig. 5. Schematic for lab tests performed on the prototypes

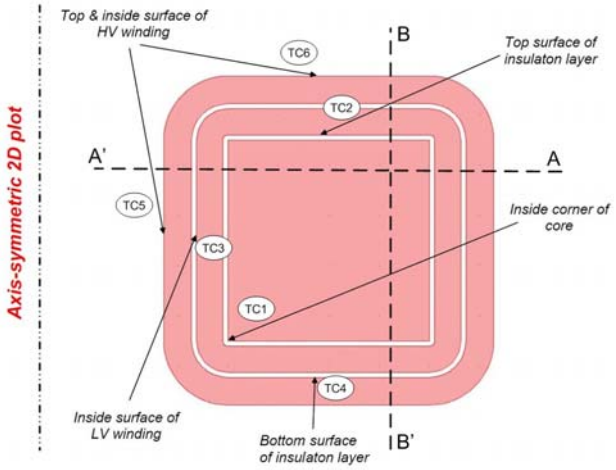

Fig. 6. Placement of thermocouples inside the prototype.

depicted in this figure are used later in section VIII to compare results. The transformer was fed from a constant voltage source while the load power was kept constant. The input power, output power and the temperatures were recorded at intervals of 30 minutes until steady state was achieved as per IEEE C57 [10]: i.e. the temperature does not change more than one degree in one hour. The difference in input and output power is the power dissipated in the transformer and is responsible for the temperature rise.

Estimation of power loss in individual windings and layers accurately is essential for this model. The mean length per turn times the total number of turns per layer would yield total resistance per layer. From this the I^2R loss can be calculated precisely.

VIII. Model Results

This section summarizes the results from the equivalent circuit, the finite element simulations, and the lab test on the prototype. As shown in Fig. 6 horizontal cross section AA' is defined as a line starting from the inner surface to the external surface. Section AA' is used to plot temperatures in the inner windings, core and outer windings. Fig. 7 presents this comparison. Similarly, cross-section BB' is defined from the bottom to the upper surface and is used to plot for bottom wind-

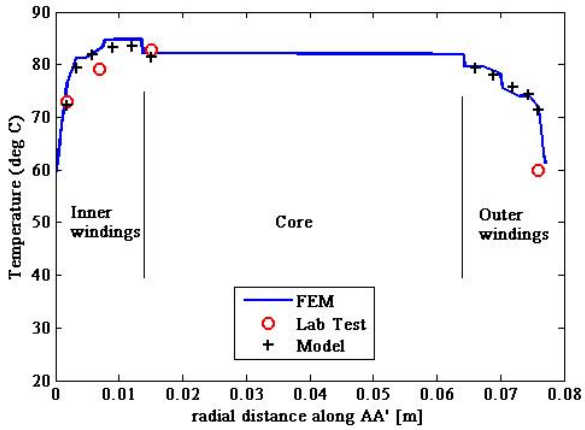

Fig. 7. Comparison of temperature distribution along section AA'

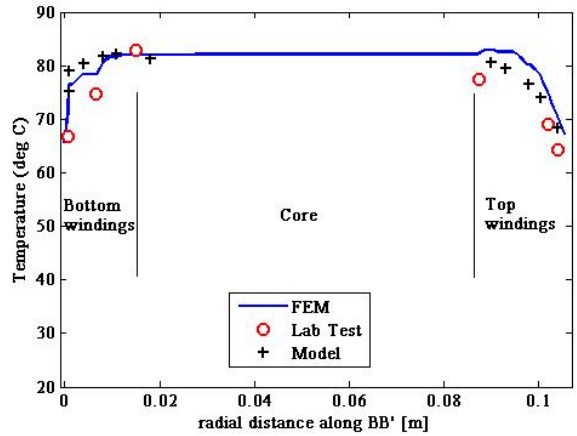

Fig. 8. Comparison of temperature distribution along section BB'.

ings, core and top windings. Fig. 8 presents the results along this section.

It is observed that the equivalent circuit behaves relatively accurately with the FEM model for the inner, outer and bottom windings. The differences in the outer winding are larger. The prototype test results are also within practical error limits of the model (max. differences of 4%). The hottest spot (HST) in this transformer is located at the inner LV winding. The probe in the prototype being outside this region was unable to catch the HST, which location we did not know when the prototype was built.

IX. Transformer in Enclosure

Distribution grade transformers are required to be enclosed in an air-tight metallic enclosure for safety reasons. The enclosure may be solid (epoxy), liquid (oil) or air filled. The tank provides additional, although small, thermal resistance to the heat flux and hence raises the operating temperature of the transformer. The tank can be modeled as a single lumped resistance in series with the ambient temperature 'voltage' source (Fig. 2), effectively raising the ambient temperature to T_{tank} given by

$$T_{\text{tank}} = T_{\infty} + Q_{loss} \times R_{\text{tank}} \tag{10}$$

where T_{tank} is the enclosure temperature and R_{tank} is the effective tank resistance.

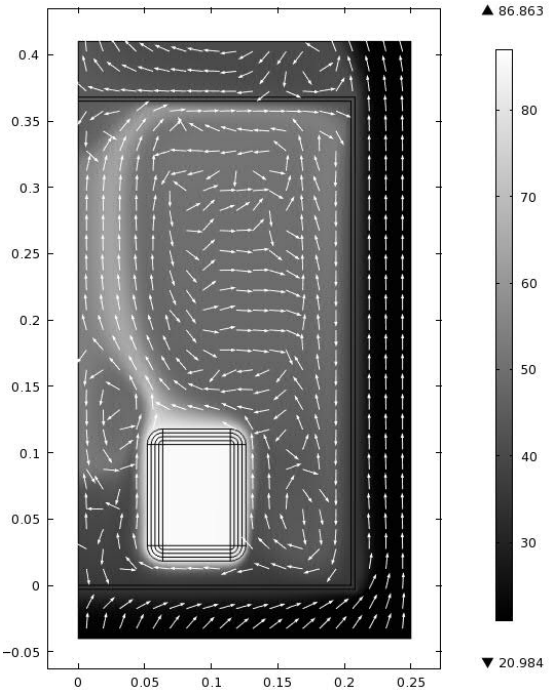

Fig. 9. FEM model of toroidal transformer enclosed in sealed enclosure under test.

The effective tank resistance, R_{tank} can be calculated as

$$\frac{1}{R_{\text{tank}}} = \frac{1}{R_{top}} + \frac{1}{R_{vertical}} + \frac{1}{R_{bottom}} \tag{1.1}$$

where R_{top}, R_{bottom}, $R_{vertical}$ are the thermal resistances of the top, bottom and vertical surfaces of the tank to the external medium. They can be evaluated from the equations (6)-(8).

All equations presented in Section V are applicable for the computation of temperature distribution within the transformer kept in an enclosure with the exception of the ambient temperature. This must be equated to the temperature of enclosure T_{tank}, since the transformer is not exposed to the surroundings at ambient temperature.

The algorithm to compute T_{tank} is presented in Appendix III.

A. Lab Tests

Various lab tests were conducted on prototypes (used in earlier sections) kept in sealed enclosures, to study the de-rating effect that the tank would have on the transformer. A dry-type arrangement (air inside enclosure) was used for this setup. To avoid exceeding the temperature limitations of the prototypes, a 75% of rated load was used for these tests. The same procedure as explained in Section VII was followed for these tests. Fig. 9 shows the transformer in the enclosure under test.

B. Finite Element Simulations

A FEM simulation with the enclosure modeled was used to compare results between the proposed model and the lab tests. Fig. 9 shows the FEM surface plot for temperature and an arrow plot for fluid velocity. The boundaries of the enclosure are closed since the fluid medium inside the enclosure is not allowed to escape. The equations solved and external boundary conditions are the same as explained in Section VI.

C. Results

Results comparing steady state temperature between the tests, FEM model and proposed model are given in Figs. 10 and 11. The results are plotted along section AA' for the horizontal and BB' for the vertical temperature distribution within the transformer.

It is observed that the model predicts the temperature variation very well. The HST occurs at the same location (inner LV winding) as the transformer exposed to ambient. The maximum error is less than 4% and is observed around the HST.

X. Consolidated Results

A concise report of all the tests conducted on the prototypes is presented in Table 1. Five prototypes (3 standard and 2 encapsulated in epoxy) of various power ratings with thermocouples installed as described in Fig. 6 were tested until steady state was achieved as per IEEE C57 [10]. The load column gives the constant electrical load connected at the transformer terminals. It is observed that encapsulation or enclosing the transformer leads to a de-rating. The comparison of the HST from the tests, model and FEM are provided. It must be noted that all the results are within practical engineering error limits (less than 4%).

XI. Conclusions

The paper has presented a model that provides detailed insight into the variation of temperature within a toroidal transformer. The equivalent electrical circuit accurately models the non-linear effects of convection and radiation and takes substantially less computational effort when compared to FEM. The new model takes into account all geometric and electric parameters such as: physical dimensions, insulation thickness, number of turns, number of layers and conductor gauge. The model accurately predicts the hot-spots which knowledge is essential for the transformer designer. The model has been validated against transient FEM simulations and measurements on actual transformers. The model if this paper is suitable to be used as an important component in a transformer design computer program.

XII. Appendix I – Prototype Transformer Details

120 / 120 Volt, 4 kVA, Rated current 33.33 A
Core ID: 12.7 cm
Core OD: 22.86 cm
Core height: 7.62 cm
No. of layers in primary and secondary: 2 each
Turn distribution for each layer: [118, 46, 105, 59]
Conductor gauge: AWG 9
Insulation (Mylar) thermal conductivity (k): 0.2 [W/(m.K)]
Rated core loss: 14.9 [W]
Full load primary winding loss: 40.8 [W]
Full load secondary winding loss: 48.9 [W]

TABLE I
Result Comparison for Various Prototypes and Configurations

HST for Free Air Tests				
Rating	Load	HST (Test)	HST (Model)	HST (FEM)
1 kVA	1 kW	83.9	85	85.5
2 kVA	2 kW	78.5	78.8	80.4
4 kVA	4 kW	82.8	83.5	84.7
HST for potted Transformer Tests				
1 kVA	1 kW	86.4	88.5	88.8
4 kVA	3.7 kW	78.5	80.6	80.2
HST for Transformer in Enclosure Tests				
2 kVA	1.25 kW	81.7 T_{tank} = 43	78.7 T_{tank} = 46.2	80.4 T_{tank} = 45.4
4 kVA	3 kW	89.1 T_{tank} = 48.9	86.6 T_{tank} = 44.8	86.9 T_{tank} = 43.9

XIII. Appendix II

The algorithm to compute temperature distribution within transformer is given in Fig. 12

XIV. Appendix III

The algorithm to compute T_{tank} is given in Fig. 13.

XV. Acknowledgment

The authors gratefully acknowledge the contributions of Iván Hernández and Noel Augustine for their continuous support to the research work. The authors are also thankful to Chandira Prabhu for conducting all the tests and providing results presented in the paper. Finally, the authors would like to thank Mr. Ulrik Poulsen of Bridgeport Magnetics for his fast response and expertise building the prototypes.

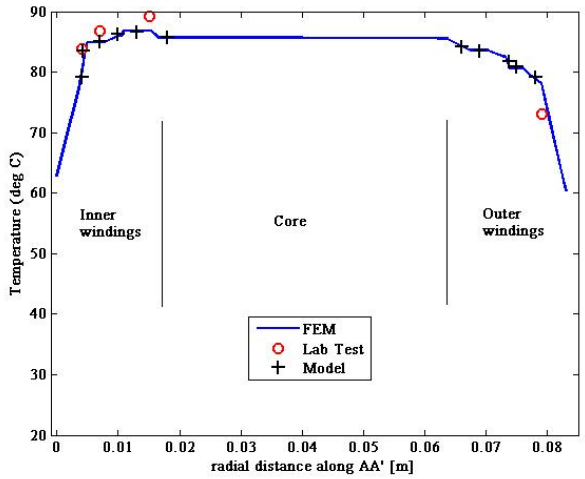

Fig. 10. Comparison of temperature distribution along section AA' for transformer in sealed enclosure

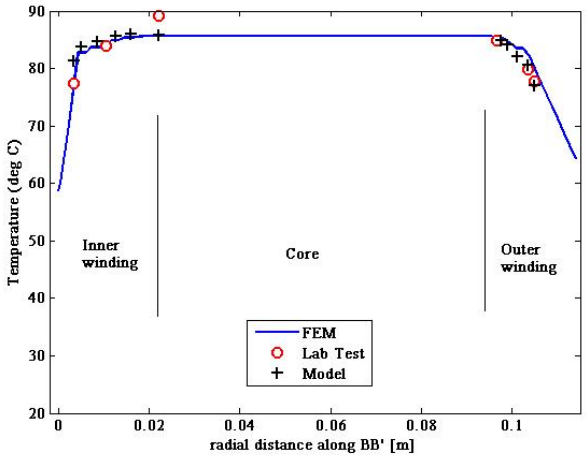

Fig. 11. Comparison of temperature distribution along section BB' for transformer in sealed enclosure

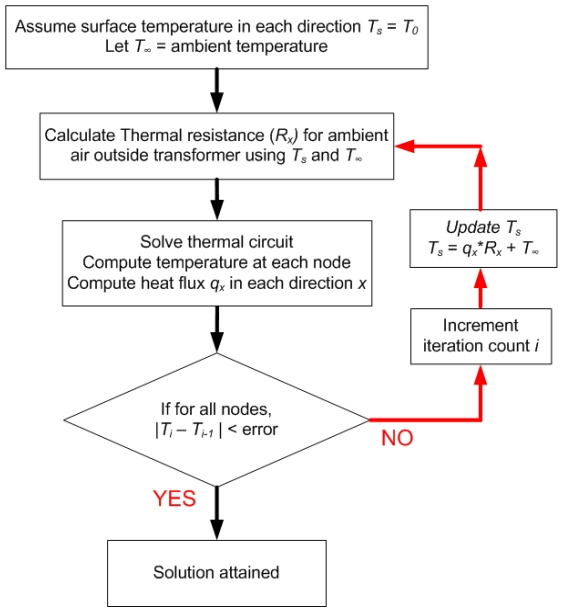

Fig. 12. Algorithm to compute temperature distribution in a transformer

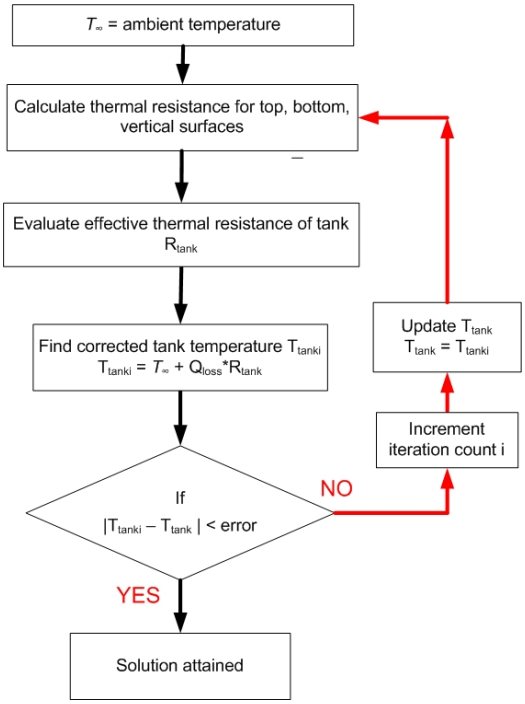

Fig. 13. Algorithm to compute temperature of the transformer tank

XVI. References

[1] F. A. Furfari and J. W. Coltman, "The Transformer", IEEE Industry Applications Magazine, Jan./Feb. 2002, pp. 11-12.

[2] Colonel Wm. T. McLyman, "Transformer and Inductor Design Handbook", 3rd Ed, New York: Marcel Dekker, Inc., 2004.

[3] M. van der Veen, "Modern High-end Valve Amplifiers: Based on Toroidal Output Transformers", Elektor Electronics Publishing, 1999.

[4] G. Swift, T. S. Molinski and W. Lehn, "A Fundamental Approach to Transformer Thermal Modeling- Part I: Theory and Equivalent Circuit," *IEEE Transactions on Power Delivery*, vol. 16, no. 2, pp.171-175, April 2001.

[5] O. A. Amoda, D. J. Tylavsky, G. A. McCulla and W. A. Knuth, "A New Model for Predicting Hottest-Spot Temperatures in Transformers," *The 40th North American Power Symposium*, pp.1-8, 2008

[6] D. Susa, M. Lehtonen and H. Nordman, "Dynamic Thermal Modeling of Power Transformers," *IEEE Transactions on Power Delivery*, vol. 20, no. 1, pp.197-204, Jan 2005.

[7] I. Hernández, F. de León, and P. Gómez, "Design Formulas for the Leakage Inductance of Toroidal Distribution Transformers", paper submitted to the IEEE Transactions on Power Delivery.

[8] P. Gómez, F. de León, and I. Hernández, "Impulse Response Analysis of Toroidal Core Distribution Transformers for Dielectric Design", *IEEE Transactions on Power Delivery*, Vol. 26, No. 2, April 2011, pp. 1231-1238.

[9] Comsol Multiphysics, *Heat Transfer Module User's Guide*, Comsol AB Group, 2006, pp. 1-222.

[10] *IEEE Standard Test Code for Dry-Type Distribution and Power Transformers*, IEEE Standard C57.12.91-1995, June. 1995.

[11] O. G. Martynenko, P. P. Khramtsov, *Free convective Heat Transfer*, Springer-Verlag Berlin Heidelberg, 2005.

[12] R. B. Bird, W. E. Stewart and E. N. Lightfoot, *Transport Phenomena*, 2nd ed., John Wiley and Sons. Inc., 2007.

[13] S. Kakac and Y. Yener, *Convective Heat Transfer*, 2nd ed. CRC Press, 1995.

[14] M. N. Ozisik, *Heat Conduction*, 2nd ed., John Wiley and Sons. Inc., 1993.

XVII. BIOGRAPHIES

Sujit Purushothaman (S'09) received his B.E. degree in electrical engineering from Mumbai University (Sardar Patel College of Engineering), India in 2005. His work experience includes testing and development of medium voltage switchgear for Siemens India. He received his Master's degree in 2009 and is currently pursuing his Ph.D. at Polytechnic Institute of NYU. His research interest includes power system transients, subsynchronous resonance damping, machine design and modeling and thermal modeling of electrical machines.

Francisco de León (S'86–M'92–SM'02) received the B.Sc. and the M.Sc. (Hons.) degrees in electrical engineering from the National Polytechnic Institute, Mexico City, Mexico, in 1983 and 1986, respectively, and the Ph.D. degree from the University of Toronto, Toronto, ON, Canada, in 1992. He has held several academic positions in Mexico and has worked for the Canadian electric industry. Currently, he is an Associate Professor at the Polytechnic Institute of NYU, Brooklyn, NY. His research interests include the analysis of power definitions under nonsinusoidal conditions, the transient and steady-state analyses of power systems, the thermal rating of cables and transformers, and the calculation of electromagnetic fields applied to machine design and modeling.

Comparing the *T* and π Equivalent Circuits for the Calculation of Transformer Inrush Currents

Francisco de León, *Senior Member, IEEE,* Ashkan Farazmand, and Pekir Joseph, *Student Member, IEEE*

***Abstract*— The most commonly used equivalent circuit for transformers is the traditional (Steinmetz) *T*-equivalent proposed towards the end of the 19th century. This model has two leakage impedance branches and one magnetizing branch. The *T* model properly represents the terminal behavior of the transformer for most low-frequency operating conditions. There exists another model derived from the principle of duality between magnetic and electric circuits, the π equivalent circuit, which has two magnetizing branches and one leakage branch. This paper shows that while the two equivalent circuits provide the same accuracy in steady state, better accuracy for the calculation of inrush currents is obtained with the π-equivalent circuit. Laboratory tests performed on three transformers with different characteristics demonstrate that inrush current simulations with the *T* equivalent circuit can have errors of up to 73%, while the π equivalent predicts the measurements in every case within a few percent.**

***Index Terms*— Duality, inrush currents, transformer equivalent circuits, transformer modeling.**

I. Introduction

FOR longer than a century the generally accepted equivalent circuit for a two-winding transformer has been the *T* equivalent. This model has the leakage inductance (L_s) divided into two branches, one is associated with the primary (L_{s1}) and another one associated with the secondary winding (L_{s2}). The model is completed with a shunt magnetizing branch (composed by the parallel R_m, L_m); see Fig 1. The originator of the equivalent circuit seems to be Steinmetz in 1897 [1]. A detailed discussion of the physical meaning of the elements of the *T* equivalent circuit is also given in [1].

As early as 1925, Boyajian [2] demonstrated the impossibility of a physically meaningful resolution of the leakage inductance as belonging partially to the primary winding and partially to the secondary winding (as it is done in Fig. 1). The leakage inductance can only be defined (or measured) for a pair of windings. Therefore, the *T* equivalent circuit should be seen only as a terminal equivalent circuit since its elements do not have any physical relationship with the building components of a transformer (core and windings).

Cherry [3] in 1949 showed that equivalent circuits for transformers could be conveniently obtained from the principle of duality between magnetic and electric circuits. When duality is applied to a single-phase transformer (both core and shell types), the obtained π model has only one leakage inductance branch in series and two shunt magnetizing branches (see Fig 2). In 1951 Boyajian [4] discussed the benefits of the π equivalent circuit emphasizing the unity of the leakage reactance between a pair of windings.

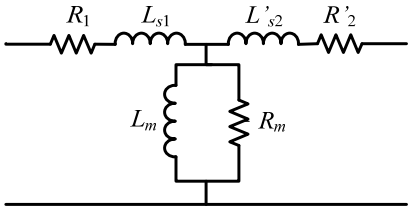

Fig. 1. *T* equivalent circuit

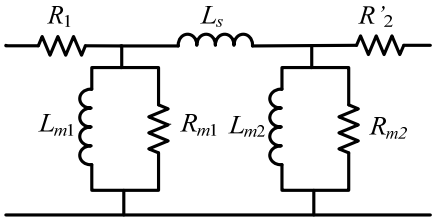

Fig. 2. π equivalent circuit

In 1953, Slemon [5] generalized the theory of duality and showed how nonlinearities can be introduced into the circuit elements of the π equivalent since they have a one-to-one relationship with the transformer flux paths. Duality-derived models have long been used for the calculation of electromagnetic transients [6]-[8]. However, they have not made the transition to steady state. The reason is perhaps that for steady state studies (not involving heavy saturation), the *T* model gives almost perfect results. Moreover, for the most common power system studies such as: load flow, short circuit, and stability, the (shunt) magnetizing branch, whose impedance is normally very large when compared to the (series) leakage impedance, is often neglected. This renders the two circuits identical.

This paper shows, experimentally and analytically, that there are conditions where the *T* equivalent circuit is not capable of properly representing the transformer under heavy saturation conditions. For example, when a transformer has large leakage inductance and the core saturates, the *T* equivalent circuit fails to reproduce the terminal behavior. Errors in the order of 73% were measured with the *T* equivalent circuit in the inrush currents for transformers with relatively large leakage inductance.

F. de León, A. Farazmand, and P. Joseph are with the Department of Electrical and Computer Engineering, Polytechnic University, Six Metrotech Center, Brooklyn, NY, 11201. (e-mails: fdeleon@poly.edu, afaraz01@students.poly.edu, pekirj@yahoo.com).

To explain the reasons why the π model performs better than the *T* model three existent transformers with different parameters were selected for the experimental study: (1) A standard transformer (T_S), which is characterized by typical leakage and magnetizing inductance values. (2) A standard torodial transformer (T_T), which is characterized by having large magnetizing inductance and very small leakage inductance. (3) A second toroidal transformer (T_L) designed with no overlapping sectored windings of 180˚. This produces a very large leakage inductance. The geometrical information is given in Appendix A.

In the next Section, the parameters of the equivalent circuit for each transformer are measured and compared. In Section III the air-core inductance, essential for the proper calculation of inrush currents, is computed with 3D finite elements simulations. In Section IV the inrush performance of the two models is compared. In Section V a parametric analysis on how the division of the leakage and magnetizing inductances affect the transformer inrush current is presented. Finally, in Section VI, the large errors obtained with the *T* model are explained by analyzing the variation of the open circuit impedance as the core saturates and the leakage inductance increases.

II. Parameter Measurement

Accurate determination of the transformer magnetizing and leakage parameters is of paramount importance to produce a correct comparison of model performance. To determine the parameters the procedures of the IEEE Standard C57.12.91-1995 [9] for open circuit and short-circuit tests were followed. The measurements of instantaneous voltage and current are obtained very precisely using a YOKOGAWA 2 MHz power analyzer (PZ4000), with a sampling rate of 20 μs. From the measuring system, 833 samples per cycle of voltage and current are obtained. The *rms* values for voltage and current are computed from basic principles as follows:

$$v_{rms} = \sqrt{\frac{1}{T}\int_0^T v^2(t)\,dt} \quad ; \quad i_{rms} = \sqrt{\frac{1}{T}\int_0^T i^2(t)\,dt} \tag{1}$$

The active power is computed from the average of the instantaneous power as:

$$P = \frac{1}{T}\int_0^T v(t)\,i(t)\,dt \tag{2}$$

The reactive power is calculated with the following formula:

$$Q = \sqrt{(v_{rms} i_{rms})^2 - P^2} \tag{3}$$

A. Open Circuit Test

The low-voltage winding of the transformer is energized with rated voltage keeping the high-voltage side in open-circuit. The terminal voltage of the high-voltage (open) side and current of the low-voltage (connected) side are captured.

B. Short-Circuit Test

The high-voltage winding is energized with the low-voltage winding short-circuited. The voltage applied is varied from 4% to 20% of the rated voltage to get the rated current in the low-voltage winding (see Table I).

TABLE I
Results of the Standardized Tests on the Four Transformers

Transformer	T_S Standard Leakage	T_T Reduced Leakage	T_L Enlarged Leakage
V_{oc} [V]	120.18	120.04	120.19
I_{oc} [A]	5.3297	0.30886	0.254976
P_{oc} [W]	39.08	10.18	13.44
Ratio	1:1	1:1	1:1
Rating [kVA]	1	1	1
V_{sc} [V]	5.15	5.08	24.73
I_{sc} [A]	8.38	8.73	8.75
P_{sc} [W]	40.351	43.9859	46.871

C. Calculation of Circuit Parameters

Table I shows the results of the standardized open circuit (oc) and short-circuit (sc) tests (at 60 Hz) for the three transformers under study. The parameters of the equivalent circuits are computed with the following expressions:

$$R_1 + R'_2 = \frac{P_{sc}}{I_{sc}^2} \tag{4a}$$

$$L_s = \frac{1}{2\pi f}\sqrt{\left(\frac{V_{sc}}{I_{sc}}\right)^2 - \left(R_1 + R'_2\right)^2} \tag{4b}$$

$$R_m = \frac{(V_{oc} - R_1 I_{oc})^2}{P_{oc}} \quad ; \quad L_m = \frac{(V_{oc} - R_1 I_{oc})^2}{2\pi f\, Q_{oc}} \tag{5}$$

where P_{sc} and P_{oc} are the active powers computed from the short circuit and open circuit tests, respectively. Q_{oc} is the open circuit reactive power. V_{sc} and I_{sc}, are the *rms* values of short circuit voltages and currents, respectively. V_{oc} and I_{oc} are the *rms* values of open circuit voltages and currents, respectively. L_s is the total (series) leakage inductance. R_m is the magnetizing resistance, L_m is the magnetizing inductance, R_1 and R_2 are the primary and the secondary *ac* resistances, respectively, and f=60 Hz.

The total series *ac* resistance $R_1 + R'_2$ is computed from (4a). Individual break down of the resistances is needed for the equivalent models. Additionally, primary and secondary leakage inductances are also needed for the *T* model. When no information is given on the value of the individual *dc* resistances, it is accepted to divide the leakage (and *ac* resistance) equally into the two windings [10]. For this paper, measurement of the *dc* resistance was performed. Therefore, the leakage inductance and *ac* resistance are divided into two as it is traditionally done in proportion to the *dc* resistances [11]; see Table II. In Section V, this division of the leakage impedance is varied over a wide range to gauge the effect of having more or less leakage to each side. The magnetizing parameters of the *T* model are obtained directly from (5).

TABLE II
CIRCUIT PARAMETERS FOR *T* AND π MODELS

Transformer	T_S Standard Leakage	T_T Reduced Leakage	T_L Enlarged Leakage
R_1 [Ω]	0.251	0.277	0.306
R'_2 [Ω]	0.324	0.300	0.305
L_{s1} [mH]	0.302	0.111	4.393
L'_{s2} [mH]	0.390	0.121	4.385
R_m [Ω]	369.53	1,415.97	1,074.71
L_m [mH]	71.91	1,284.73	1,669.60
L_s [mH]	0.692	0.232	8.778
R_{m1} [Ω]	739.06	2,831.94	2,149.42
R_{m2} [Ω]	739.06	2,831.94	2,149.42
L_{m1} [mH]	143.82	2,569.46	3,339.21
L_{m2} [mH]	143.82	2,569.46	3,339.21
L_m/L_s	103.89	5,537.63	190.20

For the π model the leakage inductance is obtained directly from (4b) and the magnetizing parameters are the double of those obtained from (5) [8]. Therefore, $R_{m1} = R_{m2} = 2\,R_m$ and $L_{m1} = L_{m2} = 2\,L_m$. Also in Section V, this division of the magnetizing impedance is varied over a wide range to determine the effect of assigning more or less magnetizing to each side. The parameters computed from rated measurements are shown in Table II.

D. Hysteresis Cycles

A family of hysteresis curves were obtained for each of the three transformers under test. These hysteresis curves are acquired from the measurement of the instantaneous values of voltage and current. Faraday's Law is then used to convert the induced voltage into flux. The hysteresis cycles of transformers T_S, T_T, and T_L are shown in Fig. 3. In Appendix C the numerical values of the upper part of the cycles are given (as required by the EMTP-RV [12]).

One can appreciate from Fig. 3 that the standard transformer (T_S) shows a traditional hysteresis cycles. The toroidal transformers (T_T and T_L) have a flat and narrow hysteresis cycles. This is so because there are no gaps in the core. Fig. 4 shows a zoom on the hysteresis cycles of the toroidal transformers. Note that the transformer with enlarge leakage T_L has a slightly wider cycle, but the saturation flux is the same.

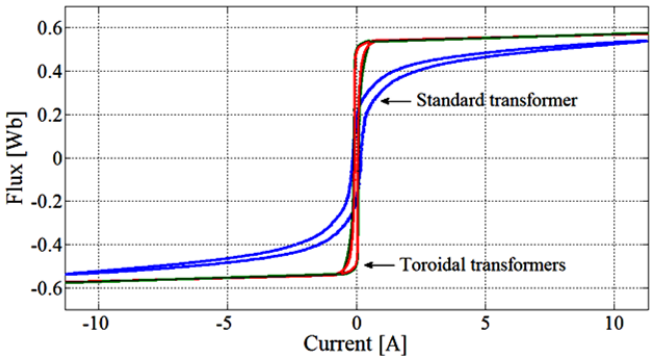

Fig. 3. Hysteresis cycles of the transformers T_S (standard design), T_T (reduced leakage), and T_L (enlarged leakage).

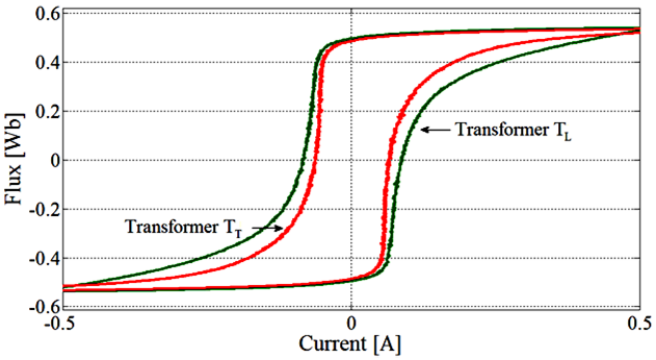

Fig. 4. Hysteresis cycles of the toroidal transformers (T_T and T_L)

III. AIR-CORE INDUCTANCES

It was not possible to measure the deep saturation section region of the hysteresis loops in the lab due to the large power requirements (high-voltage and high-current). Yet this region is of paramount importance to compute properly the inrush currents. 3-D finite element (FEM) simulations were performed to determine the air-core inductance. The commercial program COMSOL Multyphisics was used for this purpose [13]; see Appendix B.

The dimensions of the low voltage winding were used for the FEM simulations using air cores. The volume magnetic energy is extracted directly from COMSOL and then the inductance is calculated using the following formula:

$$L_{air-core} = \frac{2W}{I^2} \tag{6}$$

Table III gives the air-core inductances of the three transformers studied in this paper. Note, however that the construction details of the standard transformer T_S are not known. Therefore, an estimation was obtained from the inrush tests. The hysteresis curve is extended using the air-core inductances as the slope from the last measured point to infinity. These values are included in the tables of Appendix C.

TABLE III
AIR CORE INDUCTANCE FOR THE TRANSFORMERS

Transformer	T_S Standard Leakage	T_T Reduced Leakage	T_L Enlarged Leakage
Air-core Inductance	1000 [μH]	316 [μH]	463 [μH]

IV. MODEL COMPARISON

A. Description of the Inrush Current Experiments

Starting with the transformer core demagnetized, the worst conditions (maximum inrush currents) occur when the energization coincides with the voltage wave zero-crossing [14]. This situation can be reproduced in the laboratory by connecting the transformer through a zero-crossing detecting switch as shown in Fig. 5. To obtain accurate and consistent inrush current measurements, any remanence in the transformer from the previous energization must be removed [15]. The remanence removal process was done by gradually reducing the voltage to zero before de-energizing the transformer from the source.

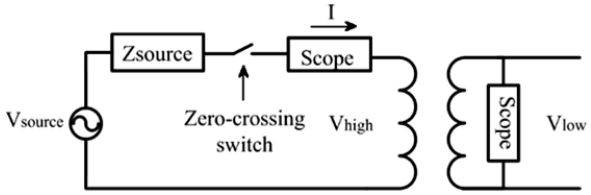

Fig. 5. Model of experimental set up for measuring inrush currents.

A zero-crossing switch consisting of voltage regulators, optic isolators, digital logic control circuits, and MOSFETs is used to switch-on the transformer. When the source voltage crosses zero, the switch is closed and the waveforms of inrush current are captured with the power analyzer. The results are compared with simulations in the next section).

B. Simulations versus Measurements

The EMTP-RV [12] was used for the simulation of the tests described in Fig. 5 using the two equivalent circuits (Fig. 1 and Fig. 2). The non-linear characteristics of all inductors representing iron-core components are modeled with the built-in hysteresis fitter (using the data computed in the previous section). The short-circuit impedance of the source was measured, which is almost purely resistive with a value of *Zsource* = 0.1444 Ω. Figs. 6, 7, and 8 compare the results obtained by simulation using the *T* and π models against the measurements for the three transformers under study.

Fig. 6 shows the results for the standard transformer T_S. The peak value of the inrush current using the π model is 121.1 A, which is very close to the experiment result (123.7 A). In this case the difference is only 2%, while the T model gives 111.7 A, which corresponds to 10% difference with respect to the experiment result. The current shape of both models follows the same path for low currents and only towards the peak they separate. The peak of the measured inrush current is about 10 times larger than the rated 11.78 A peak (8.33 A rms).

Fig. 7 shows the results for the toroidal transformer T_T, whose main characteristics are to have very small leakage inductance and very large magnetizing inductance (see Table II). The π model and experiment give the same value for the first peak (254.5 A), while the *T* model shows 241.4 A. In this case for the *T* model the difference is about 5% at the peak with the experiment result. For this transformer the measured inrush current is about 22 times larger than the rated current.

Fig. 8 shows the results for the toroidal sector wound transformer T_L, whose main features are to have a very large leakage inductance and also a very large magnetizing inductance (see Table II). In this case, the measured peak of the inrush current is 201.4 A peak (about 17 times larger than the rated current).

The π model gives 179.4 A at the first peak, which represents a difference of 10.9% with respect to the experiment result, while the *T* model yields 54.9 A, which corresponds to a very large error of 72.7% at the peak.

Note that, the measured peak inrush current of transformer T_T is about 26% larger than the peak inrush current of transformer T_L. This is because of the larger leakage inductance value of transformer T_L in comparison to T_T (almost 38 times) which limits the inrush current considerably.

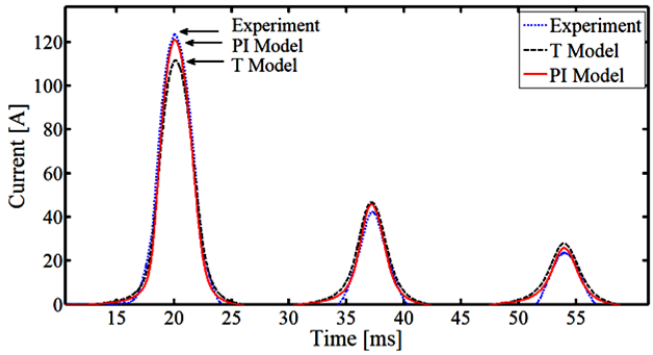

Fig. 6. Inrush current comparison: experimental versus simulated using *T* and π models for transformer T_S (standard design).

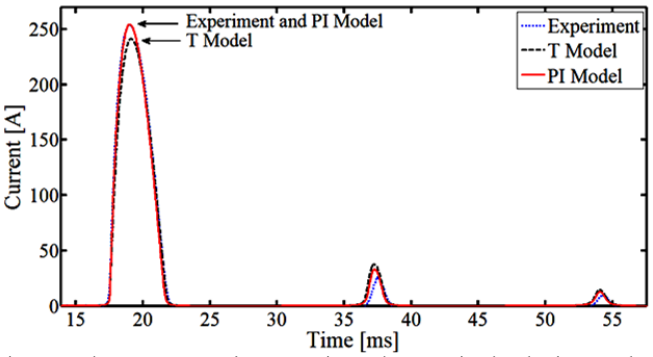

Fig.7. Inrush current comparison: experimental versus simulated using *T* and π models for transformer T_T (very small leakage inductance).

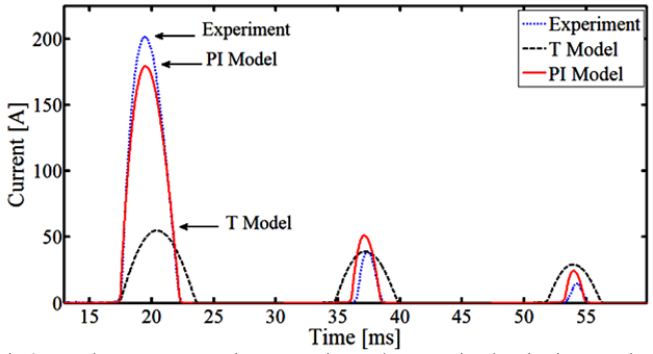

Fig.8. Inrush current comparison: experimental versus simulated using *T* and π models for transformer T_L (very large leakage inductance).

For all three transformers the π model gives more precise results than the *T* model. When the leakage inductance is small (transformers T_T and T_s) the *T* model results are also acceptable and relatively close to the experiment, but when the leakage inductance is large (transformer T_L), the *T* and π models behave quite differently: the *T* model shows a very large error, while the π model is close to the experimental results.

From the results of the simulations and measurements of this section, one can conclude that model selection plays an important role in the calculation of inrush currents when the leakage inductance is large. We make the statement that the π model should be always used, not only because its elements have a clear physical meaning, but also because large errors may appear when using the traditional *T* model. Both circuits are very simple, the π model has only one more circuit element (7 versus 6) than the *T* model, but the π equivalent may provide better results under heavy saturation conditions.

V. Parametric Studies

In this section, a parametric analysis of how the division of the leakage and magnetizing inductances affect the calculated inrush currents using the *T* and π *models* is presented.

Transformer T_L has been selected to illustrate the parametric simulations because this is the one that presents larger variations; see Table IV. The first column presents a division factor *a* used to split the total leakage inductance (L_s) into primary and secondary sides of the *T* model. For example, the first row (corresponding to $a = 0$) presents the case when all leakage inductance is entirely on the secondary side of the *T* model. In the next row ($a = 10\%$), 10% of the leakage is placed on the primary side and 90% on the secondary side. In the last case ($a = 100\%$), all the leakage inductance is on the primary side of the transformer.

The last column of Table IV presents the errors in the calculated peak currents between the *T* model and the experimental results. From the results, it is obvious that increasing the primary side leakage (L_{s1}) limits the inrush current considerably, which causes large errors. For the case in which the division factor is 50% [10], the error is 71.97%; when the leakage inductance is divided based on the *dc* resistances (as recommended in [11]), the error is 72.7%; and the error is zero when only 2.7% of the total leakage inductance is on the primary side of the transformer. Fig. 9 compares the inrush current waveforms for five different cases using a 25% division factor. From the figure, one can observe that the inrush current computed with the *T* model show a large sensitivity especially at the beginning.

To study the splitting of the magnetizing impedance in the π model, a division factor of 25% has been selected. The total magnetizing current between the two magnetizing branches is divided proportionally. Remember that the magnetizing model is nonlinear since it includes saturation and hysteresis. As it is shown in Table V, the first and last cases (with division factors of 0 and 100%, respectively) are equal to the cases with one magnetizing branch. Therefore, for these two cases the results are exactly the same as the first and last cases of *T* model (see Table IV).

In all other cases, the error is smaller than for the *T* model. The error is zero when the division factor is about 32.5%, and for a 50% division factor, the error is 10.9% (as presented in Section IV). Fig. 10 compares the inrush current waveforms for the different cases with the experiment result. Analyzing Figs. 9 and 10 one can see that the calculations are less sensitive to the division factor in the π model than in the *T* model.

TABLE IV
Parametric Study of *T* Model (Leakage Inductance Division)

a (%)	L_{s1} [mH]	L_{s2} [mH]	Peak Current [A]	Error [%]
0	0.000	8.778	230.36	14.38
10	0.878	7.900	139.75	-30.61
20	1.756	7.022	100.72	-49.99
30	2.633	6.145	78.83	-60.86
40	3.511	5.267	64.78	-67.84
50	4.389	4.389	54.99	-72.70
60	5.267	3.511	47.78	-76.28
70	6.145	2.633	42.24	-79.03
80	7.022	1.756	37.86	-81.20
90	7.900	0.878	34.3	-82.97
100	8.778	0.000	31.35	-84.43
Case with zero error:				
2.2	0.192	8.586	201.4	0.00

TABLE V
Parametric Study of π Model (Magnetizing Inductance Division)

a (%)	Peak Current [A]	Error [%]
0	230.3	14.38
25	211.3	4.92
50	179.4	-10.92
75	128.2	-36.35
100	31.34	-84.43
Case with zero error:		
32.5	201.4	0.00

VI. Analysis of the Terminal Impedance

In this section, the large errors obtained with the *T* model are explained by analyzing the variation of the open circuit impedance as the core saturates (L_m reduces). In addition, the effect of increasing the leakage inductance (L_s) is presented. The (open circuit) equivalent impedance for the *T* and π equivalent circuits can be computed from series-parallel simplifications of the circuits of Fig. 1 and Fig. 2, respectively, as follows:

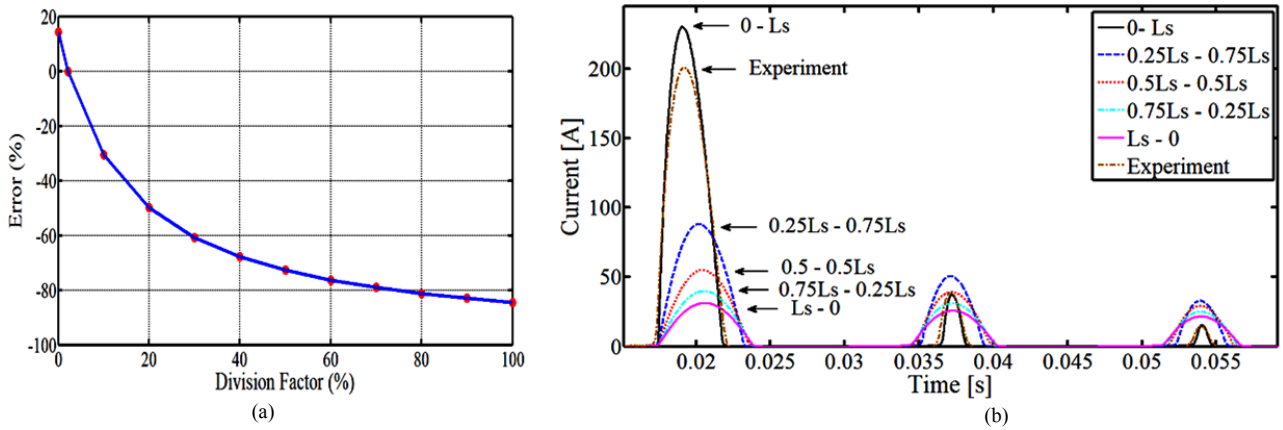

Fig.9. Inrush current comparison using *T* model for transformer T_L under different division factors for the leakage inductance. (a) Error with respect to the experiment; (b) Inrush currents waveforms.

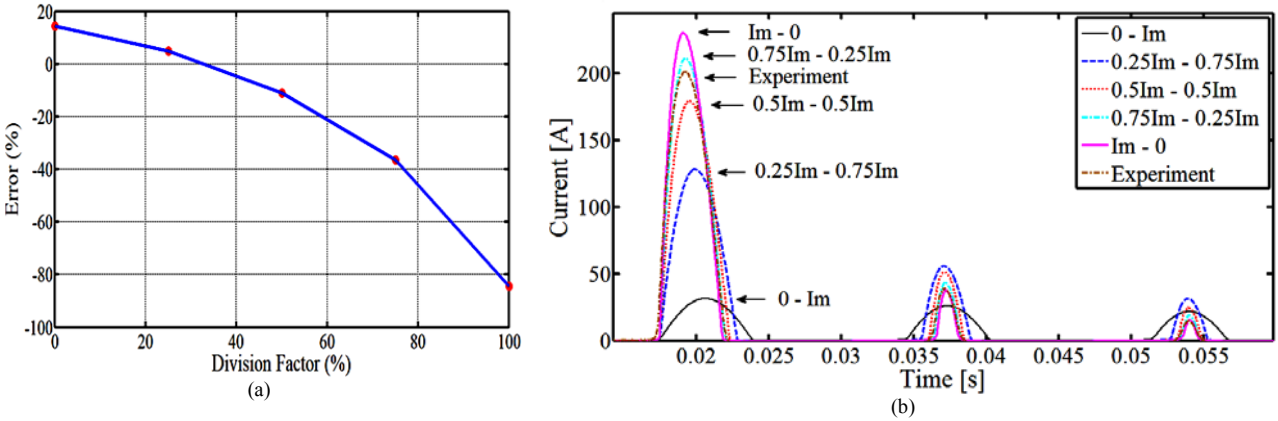

Fig.10. Inrush current comparison using π model for transformer T_L under different division factors for the magnetizing impedance. (a) Error with respect to the experiment; (b) Inrush currents waveforms.

$$Z_T = R_1 + j\omega L_{s1} + \frac{1}{\frac{1}{R_m} + \frac{1}{j\omega L_m}} \tag{7}$$

$$Z_\pi = R_1 + \frac{1}{\frac{1}{R_{m1}} + \frac{1}{j\omega L_{m1}} + \frac{1}{j\omega L_s + \frac{1}{\frac{1}{R_{m2}} + \frac{1}{j\omega L_{m2}}}}} \tag{8}$$

Using the values for the standard transformer (T_S) from the first column of Table II, we find the equivalent circuits of Fig. 11 and Fig. 12.

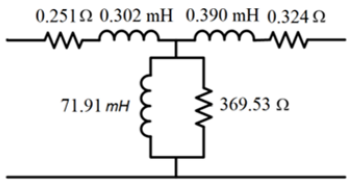

Fig. 11. *T* equivalent circuit for the T_S transformer at nominal voltage.

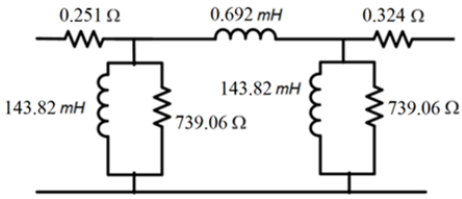

Fig. 12. *π* equivalent circuit for the T_S transformer at nominal voltage.

The effect of increasing the leakage inductance on the terminal impedance is studied varying the parameters of the equivalent circuits of Figs. 11 and 12. The leakage inductances, L_s together with L_{s1} and L_{s2}, were increased (one thousand times) in small steps. Fig. 13 shows the terminal (open circuit) impedance for the *T* and *π* models against the leakage inductance (normalized with the magnetizing inductance L_m). One can see that for small L_s / L_m ratios both circuits give the same terminal impedance. This is the normal region because L_m>>L_s for most transformers. However, as the ratio L_s / L_m increases the impedance of the *T* model increases much faster than the impedance of the *π* model. Under heavy saturation conditions L_m is small. This explains why the *T* model under predicts the inrush currents for transformers with large leakage inductance (see Fig. 8).

To study the effect on the open circuit impedance of the reduction of the magnetizing inductance due to saturation, L_m together with L_{m1}=L_{m2}= 2 L_m, were decreased in small steps to a value one thousand times smaller. The terminal impedance calculations (shown in Fig. 14) indicate that the saturation of the core by itself is not responsible for the large terminal impedance differences between the *T* and *π* models. When the leakage inductance of the transformer is increased 10 times from 0.692 mH to 6.92 mH the impedance variation of Fig. 15 is obtained. Small differences exist when the magnetizing inductance is large (not saturated), but larger differences can be observed when the magnetizing inductance is small (saturated).

The results of this section explain why both models give about the same inrush current for transformers with small leakage inductance; see Figs. 6 and 7. Looking at the topology of the two circuits (Figs. 11 and 12) one can observe that in the *T* model the primary winding leakage inductance (L_{S1}) limits the circulation of current to the magnetizing branch. This prevents large currents (especially inrush when the core saturates) to be drawn by the transformer. In the *π* model the path of the inrush current is open to the one of the magnetizing branches. Therefore, in this case the *π* model is more precise than the *T* model (see Fig. 8).

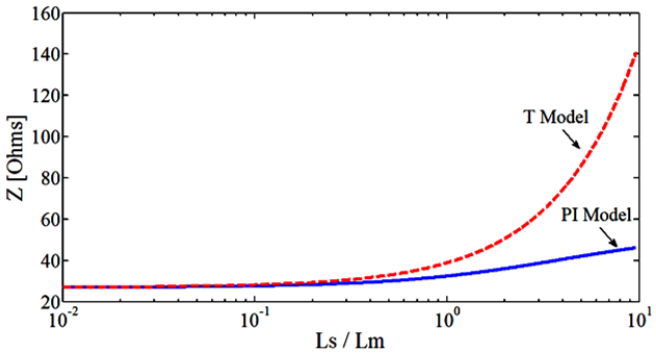

Fig.13. Variation of the terminal (open circuit) impedance with respect the ratio of leakage versus magnetizing inductances increasing the leakage inductance.

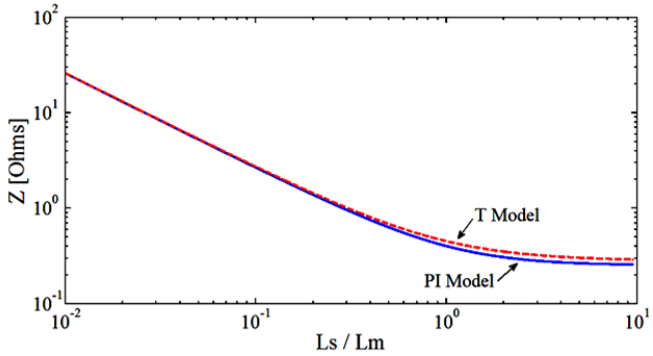

Fig.14. Variation of the terminal (open circuit) impedance with respect the ratio of leakage versus magnetizing inductances reducing the magnetizing inductance.

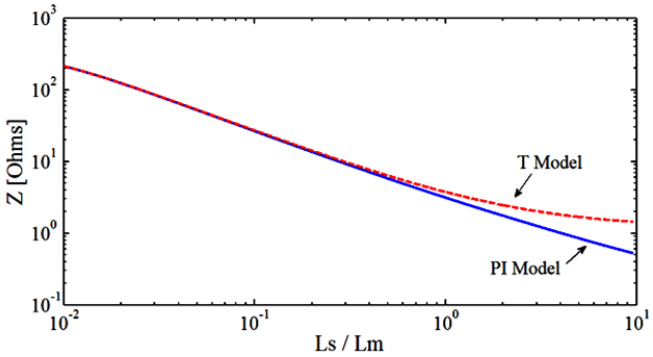

Fig.15. Variation of the terminal (open circuit) impedance with respect the ratio of leakage versus magnetizing inductances for an increased leakage inductance transformer.

VII. Conclusions

This paper has shown experimentally that the traditional *T* model of transformers may yield large errors when computing inrush currents. This is especially true when the transformers have large leakage inductance. Better accuracy for the calculation of inrush currents has been obtained with the π equivalent circuit. Laboratory tests performed on several transformers demonstrate that inrush current simulations with the *T* equivalent circuit could under predict the inrush currents by as much as 72.7%, while the π equivalent circuit predicts the measurements with a small percent error.

Physical, numerical, and analytical explanations on the performance difference of the two models were given. The topology of the *T* model, having the primary winding leakage inductance element before a magnetizing branch, is the cause for the model inaccuracies since it (incorrectly) limits the circulation of current to the magnetizing branch when the core saturates.

VIII. Acknowledgements

The authors would like to express their gratitude to Mr. Rajesh Kumar and Mrs. Xiaojing Xu, both ex-graduate students of NYU-Poly, for their help during the initial experimental stages of this project. We also would like to thank Mr. Baris Kovan, current graduate student of NYU-Poly, for performing the finite element simulations to compute the air-core inductance. The efforts of Mr. Noel Augustine with the finite elements simulations are also recognized.

IX. Appendix A – Construction Information of the Toroidal Transformers under Test

Core Dimensions [inches]			Winding Characteristics			
Internal Diameter	Outer Diameter	Height	Primary winding		Secondary winding	
			Number of Turns	Wire gauge	Number of Turns	Wire gauge
3.375	5.875	2	196	13	196	13

X. Appendix B – Air-Core Inductance

Since it was not possible to measure the air-core inductance in the lab because of the high power requirements, 3D finite element simulations were performed. Figs. 16(a) and 16(b) show the top view of the distribution of the magnetic flux density for the T_T and T_L transformers respectively. Transformer T_T has the winding distributed over the entire 360˚, while transformer T_L occupies only 180˚. From Fig. 16(a), one can see that the field is mostly contained inside the coil with higher flux densities towards the inner diameter. Fig. 16(b) shows that for the T_L transformer the flux density is concentrated inside the wound semi-circle, but the return through the air is quite scattered.

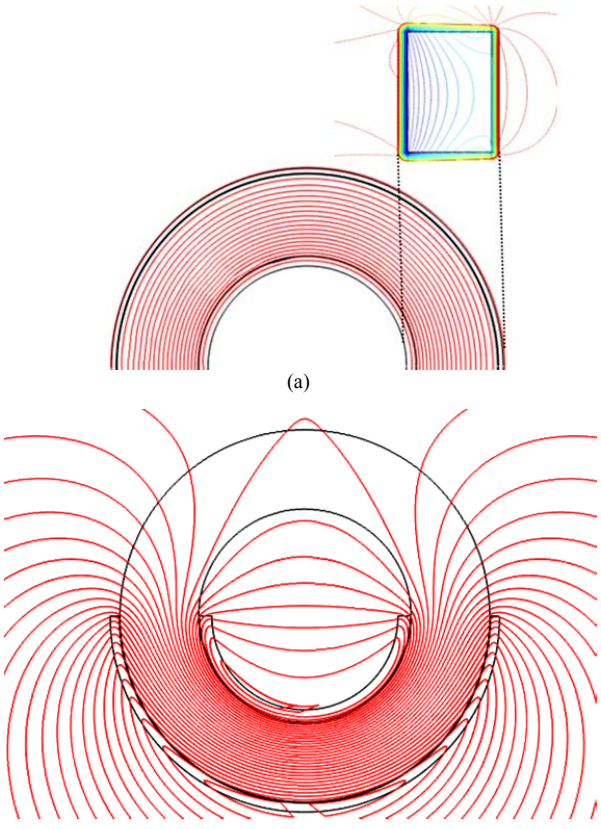

(a)

(b)

Fig.16. (a) Magnetic flux density for the T_T transformer, (b) Magnetic flux density for the T_L transformer.

XI. Appendix C – Values of the Hysteresis Cycles

Tables VI and VII present the numerical values of the hysteresis cycles used for the *T* and π models for the three transformers. Note that because the π model has two shunt inductors the value of the current is half for the same flux.

TABLE VI
NUMERICAL VALUES OF THE HYSTERESIS CYCLE OF TRANSFORMERS (T-MODEL)

T_S (Standard Leakage)		T_T (Reduced Leakage)		T_L (Enlarged Leakage)	
I [A]	Flux [Wb]	I [A]	Flux [Wb]	I [A]	Flux [Wb]
0.1873	0	0.0598	0	0.0992	0
0.2025	0.0351	0.0714	0.0619	0.1024	0.0323
0.2739	0.1030	0.0793	0.1823	0.1119	0.0955
0.3148	0.1366	0.0897	0.2115	0.1224	0.1269
0.4082	0.1700	0.1031	0.2683	0.1258	0.1579
0.5248	0.2030	0.1117	0.2958	0.1334	0.1886
0.7024	0.2354	0.1312	0.3226	0.1463	0.2188
0.9172	0.2673	0.1520	0.3485	0.1647	0.2485
1.1522	0.2986	0.1593	0.3736	0.1781	0.2775
1.4849	0.3291	0.1978	0.3978	0.2030	0.3059
1.9048	0.3588	0.2283	0.4210	0.2301	0.3335
3.3269	0.4153	0.3082	0.4641	0.3009	0.3860
4.4774	0.4420	0.3906	0.4840	0.3492	0.4108
6.0106	0.4675	0.4938	0.5026	0.4059	0.4346
8.0034	0.4918	0.6799	0.5201	0.4767	0.4573
10.2941	0.5147	0.9827	0.5362	0.5560	0.4787
12.7635	0.5362	1.5833	0.5509	0.6588	0.4989
15.2251	0.5562	2.8455	0.5641	0.7828	0.5177
17.7922	0.5749	5.1459	0.5758	0.9642	0.5351
20.3166	0.5920	9.6796	0.5859	1.2713	0.5506
22.7446	0.6074	17.9407	0.5941	1.8412	0.5636
25.0224	0.6213	29.6356	0.6002	2.8446	0.5739
27.2454	0.6335	40.0726	0.6042	4.6666	0.5816
29.3236	0.6440	45.7422	0.6062	8.2994	0.5872
30.6528	31.2725	46.8378	0.6066	15.2306	0.5912
33.0559	0.6600	600	0.7814	23.6656	0.5937
34.5354	0.6653			30.3695	0.5952
35.6353	0.6690			34.4554	0.5960
36.1479	0.6709			35.8700	0.5962
400	1.0348			600	0.8574

TABLE VII
NUMERICAL VALUES OF THE HYSTERESIS CYCLE OF TRANSFORMERS (PI-MODEL)

T_S (Standard Leakage)		T_T (Reduced Leakage)		T_L (Enlarged Leakage)	
I [A]	Flux [Wb]	I [A]	Flux [Wb]	I [A]	Flux [Wb]
0.0936	0	0.0299	0	0.0496	0
0.1013	0.0351	0.0357	0.0619	0.0512	0.0323
0.1370	0.1030	0.0397	0.1823	0.0560	0.0955
0.1574	0.1366	0.0449	0.2115	0.0612	0.1269
0.2041	0.1700	0.0516	0.2683	0.0629	0.1579
0.2624	0.2030	0.0558	0.2958	0.0667	0.1886
0.3512	0.2354	0.0656	0.3226	0.0732	0.2188
0.4586	0.2673	0.0760	0.3485	0.0823	0.2485
0.5761	0.2986	0.0797	0.3736	0.0890	0.2775
0.7424	0.3291	0.0989	0.3978	0.1015	0.3059
0.9524	0.3588	0.1141	0.4210	0.1150	0.3335
1.6635	0.4153	0.1541	0.4641	0.1504	0.3860
2.2387	0.4420	0.1953	0.4840	0.1746	0.4108
3.0053	0.4675	0.2469	0.5026	0.2029	0.4346
4.0017	0.4918	0.3400	0.5201	0.2383	0.4573
5.1470	0.5147	0.4913	0.5362	0.2780	0.4787
6.3818	0.5362	0.7916	0.5509	0.3294	0.4989
7.6126	0.5562	1.4227	0.5641	0.3914	0.5177
8.8961	0.5749	2.5729	0.5758	0.4821	0.5351
10.1583	0.5920	4.8398	0.5859	0.6357	0.5506
11.3723	0.6074	8.9703	0.5941	0.9206	0.5636
12.5112	0.6213	14.8178	0.6002	1.4223	0.5739
13.6227	0.6335	20.0363	0.6042	2.3333	0.5816
14.6618	0.6440	22.8711	0.6062	4.1497	0.5872
15.6362	0.6528	23.4189	0.6066	7.6153	0.5912
16.5280	0.6600	300	0.7814	11.8328	0.5937
17.2677	0.6653			15.1848	0.5952
17.8176	0.6690			17.2277	0.5960
18.0740	0.6709			17.9350	0.5962
200	1.0348			300	0.8574

XII. REFERENCES

[1] C. P. Steinmetz, *Theory and Calculation of Alternating Current Phenomena*, McGraw Publishing Company, 1897. First Edition Available through Open Library http://openlibrary.org.

[2] A. Boyajian, "Resolution of Transformer Reactances into Primary and Secondary Reactances", AIEE Transactions, Vol xx, No. yy, .pp. 805-810, June 1925.

[3] E. C. Cherry, "The Duality Between Interlinked Electric and Magnetic Circuits and the Formation of Transformer Equivalent Circuits", Proc. Of the Physical Society, Vol (B) 62, Feb. 1949, pp. 101-111.

[4] L. F. Blume, A. Boyajian, G. Camilli, T.C. Lenox, S. Minneci, and V.M. Montsinger, *Transformer Engineering: A Treatise on the Theory, Operation, and Application of Transformers*, p. 70, John Wily & Sons, 1951.

[5] G. R. Slemon, "Equivalent circuits for transformers and machines including nonlinear effects," Proc. Inst. Elect. Eng., pt. IV, vol. 100, pp. 129–143, 1953.

[6] F. de León and A. Semlyen, "Complete Transformer Model for Electromagnetic Transients," IEEE Transactions on Power Delivery, Vol. 9, No. 1, January 1994, pp. 231-239.

[7] J. A. Martinez and B. Mork, "Transformer Modeling for Low- and Mid-Frequency Transients – A Review", IEEE Transactions on Power Delivery, Vol. 20, No. 2, April 2005, pp. 1525-1632.

[8] F. de León, P. Gómez, J. A. Martinez-Velasco, and M. Rioual, Chapter 4, "Transformers" in *Power System Transients: Parameter Determination* (Edited by J.A. Martinez-Velasco), CRC Press, Boca Raton FL, 2009, pp. 177-250.

[9] IEEE Std C57.12.91-1995, "IEEE Standard Test Code for Dry-Type Distribution and Power Transformers", Recognized as an American National Standard (ANSI).

[10] V. Del Toro, "Principles of Electrical Engineering", Second Edition, Prentice-Hall, Englewood Cliffs, New Jersey, 1972.

[11] Staff of the Department of Electrical Engineering of Massachusetts Institute of Technology, "Magnetic Circuits and Transformers", John Wiley and Sons, New York, 1943.

[12] DCG-EMTP (Development coordination group of EMTP) Version EMTP-RV, Electromagnetic Transients Program. [Online]. Available: http://www.emtp.com.

[13] Comsol Multiphysics 4.2a User's Guide, Burlington, MA, 2011.

[14] A. Greenwood, "Electrical Transients in Power Systems", Second Edition, John Wiley & Sons, New York 1991, pp. 113-116.

[15] B. Kovan, F. de León, D. Czarkowski, Z. Zabar, and L. Birenbaum, "Mitigation of Inrush Currents in Network Transformers by Reducing the Residual Flux with an Ultra-Low-Frequency Power Source", IEEE Transactions on Power Delivery, Vol. 26, No. 3, July 2011, pp. 1563-1570.

XIII. BIOGRAPHIES

Francisco de León (S'86–M'92–SM'02) received the B.Sc. and the M.Sc. (Hons.) degrees in electrical engineering from the National Polytechnic Institute, Mexico City, Mexico, in 1983 and 1986, respectively, and the Ph.D. degree from the University of Toronto, Toronto, ON, Canada, in 1992. He has held several academic positions in Mexico and has worked for the Canadian electric industry. Currently, he is an Associate Professor at Polytechnic Institute of NYU, New York. His research interests include the analysis of power phenomena under nonsinusoidal conditions, the transient and steady state analyses of power systems, the thermal rating of cables, and the calculation of electromagnetic fields applied to machine design and modeling.

Ashkan Farazmand was born in Tehran, Iran, in 1983. He received his M.Sc. (Hons.) from the University of Tehran in 2009, and is currently pursuing a Ph.D. in Electrical Engineering from the Polytechnic Institute of NYU, Brooklyn, New York. His research interests are design and analysis of transformers, electrical transients, derating of electrical machines under non-sinusoidal and unbalanced conditions, and power quality.

Pekir Joseph (S'09) was born in Brooklyn, New York in 1987. He received his Bachelor degree in Electrical Engineering in 2009 and his Master's degree in Power System Engineering in 2011, both, at the Polytechnic Institute of New York University. His research interests are in electrical transients, switching surges, relay protection and coordination, transmission and distribution, and inrush currents in transformers.

A Comparative Study on π and T Equivalent Models for the Analysis of Transformer Ferroresonance

Saeed Jazebi, *Student Member, IEEE*, Ashkan Farazmand, Brahadeesh Perinkolam Murali, and Francisco de León, *Senior Member, IEEE*

***Abstract*—The performance of the T and the π equivalent models used to represent transformers are tested under ferroresonance. Comparisons between simulations and laboratory experiments show the superiority of the π equivalent circuit.**

***Index Terms*—Ferroresonance, transformer modeling.**

I. Introduction

FERRORESONANCE may cause severe temporary over-voltages and damage the internal or external insulation of transformers. To predict possible over-voltages, proper modeling of ferroresonance is required for computer simulation. The T equivalent circuit is the most common representation of a two winding transformer [1]; see Fig. 1(a). An alternative, the π model [2], is a duality derived representation for a transformer that has advantages over the T model; see Fig. 1(b). In this paper, the T and π models are compared using time-domain simulations against laboratory experiments. The results show that the T model may produce large errors while the π model predicts properly the occurrence of ferroresonance. All simulations in the paper are carried out with the EMTP considering detailed representation of the hysteresis curves (except when noted) including non-linear magnetization and losses.

II. Simulations Versus Laboratory Experiments

Two 1 kVA, 120:120 V transformers (T1 and T2) with electrical parameters presented in Table I are selected. T1 has typical impedance parameters for a small power transformer, while T2 has been selected because it has a substantially larger leakage inductance and serves to accentuate the differences between the two circuits. The equivalent circuits for the experimental setup are depicted in Fig. 1. The parameters are obtained from the standard impedance and open circuit tests according to the IEEE Std C57.12.91-1995.

A large number of experiments have been carried out with the secondary of the transformers open circuited and applying rated voltage. Ferroresonance is chaotic and depends on initial conditions. To get consistent results, the core was demagnetized and the series capacitor was discharged before each experiment. We made sure that the results were consistent, and not affected by the chaotic nature of ferroresonance. Only three cases are discussed here. The first test is on T1 when a 20 μF capacitance was connected in series with the terminals. Both models show the occurrence of ferroresonance with voltages within a few percent error when compared to the experiments (details are not presented).

TABLE I
Electrical Parameters of Transformers

Code	R_1 (Ω)	R'_2 (Ω)	R_m (Ω)	L_s (mH)	$L_{m\text{-}lin}$ (mH)	$L_{m\text{-}sat}$ (mH)
T1	0.277	0.300	1,415.9	0.23	1,284.7	316
T2	0.306	0.305	1,074.7	8.78	1,669.6	463

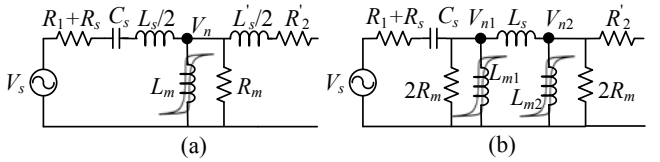

Fig. 1. Equivalent circuit of the experimental setup; a) π model; b) T model.

In the second experiment, ferroresonance occurs on T2 with the series 20 μF capacitance (see Figs. 2 and 3). Note however, that the T model exhibits a completely different behavior than the measurements. The mismatch is evident in both voltage and current; and even the frequency of oscillation is different. The computed overvoltage is 44 % higher than the experimental result. On the other hand, the current and voltage of the π model are visibly correct with a relative difference of maximum about 5% with respect to the experimental results.

The third experiment presents ferroresonance between T1 and a 60 μF capacitance. The voltage waveforms are presented in Fig. 4. One can note that the experiments and the π model show a normal operating condition (no ferroresonance), but the T model predicts ferroresonance.

III. Discussion

During ferroresonance, transformers have transitions between the linear and the nonlinear regions of the hysteresis curve. In this section, to study the performance of the transformers, the nonlinearities are represented by piecewise-linear models with only two sections (see Fig. 5). Parameters $L_{m\text{-}lin}$ and $L_{m\text{-}sat}$ are the slopes of the linear and deep saturation parts of the magnetizing curve respectively.

In the π model, there exist two shunt magnetizing branches with internal nodal voltages denoted V_{n1} and V_{n2}. The (internal) voltage of the T model's magnetizing branch is V_n (see Fig. 1). The relations between the internal node voltages and the source voltage, neglecting all damping components are:

$$\frac{V_n}{V_s} = \frac{2C_s L_m \omega^2}{C_s(L_s + 2L_m)\omega^2 - 2} \qquad (1)$$

S. Jazebi, A. Farazmand, B. Murali, and F. de León are with the department of Electrical and Computer Engineering, Polytechnic Institute of New York University, Six Metrotech Center, Brooklyn, NY, 11201 (e-mails: jazebi@ieee.org, afaraz01@students.poly.edu, brahadeesh.murali@gmail.com, fdeleon@poly.edu).

$$\frac{V_{n1}}{V_s} = \frac{C_s L_{m1}(L_s + L_{m2})\omega^2}{C_s L_{m1}(L_s + L_{m2})\omega^2 - L_{m1} - L_{m2} - L_s} \qquad (2)$$

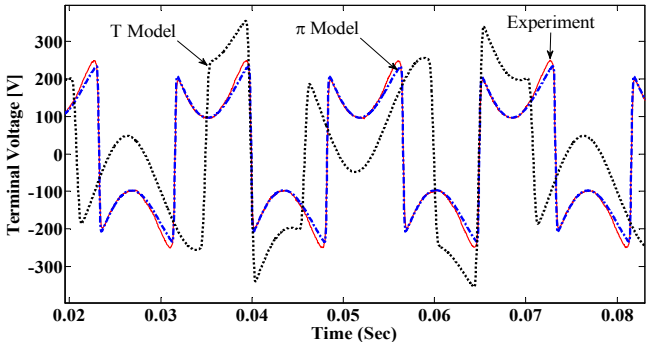

Fig. 2. Terminal voltage of T2 with 20 μF series capacitance.

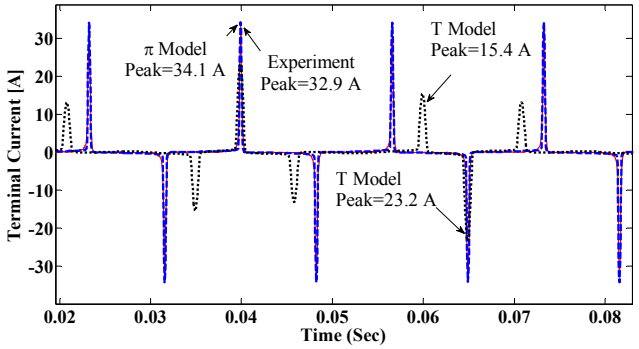

Fig.3. Terminal current of T2 with 20 μF series capacitance.

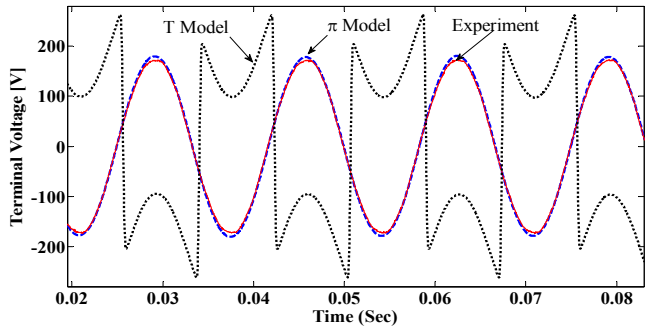

Fig. 4. Terminal voltage of T1 with 60 μF series capacitance.

$$\frac{V_{n2}}{V_s} = \frac{C_s L_{m1} L_{m2}\omega^2}{C_s L_{m1}(L_s + L_{m2})\omega^2 - L_{m1} - L_{m2} - L_s} \qquad (3)$$

To highlight the difference in the resonance behavior of the two equivalent circuits, three cases are investigated:

1) L_m=0.5L_{m1}=0.5L_{m2}=$L_{m\text{-}lin}$ (non-saturated conditions)
2) L_m=0.5L_{m1}=0.5L_{m2}= $L_{m\text{-}sat}$ (saturated conditions)
3) L_m=0.5L_{m1}=$L_{m\text{-}sat}$, 0.5L_{m2}=$L_{m\text{-}lin}$ (L_m and L_{m1} saturated and L_{m2} non-saturated)

The saturation status (instantaneous flux) depends on the instantaneous voltages applied to the non-linear inductances; see (1) to (3). In the first case, it is assumed that both models are working in the linear part of the magnetizing curve. The second case is when both T and π models are saturated. Due to the leakage inductance between the magnetizing branches in the π model, there are differences between V_{n1} and V_{n2}. Differences become more noticeable for transformers with large leakage inductance. Thus, it is possible that L_{m1} goes into saturation while L_{m2} is still working in its linear part; this situation corresponds to Case 3. For transformer T2, the terminal voltage versus the value of the series capacitance is presented in Fig. 6. The figure shows that the resonance behavior of T and π models is quite different at various operating conditions. This can also be observed from the capacitance values that would produce resonance:

$$C_\pi = \frac{L_{m1} + L_{m2} + L_s}{L_{m1}(L_s + L_{m2})\omega^2} \qquad C_T = \frac{2}{(L_s + 2L_m)\omega^2} \qquad (4)$$

where L_m, L_{m1} and L_{m2} can be substituted by $L_{m\text{-}lin}$ or $L_{m\text{-}sat}$ depending on the values of the instantaneous voltages V_n, V_{n1} and V_{n2}. Note that, the differences between C_π and C_T become larger for transformers with higher leakage inductance. For transformer T1, the resonance response of the models is much closer than for T2 (results not shown). However, sometimes the T model fails; Fig. 4 shows a case when the T model predicts ferroresonance when it does not occur in reality.

A comprehensive sensitivity analysis on transformer parameters (L_s/L_m) with respect to terminal behavior of both models for the calculation of inrush currents is presented in [3].

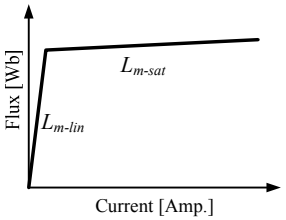

Fig. 5. Simplified magnetizing curve for T2 used for analysis purposes.

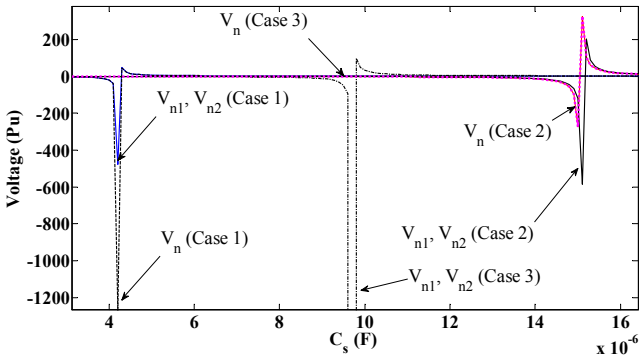

Fig. 6. Non-linear branch voltages by varying series capacitance for T2.

IV. Conclusions

This letter has shown that the T model may fail to reproduce ferroresonance measurements, while the π model predicts the measurements adequately in all tested cases.

V. References

[1] Slow Transients Task Force of the IEEE. Modeling and Analysis of System Transients Using Digital Programs Working Group "Modeling and Analysis Guidelines for Slow Transients--Part III: The Study of Ferroresonance," *IEEE Trans. Power Del.*, vol. 15, pp. 255–265, Jan. 2000.

[2] F. de León, P. Gómez, J. A. Martinez-Velasco, and M. Rioual, Chapter 4, "Transformers" in *Power System Transients: Parameter Determination*, CRC Press, Boca Raton FL, 2009, pp. 177-250.

[3] F. de León, A. Farazmand, and P. Joseph, "Comparing the T and π Equivalent Circuits for the Calculation of Transformer Inrush Currents", paper accepted for publication, *IEEE Trans. on Power Del,* July 2012.

Leakage Inductance Design of Toroidal Transformers by Sector Winding

Francisco de León, *Senior Member, IEEE*, Sujit Purushothaman, *Member*, *IEEE,* and Layth Qaseer

***Abstract*— Toroidal transformers are commonly used in power electronics applications when the volume or weight of a component is at a premium. There are many applications that require toroidal transformers with a specific leakage inductance value. A transformer with a large (or tuned) leakage inductance can be used to eliminate a (series) filter inductor. In this paper a procedure to control the leakage inductance of toroidal transformers by leaving unwound sectors in the winding is presented. Also a simple formula is obtained in this paper that can be used to design transformers with a specific leakage inductance value. The leakage inductance formula is expressed as a function of the number of turns, the geometrical dimensions of the toroidal transformer, such as: core internal diameter, external diameter and height, and the angle of the unwound sector. The formula of this paper has been obtained and validated from laboratory experiments and hundreds of three-dimensional finite element simulations. The techniques described in this paper will find applications in the design of transformers that in addition of providing voltage boosting need to double as filters.**

***Index Terms*— Leakage inductance, toroidal transformers, sector winding.**

I. Introduction

TOROIDAL transformers with enlarged leakage inductance find applications in several power electronics devices that require a transformer with a specified leakage inductance value. For example, a transformer with a large leakage inductance can be used to eliminate a series inductor for filtering or tuning. Among the applications we can find a number of converters [1]-[4] and electromagnetic noise reduction transformers [5]-[10]. Particular leakage inductance values for transformers are used to distribute the power flow of parallel paths and to limit the short circuit currents [11].

Tape wound toroidal transformers made with grain oriented silicon steel are more efficient, smaller, cooler, and emit reduced acoustic and electromagnetic noise when compared with standard transformers built on staked laminations [12]. Toroidal transformers are commonly used in the power supply of audio, video, telecommunications, and medical equipment. These transformers are finding new applications in small to medium size UPS systems and in the lighting industry (especially in halogen lighting). Aircrafts have also benefited from the advantages of toroidal transformers [13].

The equations for computing the leakage inductance of E-I transformers at 60 Hz are readily available [14], [15]. Also, available are analytical expressions for computing winding losses and leakage inductance for high frequencies [16], [17].

The theory for toroidal transformers is not nearly as advanced as the theory for E-I transformers. This may be because at this moment toroids are restricted to small powers (tens of kVA) and low voltages (possibly up to a few kilovolts). In references [18] and [19] an analytical study of the losses at high frequency was presented for toroidal inductors, but the leakage inductance was not considered.

This work was supported by the U.S. Department of Energy under Grant DEOE0000072.

F. de León is with the Department of Electrical and Computer Engineering of Polytechnic Institute of New York University, Six Metrotech Center, Brooklyn, NY, 11201 (email: fdeleon@poly.edu).

S. Purushothaman is with FM Global Research, 1151 Boston Providence Turnpike, Norwood, MA 02062 (email: sujitp@ieee.org)

L. Qaseer is with Al-Khwarizmi College of Engineering, University of Baghdad, Baghdad, Iraq (email: laythqaseer@yahoo.com).

Perhaps, due to the complexity of the winding, researchers have preferred numerical solutions such as finite elements [20], [21]. There exists a semi-empiric formula for computing the leakage inductance of small toroidal common mode chokes [22]. However, in all our cases the formula in [22] predicted erroneous values. We should mention that there is a substantial difference in the sizes of our transformers and those of [22].

In [23] an analytical formulation for computing the leakage inductance of toroidal transformers with circular cross-sectional area is derived elegantly from the solution of Maxwell Equations. In [23] the toroidal core is opened and elongated to form a linear rod with circular cross-sectional area and Fourier techniques are applied (this is possible because the rod is terminated with magnetic end planes, which are replaced by images on the infinite rod). This works well in [23] because the toroids are very small and the windings, which never overlap, cover only a small portion of the core perimeter. The transformer cores of this paper are much larger and the windings overlap. Additionally the cores here do not have circular cross-sections.

A technique to enlarge the leakage inductance using inter-winding spacing and magnetic insets is given in [24]. The technique is highly controllable and can achieve large increases in leakage inductance; however, the transformer becomes larger, heavier and more expensive. Sector winding, as advanced in this paper, produces very large increases in the leakage inductance at virtually no added cost or weight. The method of [24] is applicable for relatively small leakage inductance gains, say for a target increase of up to 5 times the natural (or minimum) leakage inductance (L_0). The method promoted in this paper will find applications when the desired leakage inductance is several orders of magnitude larger than the natural value.

Recently, in [25] a turn-by-turn formulation to compute the leakage inductance in common mode chokes was presented. A rectangular turn is broken into four straight line conductors and approximate solutions on infinitely long geometries are used for each region. Thus, the inner conductor is modeled as an eccentric conductor inside of a ferromagnetic cylinder. Similarly, the outer conductor is represented as being outside the ferromagnetic cylinder. The lateral conductors are considered as filamentary currents on top of an infinite ferromagnetic plane with the method of images. The method of [25] is applicable to toroids with a few thick turns that can be wound in only one layer (for example common mode chokes), but it is not applicable to multi-layer transformers. The frequency dependency is considered by including the resistances and the capacitances producing a wideband circuital model. Previously, in [26] a method to measure the leakage inductance of multi-winding chokes was presented. A model to describe the terminal behavior is given, but there are no equations to compute the parameters from dimensions.

The objectives of this paper are two: First is to present a methodology to increase the leakage inductance of toroidal transformers by leaving unwound sectors in the windings (see Fig. 1). Second is to propose an equation for the calculation of the leakage inductance suitable for a design program.

Although toroidal transformer manufacturers know that leaving unwound sectors increases the leakage inductance, the desired leakage inductance value is obtained by trial and error. In this paper the transformer leakage inductance is expressed as a function of the number of turns (N), the geometrical dimensions of the toroidal transformer, internal diameter (ID), external diameter (OD) and height (HT), and the angle of the unwound sector (θ).

This paper deals with a wide range of power transformer sizes of rectangular cross-sectional area. The core dimensions cover the following range: height from 1 to 6 inches; external diameter between 4 and 13 inches; and internal diameter from 1 to 10 inches. These combinations cover most of the power conditioning application today from one kVA to perhaps one hundred kVA (depending on the switching frequency). We have only experimented with unwound sector angles from 30° to 180°. It is quite possible, however, that the equations of this paper are applicable to much larger transformers with larger unwound angles. A few numerical experiments shown below indicate this, but more research is needed to make stronger claims.

The formula proposed in this paper is obtained from the observation of the behavior of the leakage inductance when the construction parameters of toroidal transformers are varied. More than 400 3D FEM (Finite Elements) simulations have been per-

formed to cover a very wide range of applications. Over 20 prototypes were built to validate the FEM simulations and proposed formula.

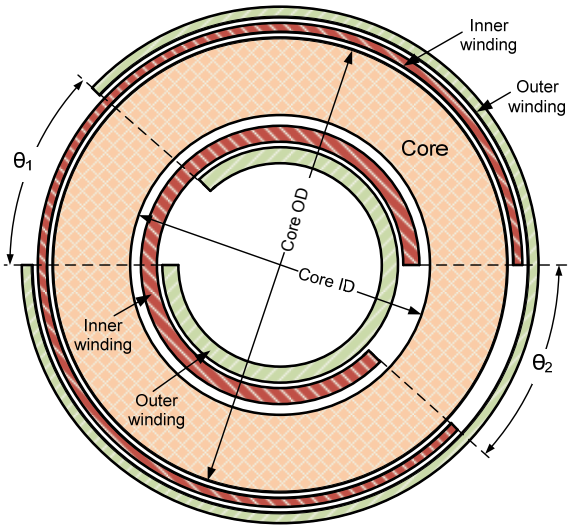

Fig. 1. Toroidal transformer with sectored windings.

II. Theoretical Considerations

To make the presentation accessible to wider audiences and to establish the nomenclature, we start by presenting the basic concepts of leakage flux for toroidal transformers. Two geometrical arrangements are discussed: toroidal transformers that are wound around the 360° and toroids with sectored windings. Leakage flux is defined for a pair of windings as the flux that links only one winding and does not link the other winding. The corresponding leakage inductance is obtained in the laboratory through the short circuit test, which consists of feeding a winding with rated current when the other winding has its terminals short-circuited. The test can be simulated with FEM to obtain the leakage inductance. Additionally, with simulations one can fully eliminate any influence from the magnetizing current, while the short circuit-test does not fully cancel the magnetizing flux.

A. Toroidal Transformers with 360° Windings

The leakage flux in a toroidal transformer, whose windings are one on top of the other for the entire 360°, is produced by the current in the windings that are equal in magnitude (i.e. $N_1I_1 = N_2I_2$), but opposite in direction. By forcing $N_1I_1 = N_2I_2$ there is no (magnetizing or leakage) flux in the core. As shown in Fig. 2 the leakage flux does not start nor it ends in the core, but closes in itself. The left-hand quadrant shows the surface plot of the distribution of the magnetic flux density while the right-hand quadrant shows the direction of the streamlines (concentric circles). Note that most of the leakage flux is in the insulation between the windings; some flux is also present in the windings, but there is no flux outside the region occupied by the windings. The leakage inductance for such geometry is computed in [24] from the energy stored yielding:

$$L_0 = \frac{N^2 \mu_0}{2\pi} \sum_{i=1}^{5} \eta_i \left(\alpha_i \, a + \phi_i \, g + \beta_i \, b \right) \qquad (1)$$

where variables η_i, α_i, β_i, and ϕ_i are computed from the radii of the windings and include the factors of partial linkage fluxes in the windings; a, b and g are the thicknesses of the inner winding, the outer winding and the insulation layers, respectively; all the details are given in the Appendix.

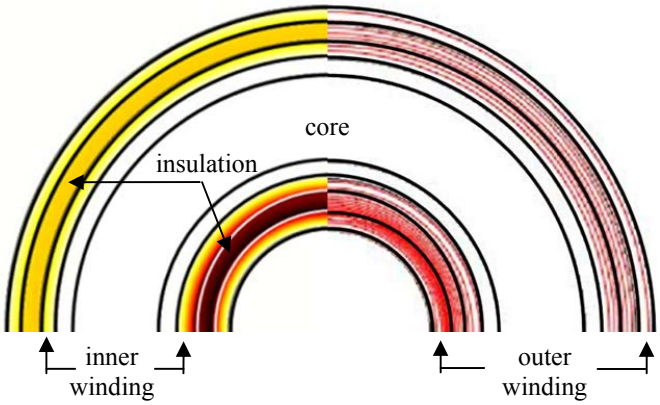

Fig. 2. Axial view of a toroidal transformer with windings covering 360°. The left-hand quadrant shows the surface plot of the distribution of the magnetic flux density while the right-hand quadrant shows the direction of the streamlines (concentric circles).

B. Sectored Wound Toroidal Transformers

In sectored wound transformers, i.e. when the windings do not cover the entire 360°, the leakage flux follows a completely different path. Fig. 3 shows the top view of the leakage flux distribution. One can see that in this case the path of the leakage flux includes a section of the core. The amount of leakage flux that a winding links depends on the sector that is not wound. From Fig. 3, it is possible to see that many lines of flux only link partially the winding. We make the remark that the shape of the leakage flux does not change significantly as the angle of the wound sector varies. However, the intensity of the leakage flux increases substantially as the unwound angle increases. It should be mentioned that the flux in the core contributes very little to the leakage inductance since the energy stored depends on the square of the magnetic field strength (H), which is very small in the core due to its high permeability.

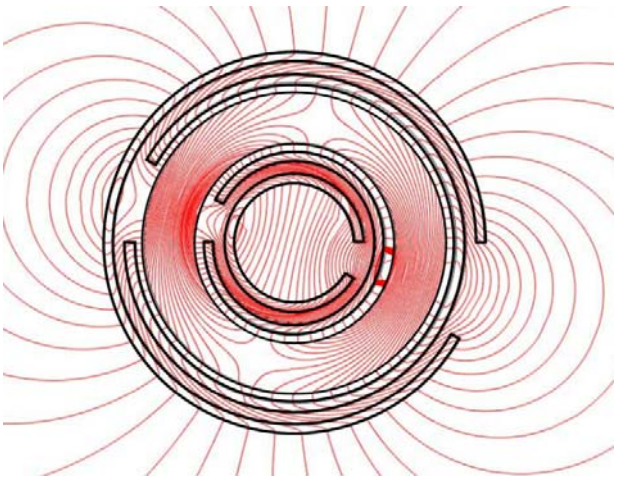

Fig. 3. Top view of the distribution of the leakage flux in a sectored wound transformer.

III. Initial Experimentation

A first set of prototypes were built consisting of 7.25 kVA transformers V_1 = 215 V, V_2 = 1,928 V. These transformers are used in a PWM application to drive a sonar amplifier. A standard toroidal transformer design for the specified power and voltage levels has a leakage inductance of under 10 μH. For those conditions an external series inductor of around 800 μH is needed to help filtering the input of the amplifier at 450 Hz. Alternatively, we designed a transformer with increased leakage inductance. The transformer parameters are N_1 = 97 turns, N_2 = 870 turns. The core dimensions are: *OD* = 175 mm, *ID* = 100 mm, *HT* = 45 mm.

Table I shows the total leakage inductance, referred to the low voltage side (N=97), of a set of prototypes built with equal unwound sectors in both windings, but displaced 180°; see Fig. 4. As a reference, note that the magnetizing inductance of these toroidal transformers is about 1 H, which is much larger than the natural inductance of L_0 = 9.3 μH (for θ =0°) and even substantially larger than the largest leakage we measured of 2.6 mH resulting from sectored windings (for θ =180°) .

Fig. 5 shows the variation of the leakage inductance with respect to the unwound angle, which seems to be perfectly quadratic. Therefore, added to the plot of Fig. 5 there is a fitted quadratic equation of the form:

$$L = K\theta^2 \qquad (2)$$

For this example, $K = 7.203\times10^{-2}$ when the unwound angle θ is given in degrees and L in μH.

TABLE I
MEASURED LEAKAGE INDUCTANCE VERSUS UNWOUND ANGLE

Point	Angle $\theta_1 = \theta_2$ [Degrees]	L (measured) [μH] N=97
0	0	L_0 = 9.3
1	15	17.6
2	30	56.7
3	45	151
4	65	320
5	80	499
6	100	777
7	120	1032
8	180	2600

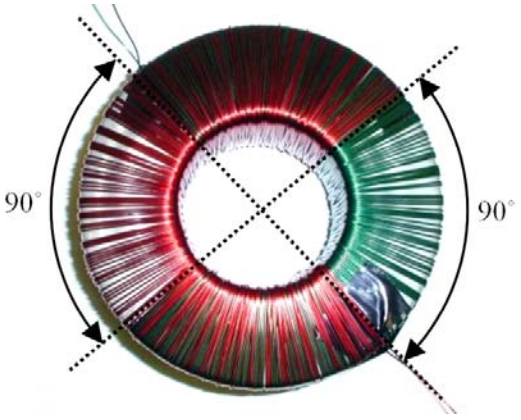

Fig. 4. Toroidal transformer with 90° sectored windings displaced 180°.

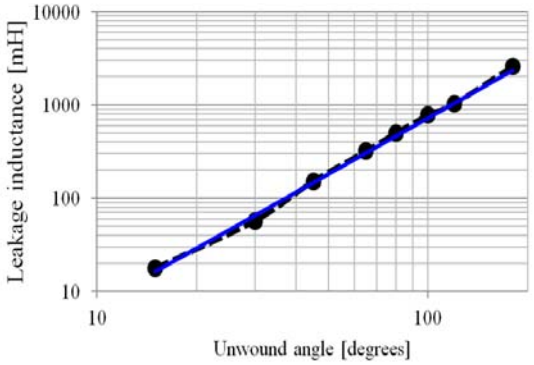

Fig. 5. Fitting a quadratic function to the experimental data.

It is difficult to control the inter-turn spacing with high speed winding machines and overlapping frequently occurs. However, "messy" windings when are elements of a sector winding strategy have relatively little effect in the leakage inductance (provided that they cover certain angle). A few experiments using "bank winding", which consists in purposely producing overlapping by changing the rotation direction around the rollers, show very little increase in the leakage inductance. However, to obtain consistent leakage inductance values, it is important to precisely control the unwound angle. For this, a physical barrier beyond which the winding cannot pass is used.

IV. Systematic Experimentation

A set of eleven prototypes was built with the purpose of shedding light on the parameters influencing the value of *K*. This set, in addition to varying the unwound sector, also included variation of other geometric parameters of the core i.e. *ID*, *OD* and *HT*. Table II gives the geometric details of the prototypes along with the leakage inductance obtained in the laboratory with short circuit (SC) test. Measurements with an LCR meter (at 60 Hz) confirmed the results of the SC tests. In Table II the value of L_0 has been added as reference. One can appreciate that L_0 is negligible for unwound angles of 90° and larger. Prototypes 1, 2 and 3 have all parameters but *ID* constant. These three prototypes can be used to study the effect of *ID* on the leakage reactance. Similarly, prototypes 3, 4 and 5 can be used to study effect of the variation of *OD* on the transformer leakage. Height variations can be studied with prototypes 5, 6 and 7. All prototypes have 400 turns on each winding.

TABLE II

Leakage Inductance Comparison between FEM and Short Circuit (SC) Tests on Prototypes with *N*=400

No	Core Dimensions [inch]			Angle θ	L_0	FEM *L*	SC test *L*	%
	OD	ID	HT	[deg]	[mH]	[mH]	[mH]	difference
1	10	8	2	180	0.322	42.71	45.27	-5.64
2	10	6	2	180	0.287	47.25	52.6	-10.17
3	10	4	2	180	0.252	51.40	53.14	-3.27
4	8	4	2	180	0.215	42.18	42.27	-0.21
5	6	4	2	180	0.179	32.72	36.65	-10.72
6	6	4	3	180	0.115	38.85	39.28	-1.10
7	6	4	1	180	0.363	26.24	28.11	-6.64
8	6	4	1	150	0.363	17.34	18.6	-6.78
9	6	4	1	110	0.363	8.80	9.14	-3.72
10	6	4	1	90	0.363	5.75	5.67	1.48
11	6	4	1	40	0.363	1.15	1.08	6.88

Although we found very little effect on the core losses at 60 Hz due to sector winding, it has been found in [27] that the core losses increase considerably due to the orthogonal flux in cut tape-wound cores at high frequencies. Therefore, although the techniques of this paper are directly applicable to ferrite cores over a wide frequency range, further investigation is needed to gauge the effect on losses for uncut tape-wound cores at high frequencies.

Measurements with the LCR meter at 1 kHz show an average reduction in the leakage inductance of about 12% from the value at 60 Hz; the larger the transformer, the larger the reduction. Further research will be carried out to model the frequency dependency of the leakage inductance in sectored winding toroidal transformers.

V. FEM Simulations

Three-dimensional (3D) finite element simulations are performed to generate additional cases needed for the derivation of a mathematical model. The leakage inductance is computed from the total energy stored in the magnetostatic field when one winding is fed with unity current in one direction and the second is fed with unity current in the opposite direction. This effectively eliminates any effect of the magnetizing current since $N_1I_1 = N_2I_2$ is strictly enforced. A total of 420 different transformer configurations were analyzed with 3D FEM simulations.

Even though the toroidal core is symmetric around the central axis, the windings are not. Each winding exists for $360^\circ - \theta$ degrees around the central axis as shown in Fig. 1; moreover the core height is not infinite in depth. Hence an axisymmetric or a two-dimensional (2D) model cannot be used to represent a sector wound toroidal transformer.

The windings are modeled as thin sheets carrying currents in opposite direction to simulate the conditions of the short-circuit test needed to measure the leakage inductance. The windings were initially modeled as volume regions with finite thickness having an impressed current density J, but it was found from many experiments that the coil thickness played only a minor role in the leakage inductance when there is an unwound sector of at least 30°. Hence the optimum FEM simulations use a current sheet to represent the windings. A cross section of the FEM model is presented in Fig. 6. It must be noted that such a 3D model consists of 100,000 to 200,000 second order finite elements and takes 30 minutes to solve using a server that has 24 cores in its CPU running at 3.33 GHz each as well as 96 GB of DDR3 RAM.

Table II shows the comparison between the experimental results and the corresponding 3D FEM simulations. One can appreciate that the simulations yield very good results when compared to the experiments. The small differences are attributed to manufacturing tolerances in the prototypes. Fig. 7 shows cuts of the front and top views of the distribution of the magnetic flux density.

The surface current densities K_{vertical} and $K_{\text{horizontal}}$ are chosen such that the total current is the same ($N_1I_1=N_2I_2$). While $K_{\text{horizontal}}$ is a function of spatial coordinates, K_{vertical} is constant in magnitude and is not a function of spatial coordinates. In a completely wound ($\theta = 0^\circ$) transformer, the leakage flux flows through the inter-winding gap, g and hence is a critical factor contributing in the leakage inductance; see [24]. In a sectored wound transformer, the leakage flux is dictated by θ, ID, OD and HT.

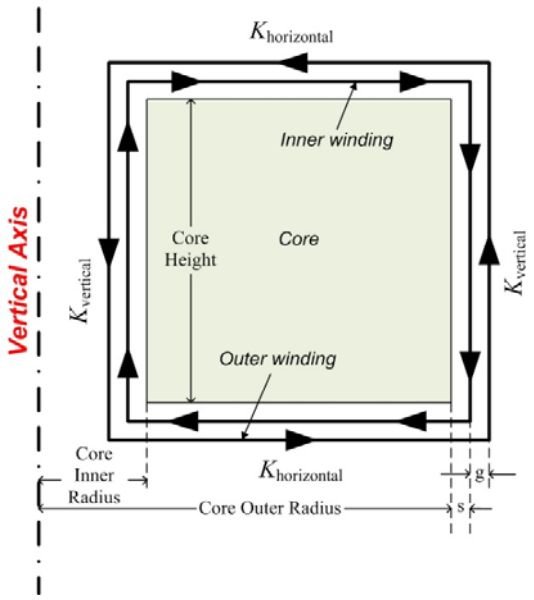

Fig. 6. Cross section of the FEM model.

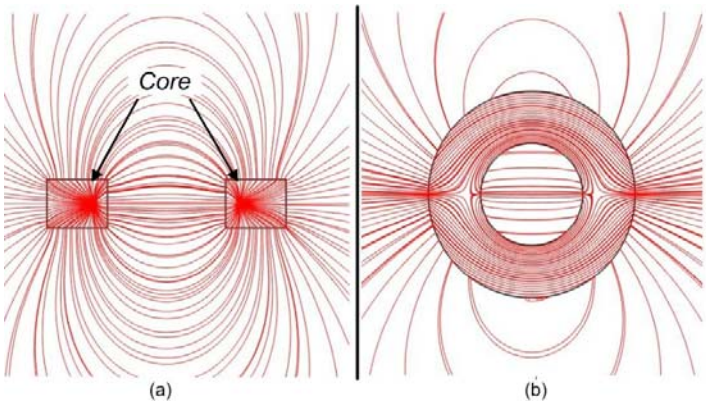

Fig. 7. FEM flux density streamline plot. (a) Front view; (b) Top view.

VI. Mathematical Model

The validation of the FEM simulations against experimental results, as shown in Table II, enables the derivation of a mathematical formula for the calculation of the leakage inductance of sectored winding toroidal transformers based on the results of FEM simulations. In this section a double regression method is employed to obtain a simple formula for the leakage inductance.

From numerous tests on transformers having the same number of primary and secondary turns of 400, it was found that there exists a linear relationship between the leakage inductance (L) and outer diameter of the core (OD). This can be written in the following form:

$$L = b_{10} + \beta_1 OD \qquad (3)$$

where L is the leakage inductance and β_1 is the contribution factor for outer diameter. Fig. 8 shows the relationship between the leakage inductance and the outer diameter, keeping all other parameters fixed (ID = 4", HT = 2"). Results are plotted for (unwound) sector angles of 60°, 70° and 80°.

Fig. 9 shows the relationship between the leakage inductance and the inner diameter (*ID*) when keeping the other parameters fixed (*OD* = 10", *HT* = 2"). Results are plotted for sector angles of 60°, 70° and 80°. It can be seen from Fig. 7 that the leakage inductance varies linearly in inverse proportion to the inner core diameter (*ID*), which can be expressed as

$$L = b_{20} + \beta_2 \ ID \tag{4}$$

where β_2 is the contribution factor for inner diameter.

We have also observed that the leakage inductance varies linearly with core height (*HT*) as:

$$L = b_{30} + \beta_3 \ HT \tag{5}$$

where β_3 is the contribution factor for core height. Fig. 10 shows the relationship between the leakage inductance and the core height when keeping all other parameters fixed (*OD* = 6", *ID* = 4"), for sector angles of 90°, 100° and 110°.

Finally, we note that the leakage inductance varies with the unwound sector angle as a quadratic function. This is given as:

$$L = b_{40} + c_1\theta^2 \tag{6}$$

where θ is the sector angle in radians. Fig. 11 shows the relationship between the leakage inductance and the unwound sector angle for a transformer keeping other parameters fixed (*OD* = 6", *ID* = 4"). Results are plotted for three cases with core height = 2", 3" and 4". The sector angle is varied from 10° to 350° to cover the entire spectrum. The slope $m = 2$ of the lines in the log-log plot confirms the quadratic variation.

Consistent with theory, all analytical formulas for the calculation of inductances reveal that they depend of the square of the number of turns. Combing the above four equations (3)–(6) into a single equation gives an inductance formula as a function of the inner diameter, outer diameter, core height, sector winding angle and the number of turns as follows:

$$L = L_0 + \mu_0 N^2 \left(\beta_1 OD + \beta_2 ID + \beta_3 HT\right) \tag{7}$$

where L_0 is the leakage inductance for a transformer with complete 360° windings or sector angle of 0°. The procedure to evaluate L_0 has been given in [24].

Exhaustive analysis of the numerical results has yielded that the contribution factors, β_i are quadratic functions of the sector angle θ as follows:

$$\begin{aligned} \beta_1 &= k_1\theta^2 \\ \beta_2 &= k_2\theta^2 \\ \beta_3 &= k_3\theta^2 \end{aligned} \tag{8}$$

β_1, β_2 and β_3 correspond to the slopes of the lines of Figs. 8, 9, and 10, respectively. Hence (7) simplifies to:

$$L = L_0 + \mu_0 N^2 \left(k_1 OD + k_2 ID + k_3 HT\right)\theta^2 \tag{9}$$

OD, *ID* and *HT* are given in inches, θ in degrees and *L* is in milli-Henry. The thickness of the windings *a* and *b* in equation (1) only affects L_0.

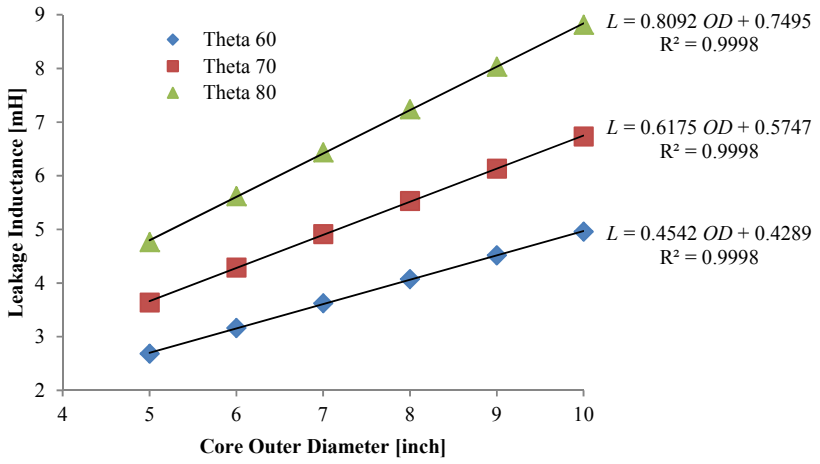

Fig. 8. Variation of leakage inductance with core outer diameter. The dots correspond to the simulated values. The trend lines and their equations are also presented.

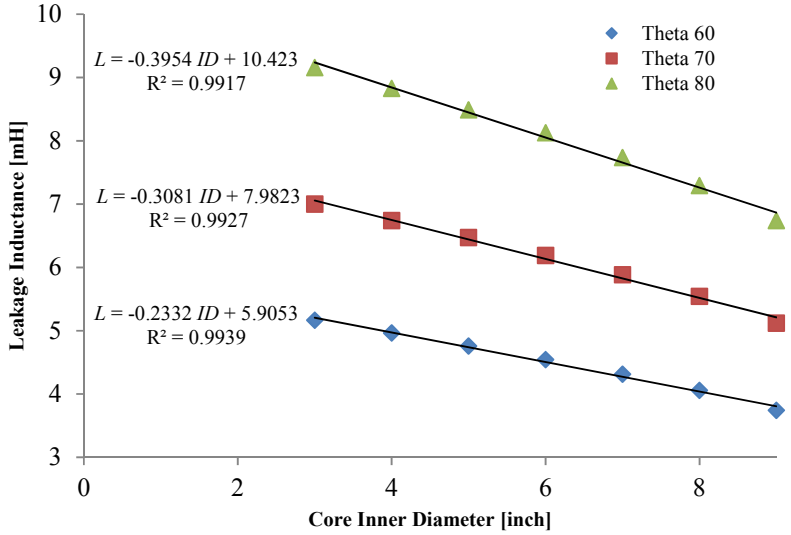

Fig. 9. Variation of leakage inductance with core inner diameter. The dots correspond to the simulated values. The trend lines and their equations are also presented.

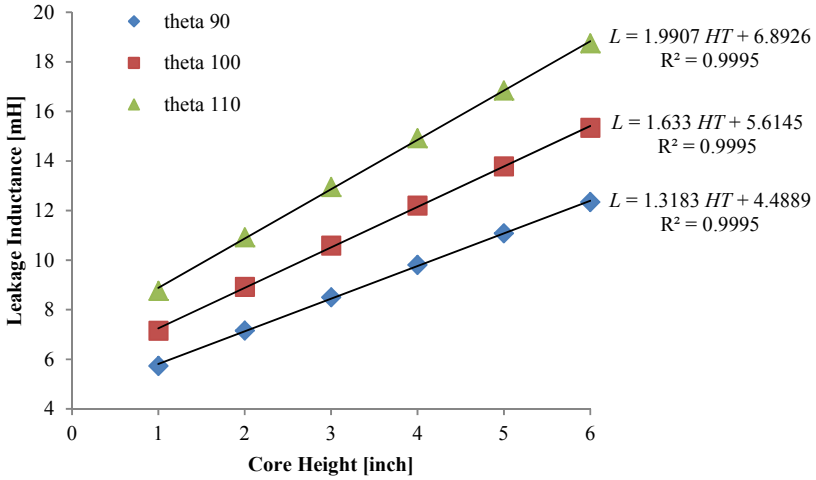

Fig. 10. Variation of leakage inductance with core height. The dots correspond to the simulated values. The trend lines and their equations are also presented.

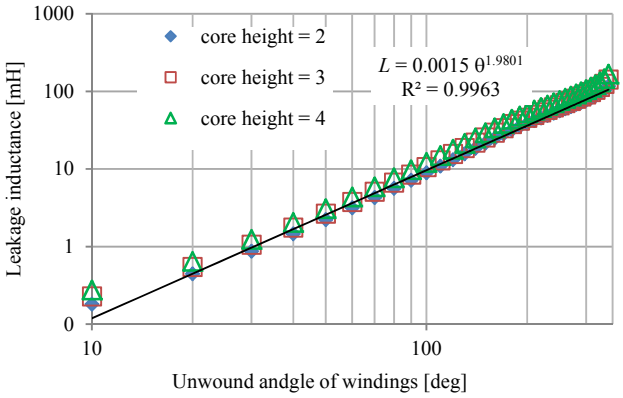

Fig. 11. Variation of leakage inductance with unwound sector winding angle. The dots correspond to the simulated values. The trend line for core height = 3 inch and its equation is also presented.

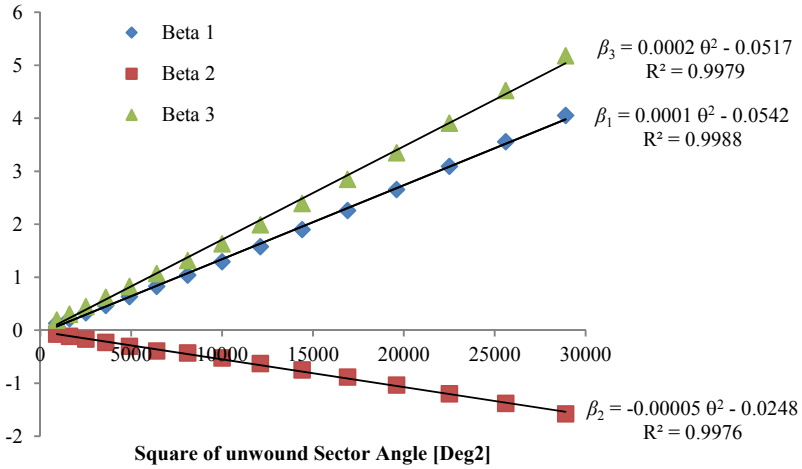

Fig. 12. Variation of β_i with unwound sector winding angle. The dots correspond to the simulated values. The trend lines and their equations are also presented.

The values of k_1, k_2 and k_3 in (9) are evaluated by a two step regression readily available in Excel. Multiple cases are generated using the FEM model described in Section V. The geometric parameters *ID*, *OD* and *HT* are varied in steps for every sector angle θ.

A linear regression is first performed on data with constant θ and the values of β_1, β_2 and β_3 are evaluated. This is repeated for various values of sector angle θ, yielding different values of β_i. 210 of the 420 cases generated by the FEM model were used for this regression. It must be noted that the coefficient of determination, R^2 is larger than 99% for all the cases indicating an excellent fit. Fig 12 shows the variation of β_i with respect to the square of the sector angle.

Fig. 12 confirms the quadratic variation of β_i with sector angle given in (8). The second regression is performed on the data plotted in Fig. 12 to satisfy (8) yielding the values of k_i as follows:

Units for *OD*, *ID*, *HT*	k_1	k_2	k_3
mm	2.6444×10^{-5}	-1.104×10^{-5}	3.178×10^{-5}
inch	6.7168×10^{-4}	-2.8043×10^{-4}	8.0723×10^{-4}

k_1, k_2 and k_3 are the contributing factors of the geometric parameters of the core *OD*, *ID* and *HT*, respectively. When the geometric dimensions of the transformer are given in mm, k_1, k_2 and k_3 have units of degree^{-2}.

The double regression used in this paper (to model the leakage inductance for sectored winding transformers) gives a good balance between simplicity and accuracy. Equation (9) is very simple, yet sufficiently accurate for engineering design. We have investigated the effects of fitting curves for other variables and ratios. For example, it was experimented with ratios of OD/ID, differences (OD-ID), compound ratios as (OD-ID)/(OD+ID), and their powers (squares and roots). Slightly more accurate results can be obtained with some combinations, however the resulting equations are substantially more intricate than (9).

VII. Results

Table III presents the comparison between 24 of the close to 250 cases used for validation of the proposed model against FEM simulations. These cases are provided to cover a wide range of core dimensions. For each set of *OD*, *ID* and *HT*, the unwound sector angle θ, is set to 60°, 120° and 240°. Most of the results match very well. It was observed that transformers with cross sectional area close to a square aspect ratio ($HT \cong (OD–ID)/2$) have errors smaller than 5%. Tall and flat looking transformers have errors smaller than 10%. If there are no special constraints on dimensions, square aspect ratio is preferred because the turn length is shorter. The value of L_0 has been included in Table III. One can appreciate that L_0 in all these cases is negligible, but this is not always the case. For smaller angles, say up to 60°, L_0 may play a role. Note that the values presented in Table III do not match with the same degree of accuracy as the cases used to fit the equations (as presented in Figs. 8 to 12). This is so because Table III gives the extremes used to validate the model; these cases represent the worst case scenarios.

To gauge the validity of the formulas for large transformers, a set of FEM simulations for unrealistically large transformers were performed. We used: *OD* = 6 m, *ID* = 4 m and *HT* = 1 m for unwound angles of 60°, 120°, 240°, and 270°. We found differences between FEM and (9) of only -6.80%, -1.56%, -2.08%, and -6.58%, respectively.

VIII. Conclusions

A methodological technique to increase considerably the leakage inductance of power toroidal transformers by leaving unwound sectors has been developed. Additionally, a formula to compute the leakage inductance for sectored wound transformers has been derived from the observation of its behavior through hundreds of 3D FEM simulations. The leakage inductance is computed with a simple formula from the physical quantities of the transformer: number of turns and core dimensions: internal and external diameter, height, and the angle of the unwound sector. Therefore, the equation is suitable for implementation in transformer design programs or even hand calculations. The FEM simulations and the formula have been corroborated experimentally with over 20 prototypes of varied sizes and winding conditions.

Acknowledgments

The first author would like to thank the people (co-workers and students) who have worked with him in this project over the past 12 years; in chronological order: Valeriu Tatu, Salvador Magdaleno, Ivan Hernandez, Noel Augustine, and Chandira Prabhu.

TABLE III

COMPARISON BETWEEN FEM AND PROPOSED MODEL (9)

No	Core Dimensions [inch]			Unwound Angle θ [deg]	L[mH]				% difference
	OD	ID	HT		FEM	L_0 (1)	Sector Model L - L_0 in (9)	Total (9)	
1	4	1	1	60	2.48	0.049753	2.33	2.380	6.05
2				120	9.11	0.049753	9.30	9.350	-2.09
3				240	35.19	0.049753	37.22	37.270	-5.77
4			4	60	4.57	0.003843	4.08	4.084	10.72
5				120	16.01	0.003843	16.32	16.324	-1.94
6				240	61.30	0.003843	65.26	65.264	-6.46
7		3	1	60	1.88	0.068701	1.92	1.989	-2.13
8				120	7.59	0.068701	7.68	7.749	-1.19
9				240	29.91	0.068701	30.72	30.789	-2.71
10			4	60	3.76	0.011310	3.67	3.681	2.39
11				120	14.63	0.011310	14.69	14.701	-0.41
12				240	57.43	0.011310	58.77	58.781	-2.33
13	12	4	2	60	5.91	0.079918	6.19	6.270	-4.74
14				120	24.30	0.079918	24.76	24.840	-1.89
15				240	94.87	0.079918	99.05	99.130	-4.41
16			6	60	8.46	0.023534	8.53	8.554	-0.83
17				120	34.28	0.023534	34.11	34.134	0.50
18				240	132.32	0.023534	136.45	136.474	-3.12
19		9	2	60	4.78	0.101876	5.18	5.282	-8.37
20				120	20.20	0.101876	20.70	20.802	-2.48
21				240	79.03	0.101876	82.81	82.912	-4.78
22			6	60	7.32	0.032882	7.51	7.543	-2.60
23				120	30.37	0.032882	30.05	30.083	1.05
24				240	117.49	0.032882	120.21	120.243	-2.32

APPENDIX – CALCULATION OF L_0

In this section, the necessary information to compute L_0 using (1) is reproduced from [24]. The geometrical arrangement and the definition of all variables are given in Fig. 13. The coefficients η_i, α_i, β_i, and ϕ_i for the different sections are given in Table V. The following relationships are needed to complete the information:

$$R_{mj} = \left(R_j + R_{j+1}\right)/2 \qquad (11a)$$

$$t_1 = 3a + 4\left(s + b + g\right) \qquad (11b)$$

$$t_2 = g + 2\left(s + b\right) \qquad (11c)$$

$$t_3 = 3b + 4s \qquad (11d)$$

TABLE V
COEFFICIENTS FOR THE DIFFERENT COMPONENTS OF THE LEAKAGE INDUCTANCE FORMULA GIVEN IN (1)

	Coefficient			
Section	η_i	α_i	ϕ_i	β_i
1	h	$\frac{R_{m1}}{3R_2^2}$	$\frac{R_{m2}}{2R_2R_3}$	$\frac{R_{m3}}{3R_3^2}$
2	h	$\frac{R_{m7}}{3R_7^2}$	$\frac{R_{m6}}{2R_6R_7}$	$\frac{R_{m5}}{3R_6^2}$
3	$\frac{R_e^2-R_i^2}{R_eR_i}$	$\frac{1}{3}$	1	$\frac{1}{3}$
4	$\frac{1}{2R_2^2}$	$\frac{R_{m1}t_1}{6}$	$R_{m2}t_2$	$\frac{R_{m3}t_3}{6}$
5	$\frac{1}{2R_6^2}$	$\frac{R_{m7}t_1}{6}$	$R_{m6}t_2$	$\frac{R_{m5}t_3}{6}$

REFERENCES

[1] J. O. Krah and J. Holtz, "Total Compensation of Line-Side Switching Harmonics in Converter-Fed AC Locomotives", IEEE Transactions on Industry Application, Vol. 31, No.6, November/December 1995, pp. 1264-1273.

[2] S. Saetieo, R. Devaraj, and D. Torrey, "The Design and Implementation of a Three-Phase Active Power Filter Based on Sliding Mode Control", IEEE Transactions on Industry Application, Vol. 31, No.5, September/October 1995, pp. 993-1000.

[3] N. Kutkut, D. Divan, and R. Gascoigne, "An Improved Full-Bridge Zero-Voltage Switching PWM Converter Using a Two-Inductor Rectifier", IEEE Transactions on Industry Application, Vol. 31, No.1, January/February 1995, pp. 119-126.

[4] M. Kheraluwala, R. Gascoigne, D. Divan, and E. Baumann, "Performance Characterization of a High-Power Dual Active Bridge dc-to-dc Converter", IEEE Transactions on Industry Application, Vol. 28, No.6, November/December 1992, pp. 1294-1301.

[5] A. Yagasaki, "Highly Improved Performance of a Noise Isolation Transformer by a Thin-Film Short-Circuit Ring", IEEE Transactions in Electromagnetic Compatibility, Vol. 41, No.3, August 1999, pp. 246-250.

[6] S. Ogasawara, H. Ayano, and H. Akagi, "An Active Circuit for Cancellation of Common-Mode Voltage Generated by PWM Inverter", IEEE Transactions on Power Electronics, Vol. 13, No. 5, September 1998, pp. 835-841.

[7] T. Yanada, S. Minowa, O. Ichinokura, and S. Kikuchi, "Design and Analysis of Noise-Reduction Transformer Based on Equivalent Circuit", IEEE Transactions on Magnetics, Vol. 34, No.4, July 1998, pp. 1351-1353.

[8] T. Yanada and O. Ichinokura, "High Performance Step-Down Noise-Reduction Transformer Constructed with C-Core", IEEE Transactions on Magnetics, Vol. 33, No.5, September 1997, pp. 3331-3333.

[9] S. Ogasawara, and H. Akagi, "Modeling and Damping of High-Frequency leakage Currents in PWM inverted-Fed AC Motor Drive Systems", IEEE Transactions on Industry Applications, Vol. 32, No. 5, September/October 1996, pp. 1105-1114.

[10] F. Forest, E. Laboure, T. A. Meynard, and V. Smet, "Design and Comparison of Inductors and Intercell Transformers for Filtering of PWM Inverter Output", IEEE Transactions on Power Electronics, Vol. 24, No. 3, March 2009, pp. 812-821.

[11] *IEEE Recommended Practice for Protection and Coordination of Industrial and Commercial Power Systems*, IEEE Standard 242-1986, Feb. 1986.

[12] Plitron Manufacturing Inc, "Toroidal Transformer Catalog", www.plitron.com.

[13] W. T. McLymann, "Transformer and Inductor Design Handbook", Marcel Dekker, 1998.

[14] K. Karsai, D. Kerenyi, and L. Kiss, "Large Power Transformers", Elsevier, 1987, p 95.

[15] G. Slemon, "Electric Machines and Drives", Addison-Wesley Publishing Company, Inc., 1992, pp. 252-255.

[16] R. Stoll, "The Analysis of Eddy Currents", Clarendon Press, Oxford, 1974.

[17] F. de León and A. Semlyen, "Time Domain Modeling of Eddy Current Effects for Transformer Transients," IEEE Transactions on Power Delivery, Vol. 8, No. 1, January 1993, pp. 271-280.

[18] K. W. E. Cheng and P.D. Evans, “Calculation of Winding Losses in High-Frequency Toroidal Inductors Using Single Strand Conductors”, IEE Proceedings on Electric Power Applications, Vol. 141, No. 2, March 1994, pp. 52-62.

[19] K. W. E. Cheng and P. D. Evans, “Calculation of Winding Losses in High Frequency Toroidal Inductors Using Multistrand Conductors”, IEE Proceedings on Electric Power Applications, Vol. 141, No. 5, September 1995, pp. 313-322.

[20] R. Prieto, J. A. Cobos, V. Bataller, O. Garcia, and J. Uceda, “Study of Toroidal Transformers by Means of 2D Approaches”, 28th Annual IEEE Power Electronics Specialist Conference PESC’97, 22-27 June, 1997, pp.621-626.

[21] R. Prieto, V. Bataller, J. A. Cobos, and J. Uceda, “Influence of Winding Strategy in Toroidal Transformers”, 24th Annual IEEE Conference of the Industrial Electronics Society IECON’98, August 31 – September 4, 1998, pp. 359-364.

[22] M. Nave, “On Modeling the Common Mode Inductor”, 1991 IEEE International Symposium on Electromagnetic Compatibility, August 1991, pp. 452-457.

[23] W.G. Hurley and D. J. Wilcox, “Calculation of Leakage Inductance in Transformer Windings”, IEEE Transactions on Power Electronics, Vol. 9, No. 1, January 1994, pp. 121-126.

[24] I. Hernández, F. de León, and P. Gómez, “Design Formulas for the Leakage Inductance of Toroidal Distribution Transformers”, IEEE Transactions on Power Delivery, Vol. 26, No. 4, October 2011, pp. 2197-2204.

[25] M. Kovacic, Z. Hanic, S. Stipetic, S. Krishnamurthy, and D. Zarko, "Analytical Wideband Model of a Common-Mode Choke", IEEE Transactions on Power Electronics, vol.27, no.7, pp.3173-3185, July 2012.

[26] A. J. Binnie and T. R. Foord, "Leakage Inductance and Interwinding Capacitance in Toroidal Ratio Transformers", IEEE Transactions on Instrumentation and Measurement, vol.16, no.4, pp.307-314, Dec. 1967.

[27] B. Cougo, A. Tuysüz, J. Muhlethaler, and J. W. Kolar, "Increase of tape wound core losses due to interlamination short circuits and orthogonal flux components," IECON 2011 - 37th Annual Conference on IEEE Industrial Electronics Society , pp.1372-1377, 7-10 Nov. 2011.

BIOGRAPHIES

Francisco de León (S’86–M’92–SM’02) received the B.Sc. and the M.Sc. (Hons.) degrees in electrical engineering from the National Polytechnic Institute, Mexico City, Mexico, in 1983 and 1986, respectively, and the Ph.D. degree in electrical engineering from the University of Toronto, Toronto, ON, Canada, in 1992. He has held several academic positions in Mexico and has worked for the Canadian electric industry. Currently, he is an Associate Professor at the Polytechnic Institute of NYU, Brooklyn, NY. His research interests include the analysis of power definitions under nonsinusoidal conditions, the transient and steady-state analyses of power systems, the thermal rating of cables and transformers, and the calculation of electromagnetic fields applied to machine design and modeling.

Sujit Purushothaman (S’09–M’13) received his B.E. degree in electrical engineering from Mumbai University (Sardar Patel College of Engineering), Mumbai, India in 2005. His work experience includes testing and development of medium voltage switchgear for Siemens in Mumbai, India. He received his Master’s and his Ph.D. degrees in electrical engineering from Polytechnic Institute of NYU in 2009 and 2011, respectively. He is currently a research engineer at FM Global Research in Norwood, MA. His research interests include power system transients, damping of subsynchronous resonance, machine design and modeling, and thermal modeling of electrical devices.

Layth Qaseer received his B.Sc., M. Sc. and Ph.D. degrees from the University of Baghdad, Baghdad, Iraq in 1979, 1993 and 2004 respectively, all in electrical engineering. Between 1979 and 2001 he has worked at national scientific research center and the ministry of industry. In 2005 he joined Al-Khwarizmi College of Engineering, University of Baghdad, Baghdad, Iraq. He was a visiting professor in the department of electrical & computer engineering at the Polytechnic Institute of New York University during the 2010-11 academic year. His areas of research interest include linear electric machines, electromagnetic systems, electrical machine design, permanent magnet synchronous motors and modeling.

Analysis, Modeling and Simulation of the Phase-Hop Condition in Transformers: The Largest Inrush Currents

Ashkan Farazmand, Francisco de León, *Senior Member, IEEE,* Kuang Zhang, *Student Member, IEEE,* and Saeed Jazebi, *Student* Member*, IEEE*

***Abstract*—Inrush currents in transformers can have very disruptive effects such as: voltage sags, false tripping of the protective devices, and mechanical stresses in the transformer windings. This paper shows that there are operating situations that may cause a transformer to draw abnormally high inrush currents. Examples include the normal operation of off-line UPS systems, interruptions, voltage sags, and notching. These conditions may produce inrush-like currents of more than twice the value of the "normal" maximum inrush caused by energizing at voltage zero-crossing. For this condition, the term "phase-hop" is used in this paper. Laboratory experiments performed on four different transformers (1 kVA) with varied characteristics show the impact of phase-hop in the magnitude of inrush currents. The experiments are also used to validate the EMTP model used for analysis of multiple cases. In addition, the behavior of the magnetic flux in a transformer under phase-hop is investigated and compared with different operating conditions using finite elements. The results of this paper have implications in transformer design and in the operation and design of UPS systems to prevent the damaging effects of phase-hop.**

***Index Terms*—inrush currents, interruptions, phase-hop, transformer modeling, UPS systems, voltage sags.**

I. Introduction

POWER quality problems are critical issues nowadays because of the increased use of power electronics loads. Interruptions and blackouts are the worst forms of power quality problems. Blackout is a complete loss of supply voltage or load current for longer than a minute [1]. Harmonics, interharmonics, power frequency variations, voltage unbalances, interruptions, notching, undervoltages, overvoltages, swells, noise, *dc* offset, voltage fluctuations, and voltage sags are common power system operation phenomena which cause power quality problems [2].

In order to solve the aforementioned problems, Uninterruptible Power Supplies (UPS) are often used [3]. UPS are designed to automatically provide emergency electricity to critical loads in case of supply voltage failure. Some UPS systems also regulate or filter the utility power [1].

This work was supported by the U.S. Department of Energy under Grant No. DEOE0000072.

A. Farazmand, F. de León, K. Zhang, and S. Jazebi are with the Department of Electrical and Computer Engineering, Polytechnic University, Six Metrotech Center, Brooklyn, NY, 11201. (e-mails: farazmand@nyu.edu, fdeleon@poly.edu, kzhang02@students.poly.edu, jazebi@ieee.org).

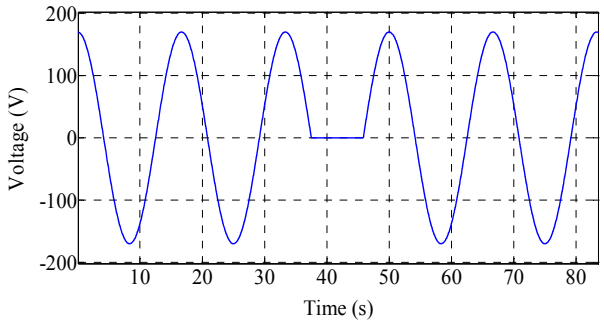

Fig. 1. Voltage wave shape of the phase-hop condition.

As it will be explained below, the operation of off-line UPS systems, interruptions, voltage sags, and notching in power systems can lead to a condition called "phase-hop" coined for the shape of the voltage wave shown in Fig. 1. When this condition occurs, there are two positive (or negative) semicycles applied consecutively to the transformer. The maximum phase-hop current has been reported as an important design parameter by engineers of the leading manufacturers of UPS systems for transformers rated at 25 kVA [4].

Phase-hop causes the transformer core to go into a deep saturation level and draws very large inrush-like currents. Transformers and protections need to be designed to prevent false tripping or damages during phase-hop. The large currents could also damage the UPS systems, or cause problems in the switching operation of the rectifiers, since they may not be designed for these abnormally large currents.

This paper introduces and investigates for the first time the effect of phase-hop on transformers. The study is performed both experimentally and with validated computer simulations. It is found that phase-hop currents can be over twice as large as the "normal" maximum inrush currents caused by switching at zero crossing.

False tripping during phase-hop is more probable than during transformer energization because of the unpredictable timing of this phenomenon. In practice, a common technique used to prevent false tripping of the protective devices during transformer energization is to add a time delay. However, the occurrence of phase-hop is not predictable and a delay cannot be applied.

The correct estimation of phase-hop currents is important for power system design. Inasmuch as their quantification is vital for UPS operation and design since UPS systems are

precisely used to provide backup power, therefore false tripping of vital loads could be disastrous.

II. Effects on Transformer Inrush Currents of Power System Electromagnetic Phenomena

The variation of the rms voltage from its nominal value is described by two parameters: the magnitude of the voltage change and its duration. Power system electromagnetic phenomena are classified in four main groups based on the duration of the disturbance: steady state variations, long duration variations, short duration variations, and transients [2].

This section discusses how interruptions, voltage sags, and notching in power systems can produce a phase-hop voltage to be applied to transformers. In this section it is assumed that a UPS system is not used to prevent these effects.

A. Interruptions

Interruptions are caused by transients that trigger utility breakers or switches to open. A voltage interruption occurs when the supply voltage decreases to less than 10% of its nominal value in one or more phase conductors. The causes for this phenomenon are: faults, component failure, switching, false breaker tripping, and malfunctions of control systems.

Depending on the duration of interruptions, they are classified in three types: momentary (0.5 cycle to 3 seconds), temporary (3 seconds to 1 minute), and sustained (greater than 1 minute) [2]. The first two types are short duration variations and the third is a long duration variation. The duration of the interruption depends on the reclosing capability and speed of the protective device. Note that an interruption of exactly 0.5 cycle produces the phase-hop voltage wave shape illustrated in Fig. 1.

B. Voltage Sags

A voltage sag is a short duration decrease of the voltage between 0.1 and 0.9 pu of the nominal voltage at the power frequency for durations of 0.5 cycle to 1 min [2]. The IEC word for this phenomenon is “dip” [5]. Sag durations are divided into three categories: instantaneous (0.5 to 30 cycles), momentary (30 cycles to 3 s), and temporary (3 s to 1 minute). The causes for this phenomenon are system faults, switching of large loads, and starting of large motors [2]. Voltage sags cause a partial phase-hop, but currents can be larger than the “normal” inrush.

C. Notching

Notching is a repetitive steady state voltage disturbance lasting less than a half cycle. It represents a phenomenon that is considered both a transient and a harmonic distortion since it occurs continuously and the frequency components related to it are high [2]. It can occur in opposite polarity to the main waveform. In this case, it is subtracted from the normal waveform. In an extreme case, notching may lead to a complete loss of voltage for up to a half cycle [3] corresponding to the phase-hop wave of Fig. 1.

Notching can be produced during the commutating action from one phase to another in the normal operation of SCR-controlled equipment, such as three-phase converters, motor controls, and inverters. In this condition, a brief short circuit between two phases occurs [3], [6].

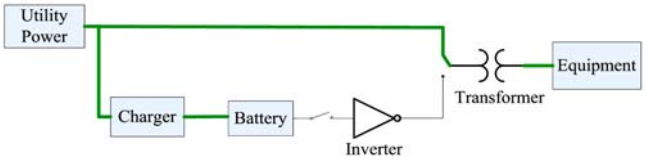

Fig. 2. Off-line UPS performance when utility power is present (normal *ac* power mode).

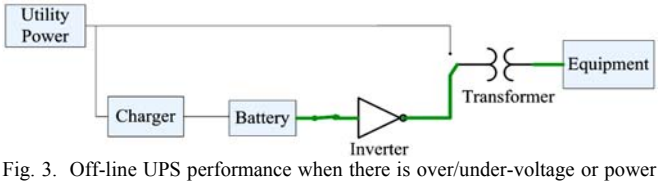

Fig. 3. Off-line UPS performance when there is over/under-voltage or power loss (inverter mode).

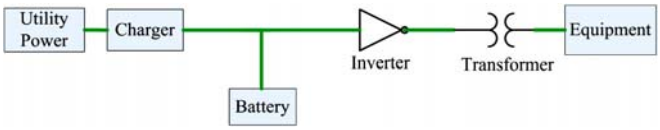

Fig. 4. On-line UPS system.

III. UPS Systems

UPS systems are intended to provide constant and regulated output voltage and power to critical loads regardless of power quality disturbances present in the mains. The objective is to prevent voltage sags, power outages, impulses, noise, overvoltages or swells, harmonic distortions, frequency variations, voltage fluctuations, and voltage surges [7], [8].

UPSs are classified into two groups: rotary and static. Rotary UPSs normally use a diesel-fueled motor generator set and static UPSs use battery as the backup power source [1]. Because there are several technical problems with rotary UPS systems, most of the modern UPSs are static [1]. There are three kinds of UPSs: off-line, line interactive, and on-line.

A. Off-line (Standby) UPS:

During the time when the utility power is present, off-line UPS systems pass the power directly to the load; the load is not isolated from the mains. During this time, the battery backup is also charged and the inverter connected to the battery is off (see Fig. 2).

When the utility voltage is below a specified value or during a utility power outage, the UPS turns on its internal *dc-ac* inverter to produce *ac* power from the battery. In this case, the equipment is connected to the inverter output mechanically (see Fig. 3).

This method saves battery life by avoiding continuous charging and discharging. However, as stated by most manufacturers, there is a switch changeover time between 4 and 10 ms to engage the UPS during an interruption [1]. Practically, this delay can be as long as 25 ms depending on the time that it takes the UPS to detect the absence of utility voltage and transfer to the battery. Therefore, during the changeover time there is a voltage drop-out to the connected equipment and the phase-hop condition is possible.

B. Line-Interactive UPS:

Line-interactive UPS is an off-line UPS connected with a tap-switching automatic voltage regulator (AVR). In this system, when the power comes from the utility line, the AVR senses the UPS output voltage. When the utility voltage is low (utility brownout), the AVR automatically switches transformer taps to increase the output voltage. When the utility voltage is large, the AVR reduces the output voltage. The set-up of this case is the same as the offline UPS (Figs. 2 and 3) with the addition of a multi-tap variable voltage auto transformer after the utility block. In this case, the load is not completely isolated from the mains power and therefore, phase-hop can occur.

C. On-Line UPS:

The on-line UPS system, as shown in Fig. 4, converts incoming *ac* power to rectified and regulated *dc* voltage and then the inverter regenerates a regulated, clean, and sinusoidal *ac* power from the *dc* voltage. Therefore, the load is isolated from the utility. This double conversion system leads to the elimination of line noise, transients, harmonic distortion, and voltage/frequency instability problems from the utility.

In this system, the load is always powered by the inverter and the battery is connected to the *dc* bus. Therefore, this is a no-break system and there is no change-over time and phase-hop will not occur. This system provides a fully charged battery backup available at all times. It has the disadvantage of shorter battery life because of the continuous charging and discharging of the battery. This UPS system is more expensive and less reliable than standby and line-interactive UPSs because there are additional components connected in series.

IV. Transformer Model

In this paper, the π model is selected to represent the transformer [9]. Tests have been performed on four different transformers (T_a, T_b, T_c, and T_d) to obtain the parameters. Transformer T_a consists of four windings. In this paper, the inner-most winding is called the first winding, the one after is called second winding, and so forth. The open circuit test is used to obtain the magnetizing parameters of the transformers as in [9]. The leakage parameters of the transformers are obtained accurately from the bucking test [10].

The total series *ac* resistance $R_1 + R'_2$ is computed from

$$R_1 + R'_2 = \frac{P_{BK}}{I_{BK}^2} \tag{1}$$

Individual breakdown of the resistances is done based on the *dc* resistance division between primary and secondary windings obtained from the *dc* test. Total leakage inductance is computed from:

$$L_s = \frac{1}{2\pi f}\sqrt{\left(\frac{V_{BK}}{I_{BK}}\right)^2 - \left(R_1 + R'_2\right)^2} \tag{2}$$

where P_{BK} is the active power computed from the bucking test. V_{BK} and I_{BK}, are the *rms* values of voltages and currents in the bucking test, respectively. L_s is the total leakage inductance. R_1 and R'_2 are the primary and the secondary *ac* resistances, respectively, and f=60 Hz. The applied voltage is 125 V rms.

The parameters computed from measurements are shown in Table I. Data given for transformer T_a is for the inner-most (first) winding. Hysteresis loops of the three transformers are obtained from Faraday's Law integrating the induced voltage to find the flux linkage as in [9].

The proper estimation of the air-core inductance is highly important to compute the inrush current precisely. 3-D finite element (FEM) simulations (using the commercial program Maxwell 14) are carried out. The air-core inductance is calculated as follows [9], [11]:

$$L_{air-core} = \frac{2W}{I^2} \tag{3}$$

where W is the volume magnetic energy (computed from FEM), and I is the winding current. Table II presents the air-core inductances of the four transformers. The air-core inductances are used to complete the hysteresis loops. They are the slopes used to extend the hysteresis loops from the final measured point (obtained from the open circuit test) to infinity. The model is implemented in the EMTP-RV [12].

V. Model Validation and Worst Phase-Hope Currents

To validate the model, laboratory experiments are performed on all four transformers under the worst possible phase-hop conditions. In this case, the phase-hop condition occurs following the moment of energizing the transformer using the zero-crossing switch. A zero-crossing and phase-hop switch is built and utilized in the laboratory to connect and disconnect transformers at specific time -instants. For the zero-crossing condition, the switch energizes the transformer when the voltage of the *ac* power source crosses zero. For phase-hop, the switch, in addition to energizing the transformer at voltage zero-crossing, opens the connection between the second and third zero-crossings, thus re-establishing power at the third zero-crossing (see Appendix for more details).

Fig. 5 shows the waveshapes and compares the results from experiments and the model for the first winding of transformer T_a. The first peak values of inrush current (caused by the first peak of the primary voltage) from experiment and simulation are 157.7 A and 162.5 A, respectively (difference of 3%). The second peak (caused by the phase-hop voltage) from experiment and simulation are 328.9 A and 330.2 A, respectively (difference of only 0.4%). Fig. 6 compares the results for transformer T_d under the abovementioned condition. The difference between the peak currents of the model and the experiment is 3.9% for the first peak and 3.3 % for the second peak. Note, however, that the inrush and phase-hop currents are much higher because transformer T_d is a toroidal transformer.

Table III and IV compare the results of the first and second peaks of inrush current under the worst case of phase-hop for all four transformers under study. Looking at Figs. 5 and 6 and Tables III and IV, one can observe a strong agreement between simulation and experimental results.

Note from Figs. 5 and 6 that the second positive peak of the voltage in the phase-hop condition is smaller than the first

peak. The reason for this is the existence of a large voltage drop in the source resistance (R_{source} = 0.1 Ω) caused by the extremely large phase-hop currents. If the short-circuit power rating of the source were larger, higher inrush (and phase-hop) currents would occur.

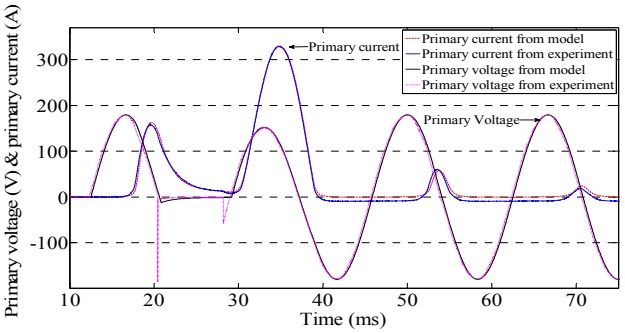

Fig. 5. Comparison of model and experiment for the worst case of phase-hop for the first winding of transformer T_a. One can see a perfect agreement between simulation and experiment.

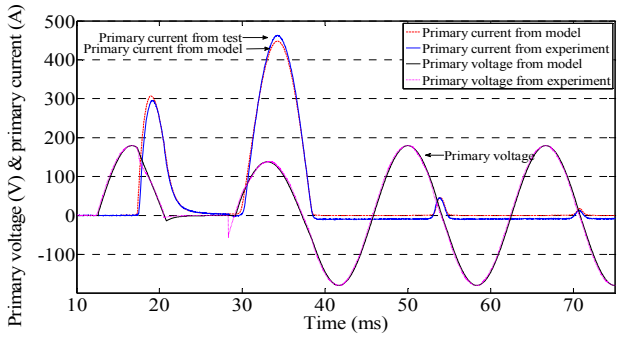

Fig. 6. Comparison of model and experiment for the worst case of phase-hop for transformer T_d. One can see a very good match between simulation and experiment.

VI. Transformers under Phase-Hop Condition

In practice, it may not be common to have the phase-hop condition right after the transformer energization (inrush). That circumstance was used in Section IV to analyze this extreme, yet possible, case of phase-hop and validate the model. The most practical and probable condition of the phase hop is when it happens during the normal operation in steady state (long after energizing the transformer for the first time). In order to simulate this condition in the EMTP and compare the results, the transformer is energized at voltage zero-crossing and after reaching the steady state, phase-hop occurs.

The results for the first winding of transformer T_a under phase-hop are shown in Fig. 7a. The first peak of inrush current is 162.5 A while the one caused by phase-hop is 313.3 A. Fig. 7b shows a closer view of the phase-hop condition for this case. Figs. 8a and 8b presents the results for transformer T_d under typical phase-hop condition. The first peak of inrush current is 307 A, and the second peak is 1.46 times higher at 446.8 A. Table V compares the results for all four transformers for the inrush currents caused by zero-crossing voltage, typical condition of phase-hop, and worst case of phase-hop through simulation. One can appreciate that the values of inrush current from the phase-hop condition are much higher than the first peak of inrush current caused by zero-crossing voltage. As an example, for transformer T_b, the peak value of inrush current under normal phase-hop condition is 2.15 times higher than the first peak of inrush current, and under the worst case of phase-hop it is 2.41 times higher.

TABLE I
CIRCUIT PARAMETERS FOR DIFFERENT TRANSFORMERS

Transformer	T_a	T_b	T_c	T_d
Rating [kVA]	1	1	1	1
Rated voltage	120	120	120	120
Turns ratio	1:1	1:1	1:1	1:1
Construction	Shell-type	Shell-type	Toroidal	Toroidal
R_1 [Ω]	0.404	0.251	0.338	0.318
R'_2 [Ω]	0.345	0.324	0.288	0.271
L_s [mH]	0.254	0.692	8.843	0.232
R_{m1} [Ω]	2656	739	2149	2832
R_{m2} [Ω]	2656	739	2149	2832
L_{m1} [mH]	822	753	3339	2569
L_{m2} [mH]	822	753	3339	2569

TABLE II
AIR CORE INDUCTANCES FOR THE FOUR TRANSFORMERS UNDER STUDY

Transformer	T_a				T_b	T_c	T_d
Winding	1st	2nd	3rd	4th			
Air-core inductance [μH]	645	850	1,069	1,300	1,000	463	316

TABLE III
FIRST PEAK VALUES OF INRUSH CURRENT FOR DIFFERENT TRANSFORMERS UNDER WORST CASE OF PHASE-HOP (EXPERIMENT VERSUS SIMULATION)

Transformer	Winding	Test [A]	Model [A]	Difference [%]
T_a	1st	157.7	162.5	3.0
	2nd	130.4	134.5	3.1
	3rd	125.2	122.3	-2.4
	4th	123.1	111.1	-9.7
T_b		149.9	153.1	2.1
T_c		208	213.2	2.5
T_d		295.4	307	3.9

TABLE IV
SECOND PEAK VALUES OF INRUSH CURRENT FOR DIFFERENT TRANSFORMERS UNDER WORST CASE OF PHASE-HOP (EXPERIMENT VERSUS SIMULATION)

Transformer	Winding	Test [A]	Model [A]	Difference [%]
T_a	1st	328.9	330.2	0.4
	2nd	291.3	272.4	-6.5
	3rd	261.7	252.5	-3.5
	4th	240.5	238.4	-0.9
T_b		353.3	368.5	4.3
T_c		402.3	360.9	-10.3
T_d		463.3	447.9	-3.3

TABLE V
COMPARISON OF MAXIMUM INRUSH CURRENT UNDER DIFFERENT CONDITIONS FOR DIFFERENT TRANSFORMERS

Transformer	Winding	First Peak (inrush) [A]	Second Peak (phase-hop) [A]	Second Peak (worst case) [A]
T_a	1st	162.5	313.3	330.2
	2nd	134.5	257.6	272.4
	3rd	122.3	237.4	252.5
	4th	111.1	222.0	238.4
T_b		153.1	329.8	368.5
T_c		213.2	359.3	360.9
T_d		307	446.8	447.9

Note that for transformers T_c and T_d, which are toroidal transformers, the difference between peak values of inrush current in the normal and the worst cases of phase-hop is small (see Table V). This is so because in these transformers the hysteresis cycles are thinner and flatter than the ones of standard transformers, because the cores have no gap. Therefore, under the worst case of phase-hop, the first spike of inrush current reached zero at the start of the second peak, while for standard transformers (T_a and T_b) the second inrush cur-

rent happens while the current is not yet zero; see Figs. 5 and 6 to compare the results for transformers T_a and T_d.

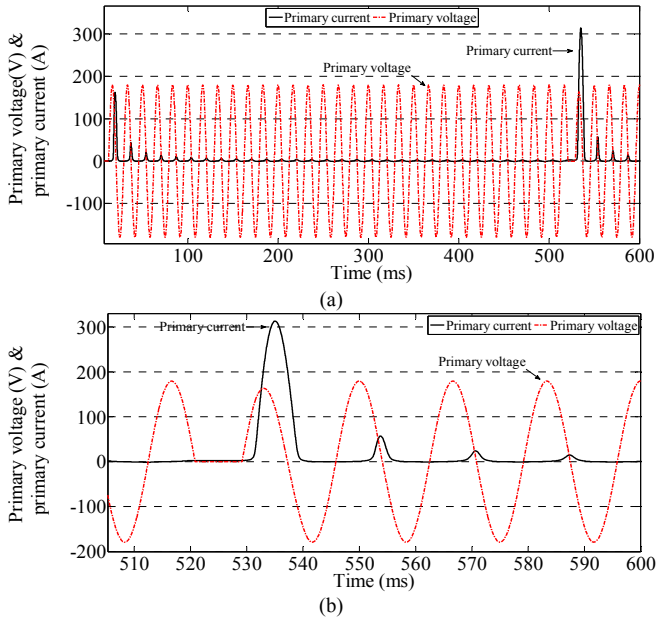

Fig. 7. Simulation of transformer Ta (first winding) under phase-hop condition; (a) transient from the beginning of excitation (b) close view of the phase-hop part.

Fig. 9 shows the effect of the duration of an interruption on phase-hop current. The primary currents and the applied voltage (primary voltage) to the first winding of the transformer T_a are presented for a zero volts interruption lasting 0.5, 0.75 and 1 cycle. One can see that the largest peak current is when the duration of the interruption is half a cycle (313.3 A), which is almost twice the normal zero-crossing inrush current (162.5 A). Under this situation, a complete instance of phase-hop occurs. The case with no inrush current is when the duration of the interruption is one full cycle. This situation corresponds to the normal sinusoidal condition since one complete cycle is eliminated. For an interruption of 0.75 cycle the peak current is 178.1 A.

An example of a voltage sag is presented in Fig. 10. The primary voltage and inrush currents under zero-crossing and 10% voltage sag lasting for 10.5 cycle are shown, for the first winding of transformer T_a. The value of inrush current caused by the sag is 274.7 A (69% larger than the zero-crossing inrush current).

Table VI summarizes the inrush current results for 0% and 5% interruptions, and for 10% and 50% voltage sags. The duration of the transient is between half a cycle (worst case) and 3600.5 cycles (around 1 minute). As shown in table VI, the worst cases of inrush-like currents occur when the fault duration is 0.5+*n* cycles; where *n*=0, 1, 2… This is so because there are two half cycles consecutively, which is the complete phase-hop. In contrast, for sags lasting 0.5+*n* cycles, there is a small flux-cancellation effect which decreases magnitude of the inrush current. To illustrate this, the 20% sag with 2.5 cycle duration (*n*=2) is depicted in Fig. 11. Note that the integral of the voltage is the flux linkage. The areas A, B, C and D cancel each other but the extra half cycle, E (highlighted in Fig. 11) leads to a decrease in the built flux. This is the reason sags with larger voltage magnitude, cause smaller inrush currents.

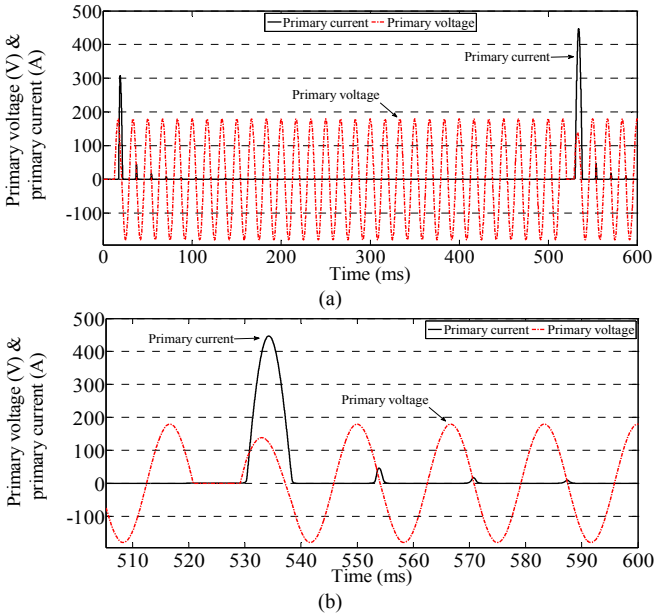

Fig. 8. Simulation of transformer T_d under phase-hop condition; (a) transient from the beginning of excitation (b) close view of the phase-hop part.

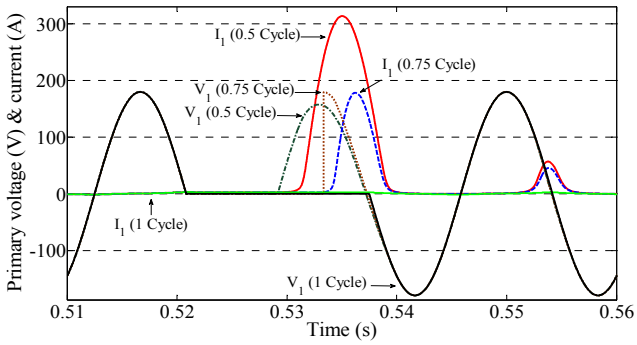

Fig. 9. Primary voltage and caused inrush current of the first winding of the transformer Ta under 0% interruption.

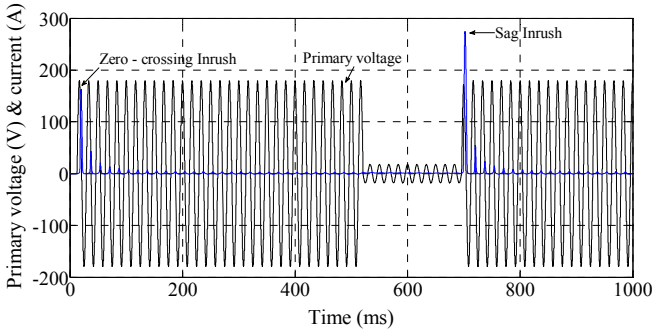

Fig. 10. Primary voltage and caused inrush current of the first winding of the transformer Ta under 10% voltage sag for 10.5 cycle duration.

In addition, a longer interruption or voltage sag causes a larger reduction in the built flux and as a result in the inrush currents (see Table VI).

To complete the study, EMTP simulations for various undervoltages were performed [2], [3]. Undervoltages lasting longer than 1 minute with magnitudes between 0.8 to 0.9 pu

were analyzed. In no case, including undervoltages lasting 0.5+*n* cycles, is the phase-hop phenomenon observed.

Form this study, it is concluded that under the phase-hop condition a very large current can be drawn by transformers due to heavy saturation of the iron core. Therefore, phase-hop should be considered in transformer and UPS design and operation to prevent its potential destructive effects. As it was shown, phase-hop can occur partially or fully depending on the magnitude and duration of electromagnetic phenomena causing distorted input voltage to the transformer.

TABLE VI
INRUSH CURRENTS UNDER DIFFERENT KINDS OF INTERRUPTIONS AND VOLTAGE SAGS FOR THE FIRST WINDING OF TRANSFORMER T_A

	Current Peak Value (A)			
	interruption	interruption	sag	sag
# of cycles	0%	5%	10%	50%
0.5	313.3	305.3	296.1	182
0.6	296.4	287.4	277.4	162.9
0.7	232.3	222.7	212.3	105.3
0.8	109.1	101.7	93.6	20.8
0.9	5.11	5	4.85	3.6
1	2.2	2.3	2.3	2.4
1.1	4.9	4.79	4.6	3.5
1.5	310.7	302.7	293.5	179.5
2.5	308.3	300.2	291	177.1
10.5	293	283.93	274.7	160.5
100.5	228.4	213.82	199.7	73.81
3600.5	201.5	184.3	166.9	37

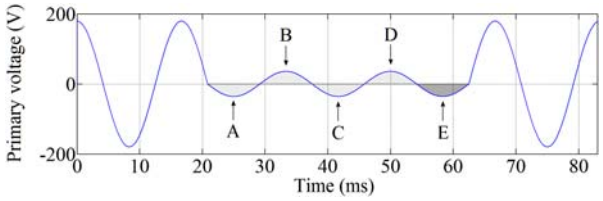

Fig. 11. 20% sag with 2.5 cycle duration

VII. PHYSICAL EXPLANATION OF THE PHASE-HOP CONDITION

Figs. 12 and 13 explain the phase-hop phenomenon physically by illustrating the behavior of the primary voltage, internal voltage, flux linkage, and current. The graphs correspond to the first winding of the transformer T_a under the worst condition of phase-hop (phase-hop following transformer energization at zero crossing). An important component of the explanation is the internal voltage (E_1), which is computed as follows:

$$E_1 = V_1 - R_1 I_1 \tag{4}$$

where V_1 is the primary terminal voltage, I_1 is the primary current, and R_1 is the primary winding *ac* resistance.

Nine points: *a*, *b*, *c*, *d*, *e*, *f*, *g*, *h*, and *i* are identified in Figs. 12 and 13 to highlight important performance stages of the transformer at different times during the inrush followed by a phase-hop transient.

The energization is done with zero residual flux (point *a*). At that instant, voltage, current, and flux are all zero. When the voltage reaches its first peak (at point *b*) a quarter of a cycle later, flux linkage is building (0.4 Wb) and the current is still small at about the value of the normal magnetizing current, 0.6 A peak. At point *c*, the internal voltage is crossing zero from positive to negative, at that moment the flux linkage presents a first peak (0.81 Wb) and the "normal" peak of the inrush currents is reached (162.5 A). Then, the phase-hop occurs and the negative semi-cycle of the voltage, between points *c* and *d* disappears (see Figs. 13a and 13b). When the terminal voltage reaches the next zero crossing at point *d*, the flux linkage has reduced a small amount, but it is still at a very high value (0.65 Wb) and the current has not reduced to zero (11.8 A). Because of the existence of a positive voltage between points *d* and *e*, the flux increases further until the transient reaches the maximum at point *e* with a flux linkage of 0.95 Wb and a phase hop current of 330.2 A, which is almost twice as large as the zero-crossing inrush current. At this time, the internal voltage is crossing zero from positive to negative. From this point on, the peaks of flux and current reduce in magnitude as the *dc* component damps. At point *f* voltage reaches its first negative peak after phase-hop, with the value of 0.3 Wb for the flux linkage and 0.31 A for the primary current. The reversing points of the hysteresis cycle in the third quadrant (points *g*, *h* and *i*) progressively decrease as the transient damps out and the flux becomes increasingly symmetric. The magnitudes of the flux linkage are -0.2 Wb, -0.26 Wb, and -0.28 Wb for these three points, respectively, which correspond to the voltage zero crossings from negative to positive.

VIII. MAGNETIC FIELD BEHAVIOR

To shed light into the internal behavior of the transformer, in this section, the magnetic field of the transformer is investigated for different operating conditions including: open circuit, normal operation (on-load), zero-crossing inrush, and phase-hop. Simulations are performed using the FEM (Finite Element Method) computer program, Maxwell 14. Magnetic flux lines are shown inside and outside of the core in Fig. 14. Note that due to the geometrical symmetry of the transformer, only a part of the core is shown.

During open circuit, the situation presented in Fig. 14(a), the magnetic field is concentrated inside the iron core (the lines in the window are the boundaries of the windings). During normal operation, when the transformer is supplying the nominal load, a part of magnetic flux "leaks" into the inter-winding region (see Fig. 14(b)). This flux is what produces the leakage inductance. In Fig. 14(c) the magnetic flux for transformer energization at zero crossing is presented. One can see that there is a considerable amount of flux in the air. In fact, the flux distribution resembles the behavior of an air-core inductor. As shown in Fig. 14(d), the flux pattern during phase-hop does not change significantly in comparison with that of the normal inrush current. However, the amplitude (seen by the concentration of lines) of the magnetic field is larger.

IX. POSSIBLE SOLUTIONS FOR PHASE-HOP

The transient phenomenon known as transformer inrush currents was first published by John Fleming in 1892 [13]. Since then, many publications have proposed techniques to limit inrush currents to prevent its destructive effects. Some of

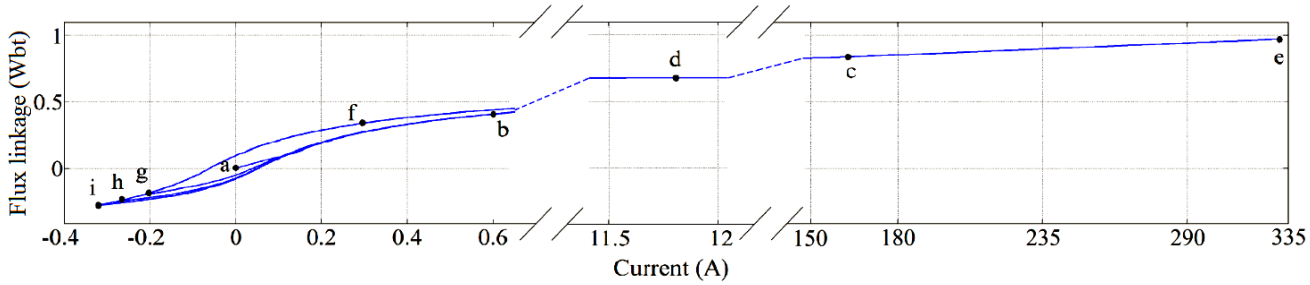

Fig. 12. Core flux linkage vs. primary current for first winding of transformer Ta under the worst condition of phase-hop.

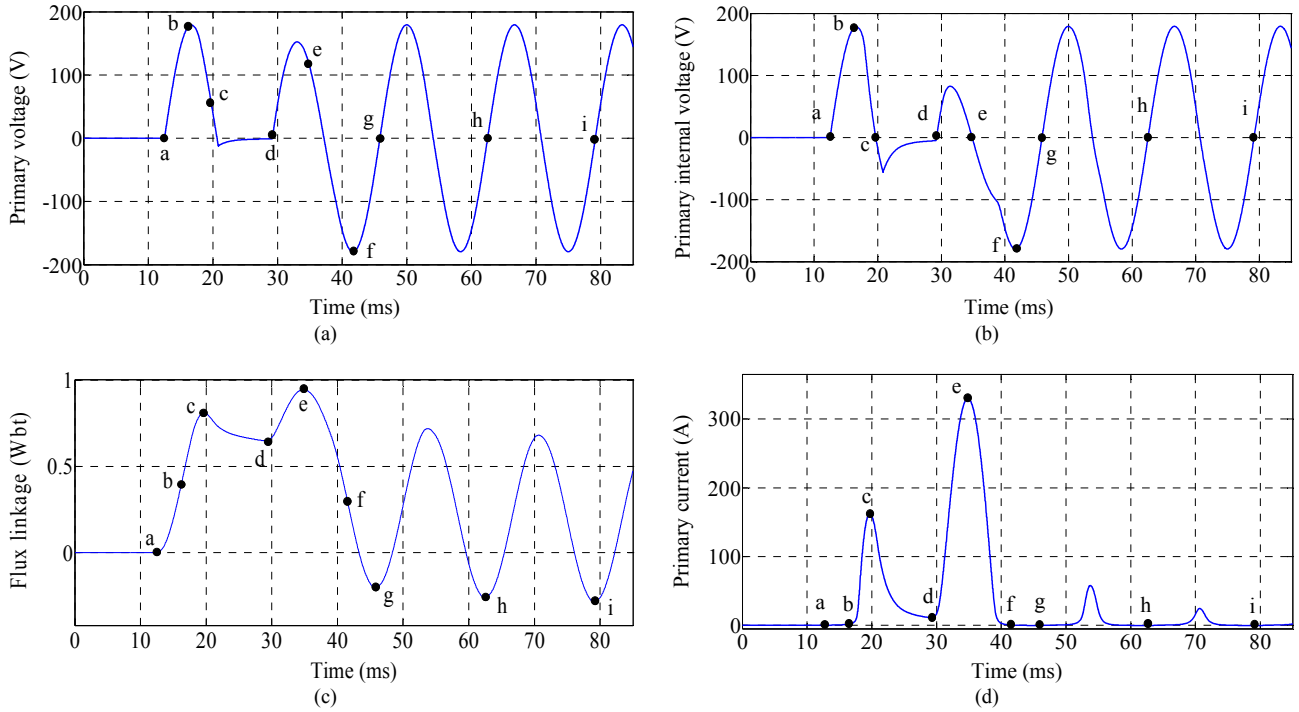

Fig. 13. (a) Primary voltage vs. time; (b) primary internal voltage vs. time; (c) core flux linkage vs. time; (d) primary current vs. time for the first winding of the transformer T_a under worst condition of phase-hop.

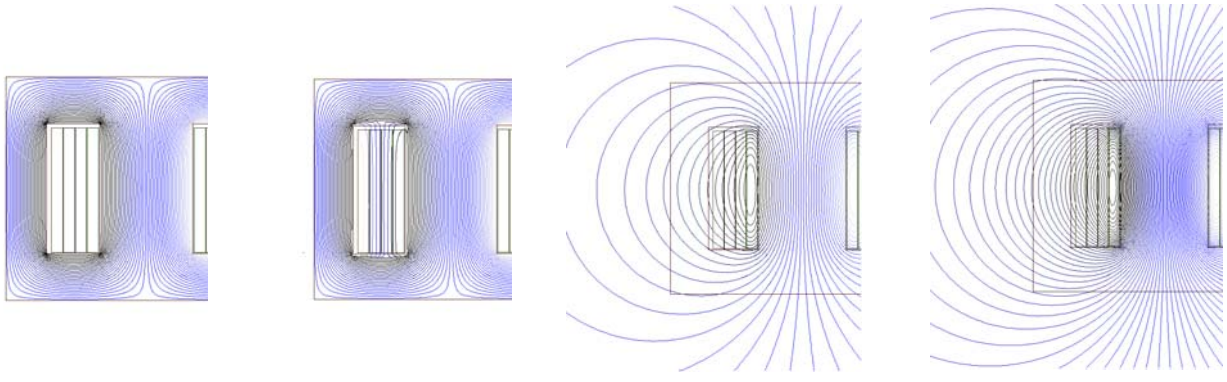

Fig. 14. Magnetic field behavior for saturated and non-saturated transformer iron core: (a) open circuit; (b) normal operating condition – transformer loaded; (c) peak condition for inrush currents at zero-crossing switching; (d) peak condition for phase-hop currents.

the methods are external (to the transformer) and others are transformer-based solutions. External solutions consist of pre-insertion impedances, negative temperature coefficient thermistors (NTC) [14], transformer core demagnetizing [15], phase-delayed switching [16], [17], and sequential phase energization [18], [19]. Transformer-based solutions consist of air gaps, virtual gaps [20], using low permeability materials for the core, and special designs with larger values of air-core inductance.

To some extent, each of the existing approaches diminishes inrush currents; however, there is a trade-off with each one of them. In addition, some methods are not applicable for phase hop. External demagnetizing techniques, for example, are not possible because there is not enough time to demagnetize the transformer core during the half a cycle between two consecutive peaks. Switching methods have some problems with the mutual effects with switches applied in the UPS system and also the reliability of the system. Implementations of pre-insertion impedance methods are very complicated due to the difficulty in the detection of the phase-hop condition. Thermistors do not work either because at the time of the phase-hop the system is already on, therefore, thermistor resistances are very small and cannot reduce the inrush current effectively. In general, there are several problems with the addition of series components with the transformer: (1) the reliability of the system reduces, and (2) depending on the voltage level the additional components need to comply with safety standards, which makes them expensive.

It seems that the best solutions to prevent the destructive effects of the phase-hop phenomena are transformer-based. Application of these methods will be treated in a forthcoming paper.

X. Conclusion

This paper has shown, for the first time, how the occurrence of the phase-hop phenomenon in transformers can lead to extremely large currents. Phase-hop can occur at any time in a power system because interruptions, voltage sags, and notching in the network are not predictable. In order to prevent these phenomena, a UPS system can be used. However, the action of off-line UPS systems may itself lead to large levels of inrush currents for the transformers located between the load and the UPS system as well.

The value of the phase-hop currents can be several times higher than the magnitude of the "normal" inrush currents that occur when a transformer is energized at voltage zero-crossing.

The extremely large currents produced by the phase-hop condition can lead to serious problems such as power quality issues, mechanical stresses on transformer windings, and false tripping of vital protections. The best techniques to prevent these serious effects seem to be transformer-based solutions.

XI. Appendix

Fig. 15 presents a block diagram of the power and control circuits implemented in the zero-crossing and phase-hop switch developed for this project. This switch consists of voltage regulators, opto-isolators, a digital logic control circuit and MOSFET switches. When the *ac* power source is on, the opto-isolator will pass the sinusoidal waveform to a comparator, which checks for a zero value. As a result, a 50% duty ratio square wave, which rising and falling edges correspond to the zero-crossing of power source, appears at the output of comparator. The first rising edge triggers the digital logic control circuit, which turns-on the switch and finally energizes the transformer.

The phase-hop circuit of the switch is essentially the same as the zero-crossing circuit except for the digital logic control circuit and an extra pair of MOSFETs. Three precise timers are utilized in the control circuit to generate the signals for switches 1 and 2 in Fig. 16. Switch 1 consists of two MOSFETs. It closes at the first zero-crossing and only opens between the second and third zero-crossings. Switch 2 is added to prevent cutting large inductive currents. When switch 2 is closed, the inrush current inside the transformer will only flow through switch 2. As a result, switch 1 and other circuit elements are protected from the high voltages caused by large *di/dt* values.

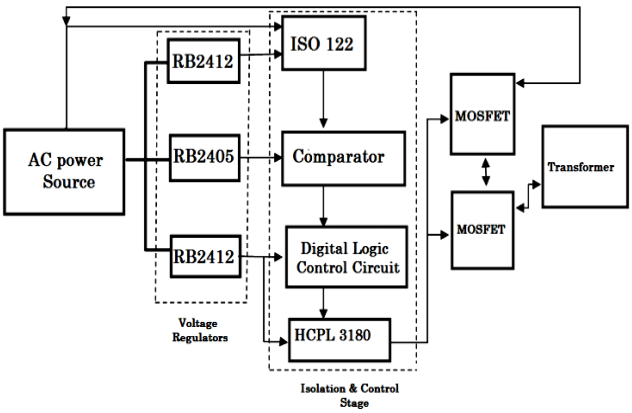

Fig. 15. Power and control circuits implemented in the zero-crossing and phase-hop switch.

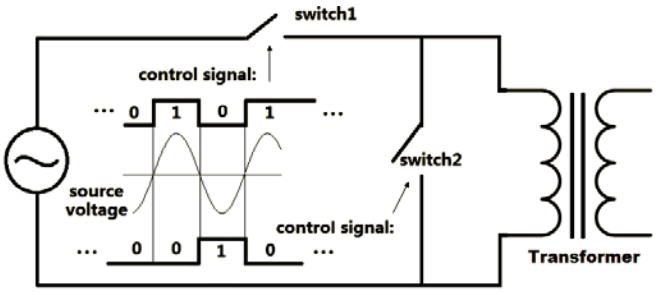

Fig. 16. Schematics of the phase-hop circuit.

XII. Acknowledgment

The authors would like to thank Mr. Nazir Mahamedau, ex-student of Polytechnic Institute of New York University, for his collaboration in building the phase-hop switch and performing the experiments during this project.

XIII. References

[1] B. W. Kennedy, "Power quality primer", McGraw-Hill Companies, 2000, pp. 122-125.

[2] *IEEE Recommended Practice for Monitoring Electric Power Quality*, IEEE Standard 1159-1995, Jun. 1995.

[3] *IEEE Recommended Practice for Powering and Grounding Electronic Equipment*, IEEE Standard 1100-1999, Mar. 1999.

[4] Private communications between engineers of American Power Conversion and Liebert with the second author, Toronto, Ontario, 1999.

[5] IEC Standard 61000-4-11, *Electromagnetic compatibility (EMC): Testing and measurement techniques- Voltage dips, short interruptions and voltage variations immunity tests,* Mar. 2004.

[6] *IEEE Recommended Practice and Requirements for Harmonic Control in Electrical Power Systems*, IEEE Standard 519-1992, Apr. 1993.

[7] J. M. Guerrero, L. G. de Vicuna, and J. Uceda, "Uninterruptible power supply systems provide protection," *Industrial Electronics Magazine, IEEE* , vol.1, no.1, pp.28-38, Spring 2007.

[8] J. Seymour," The seven types of power problems", white paper 18, Revision1, Schneider Electric – Data Center, Science Center, 2011.

[9] F. de León, A. Farazmand, and P. Joseph, "Comparing the T and pi equivalent circuits for the calculation of transformer inrush currents", *IEEE Trans. Power Delivery*, vol. 27, no. 4, pp. 2390-2398, Oct. 2012.

[10] F. de León and A. Semlyen, "Efficient calculation of elementary parameters of transformers", *IEEE Trans. Power Delivery*, vol. 7, no. 1 pp. 376-383, Jan. 1992.

[11] F. de León, S. Jazebi, and A. Farazmand, "Accurate measurement of the air-core inductance of iron-core transformers with a non-ideal low power rectifier," accepted for publication in the IEEE Trans. Power Del.

[12] J. Mahseredjian, S. Dennetière, L. Dubé, B. Khodabakhchian, and L. Gérin-Lajoie, "On a new approach for the simulation of transients in power systems," *Elect. Power Syst. Res.*, vol. 77, no. 11, pp. 1514–1520, Sep. 2007.

[13] J. A. Fleming, "Experimental researches on alternate-current transformers", *Journal of the Institution of Electrical Engineers*, vol. 21, no. 101, pp. 594-686, Nov. 1892.

[14] K. Billings and T. Morey, "Switchmode power supply handbook", 2nd ed., McGraw Hill, NY, pp. 1-6, 1989.

[15] B. Kovan, F. de León, D. Czarkowski, Z. Zabar, and L. Birenbaum, "Mitigation of inrush currents in network transformers by reducing the residual flux with an ultra-low-frequency power source", *IEEE Trans. Power Delivery*, vol. 26, no. 3, pp. 1563-1570, Jul. 2011.

[16] J. H. Brunke and K. J. Frohlich, "Elimination of transformer inrush currents by controlled switching. I. Theoretical considerations", *IEEE Trans. Power Delivery*, vol. 16, no. 2, pp. 276-280, Apr. 2001.

[17] J. H. Brunke and K. J. Frohlich, "Elimination of transformer inrush currents by controlled switching. II. Application and performance considerations", IEEE Trans. Power Delivery, vol. 16, no. 2, pp. 281-285, Apr. 2001.

[18] Y. Cui, S. G. Abdulsalam, S. Chen, and W. Xu, "A sequential phase energization technique for transformer inrush current reduction- Part I: simulation and experimental results", *IEEE Trans. Power Delivery*, vol. 20, no. 2.pp. 943-949, Apr. 2005.

[19] W. Xu, S. G. Abdulsalam, Y. Cui, and X. Liu, "A sequential phase energization technique for transformer inrush current reduction - Part II: theoretical analysis and design guide," *IEEE Trans. Power Delivery*, vol. 20, no. 2, pp. 950- 957, Apr. 2005.

[20] V. Molcrette, J. L. Kotny, J. P. Swan, and J. F. Brudny, "Reduction of inrush current in single-phase transformer using virtual air gap technique", *IEEE Trans. Magnetics*, vol. 34, no. 4, pp. 1192-1194, Jul. 1998.

Ashkan Farazmand was born in Tehran, Iran, in 1983. He received the M.Sc. (Hons.) degree in electrical engineering from the University of Tehran, Tehran, Iran, in 2009, and the Ph.D. degree (Hons.) in electrical engineering from the Polytechnic Institute of New York University, Brooklyn, NY, in 2013. Currently he is a Post-doctoral Fellow in the Electrical and Computer Engineering Department of Polytechnic Institute of New York University. His research interests are design and analysis of transformers, electrical transients, derating of electrical machines under nonsinusoidal and unbalanced conditions, and power quality.

Francisco de León (S'86–M'92–SM'02) received the B.Sc. and the M.Sc. (Hons.) degrees in electrical engineering from the National Polytechnic Institute, Mexico City, Mexico, in 1983 and 1986, respectively, and the Ph.D. degree from the University of Toronto, Toronto, ON, Canada, in 1992. He has held several academic positions in Mexico and has worked for the Canadian electric industry. Currently, he is an Associate Professor at Polytechnic Institute of NYU, Brooklyn, New York. His research interests include the analysis of power phenomena under nonsinusoidal conditions, the transient and steady state analyses of power systems, the thermal rating of cables and transformers, and the calculation of electromagnetic fields applied to machine design and modeling.

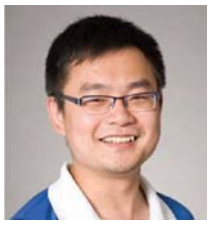

Kuang Zhang (S'12) was born in Ziyang, China, in 1990. He received the B.Eng. degree in Electronic Engineering from South China University of Technology, Guangzhou, China, in 2013, and the B.Sc. degree in Electrical Engineering from the Polytechnic Institute of New York University, Brooklyn, NY, in 2013. He is pursuing Ph.D. degree in Electrical Engineering at the Polytechnic Institute of New York University, Brooklyn, NY. His research interests include modeling, computation and measurement of transformer inrush currents. He is currently working in the areas of power electronics and power quality.

Saeed Jazebi (S'10) was born in 1983, Kerman, Iran. He received his B.Sc. and M.Sc. degrees in 2006 and 2008 in Electrical Engineering from Shahid Bahonar University, Kerman, Iran, and Amirkabir University of Technology, Tehran, Iran, respectively. He is currently a Ph.D. student at the Polytechnic Institute of New York University, Brooklyn, NY. His field of interest includes: electromagnetic design, modeling and simulation of electrical machines and power system components, statistical pattern recognition applications in power engineering, power system protection, and power quality.

Experimentally Validated Reversible Single-Phase Multi-Winding Transformer Model for the Accurate Calculation of Low-Frequency Transients

Saeed Jazebi, *Member, IEEE*, and Francisco de León, *Senior Member, IEEE*

***Abstract*—In this paper, a previously published model for the representation of the leakage inductance of multi-winding transformers is enhanced to support accurate calculations of low-frequency transients, including: inrush currents, series ferroresonance, and geomagnetic induced currents (GIC). The new circuit is obtained from the principle of duality and therefore is physically consistent. The unique characteristic of the improved model is that the very deep saturation behavior of the iron core is properly represented for each winding simultaneously (reversible model) without changing parameters. The hysteresis cycle and iron core losses are also included. In addition to its reversible terminal behavior coupled with physical consistency, the proposed model can be built with circuit elements available in EMTP-type programs and all the parameters can be computed from terminal tests. The model is validated by comparing computer simulations versus laboratory measurements for three- and four-winding transformers.**

***Index Terms*— Duality, electromagnetic transients, ferroresonance, GIC, inrush currents, multi-winding transformers.**

I. Introduction

MULTI-WINDING transformer models have broad applications in design and development of power system and power electronic devices. Several multi-winding transformer models exist in the literature. Among them, the models presented in [1]-[10] need to be acknowledged. The saturation inductance (frequently called "air-core" inductance) and winding resistance, the dominant parameters for transients when the core saturates, are different for each winding since the geometry (at the very least the radius) is different; see [11] and [12]. Therefore, inrush currents, geomagnetic induced currents (GIC), and ferroresonance occur at different levels of current and voltage for each winding. Laboratory measurements on a four-winding transformer are shown in Fig. 1. This figure demonstrates the significant difference in the transient response of the windings during inrush currents. This attribute is neither reported nor considered in publications dedicated to multi-winding transformer models.

S. Jazebi and F. de León, are with the Department of Electrical and Computer Engineering at the NYU Polytechnic School of Engineering, Six Metrotech Center, Brooklyn, NY, 11201 (e-mails: jazebi@ieee.org, fdeleon@nyu.edu).

Recently, an analytical solution for single-phase two-winding transformers was proposed based on equivalent reluctance circuits [13]. The model accurately considers the deep saturation behavior of the two windings simultaneously, and therefore, the word *reversible* was coined for this model. However, the model of [13] cannot be built with circuit elements available in EMTP-type programs. Thereafter, a dual magnetic-electric model was proposed to overcome this drawback in [14]. The model of [14] is derived from terminal measurements and is easy to implement in any EMTP-type program since it uses only standard circuit element.

It is known that the terminal behavior of the duality derived transformer models does not always match the terminal measurements performed in the laboratory; see [8] and [14]. The main contribution of this paper is to enhance the terminal behavior of the multi-winding transformer model presented in [8] and [9] to accurately represent the low-frequency behavior of different windings involving very deep saturation.

The equivalent magnetic-electrical model of this paper is derived from the principle of duality. Step-by-step guidelines to compute the parameters of the model from measurements are presented. The model includes: leakage inductances, mutual couplings, hysteresis loops, and iron core losses. The very deep saturation regions of the magnetizing branches are calculated from the solution of the equivalent circuit to match the terminal measurements. The model is compatible with all circuit simulators since only standard circuit elements are needed. The excellent agreement between simulations and laboratory measurements demonstrate that the model is accurate and perfectly reversible.

This paper deals with single-phase multi-winding transformers. The same methodology will be applied to the multi-phase multi-winding model presented in [10] in a forthcoming paper.

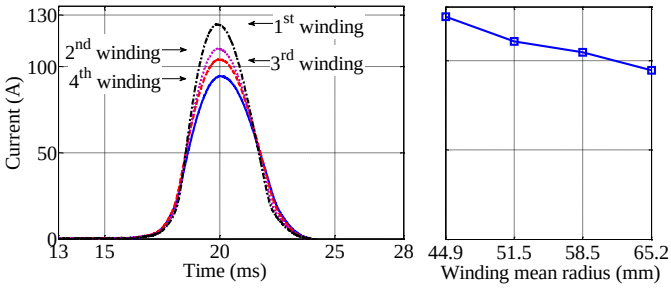

Fig. 1. Inrush current amplitudes for concentric windings with different mean radius. All windings have the same number of turns and conductor cross sectional area. The saturation inductance and the winding resistance increase for windings with larger radii, which reduce the inrush currents.

II. Modeling Principles

The structure of the model is derived from the direct application of the principle of duality to multi-winding transformers. Fig. 2 illustrates half the window of a shell-type *n*-winding single-phase transformer. The equivalent electrical circuit is depicted on top of the transformer frame. The leakage inductances are modeled with linear inductors and mutual couplings. The leakage inductances between the windings are represented by L_{ij}. The mutual inductances (M_{ij}) compensate for the missing linking flux between the windings [8], [9]. The iron core is modeled using hysteretic inductors. Also, non-linear inductors are considered for the contribution of the magnetic energy in the air [14]. The methodology replicates the physical behavior of the magnetic flux for different operating conditions. Therefore, it is in full agreement with the principle of duality and modifies the equivalent circuit for high saturation conditions. This is so because in the operating regions below the knee point (during the short circuit, normal open circuit, and nominally loaded), the value of the air inductances are negligible when compared to the iron-core inductances. However, in deep saturation the distribution of the magnetic energy completely changes, because a saturated iron core becomes linear with incremental permeability similar to air. Therefore, the magnetic flux is no longer concentrated solely in the iron core, but is distributed in the transformer window and air (see Fig. 3). Under these conditions, the flux between the windings and the core and the flux outside of the transformer window become significant since they are comparable to the flux in the core and leakage flux between the windings.

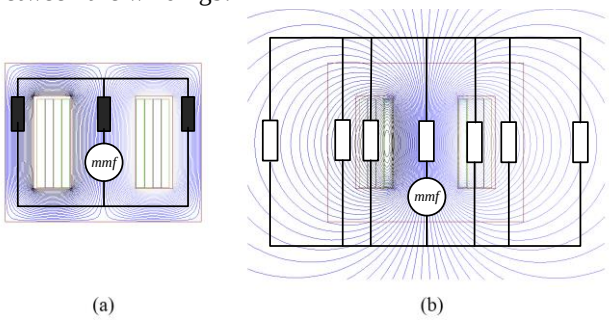

Fig. 3. Magnetic field strength and the magnetic circuit for open circuited transformer (a) normal operating region; (b) deep saturation region ($\mu_r \rightarrow 1$).

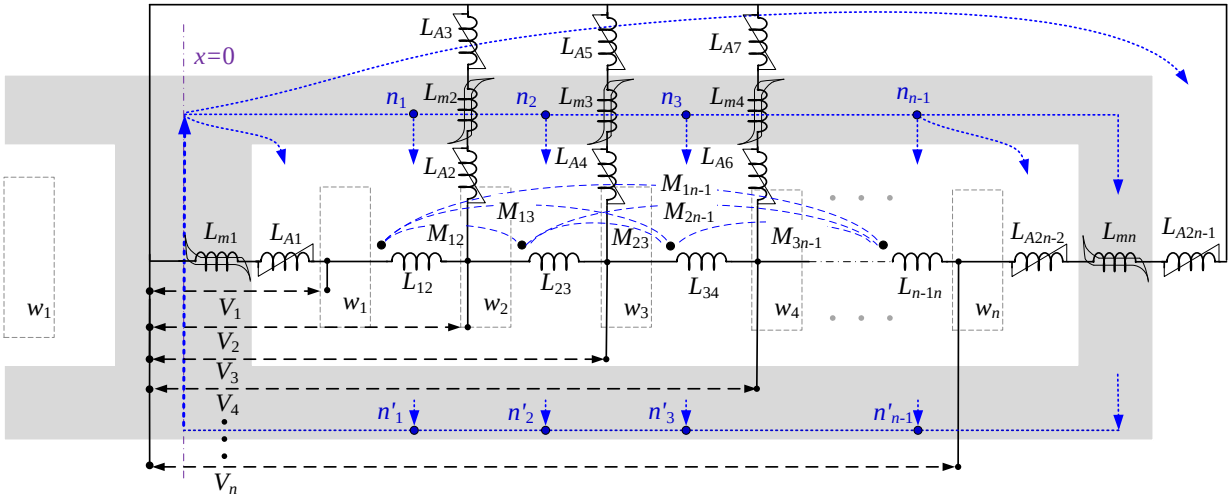

Fig. 2. Direct application of the principle of duality on a multi-winding transformer. Note that, due to the symmetry of the equivalent electrical circuit with respect to *x*=0 axis, only the right half side of the transformer window is illustrated.

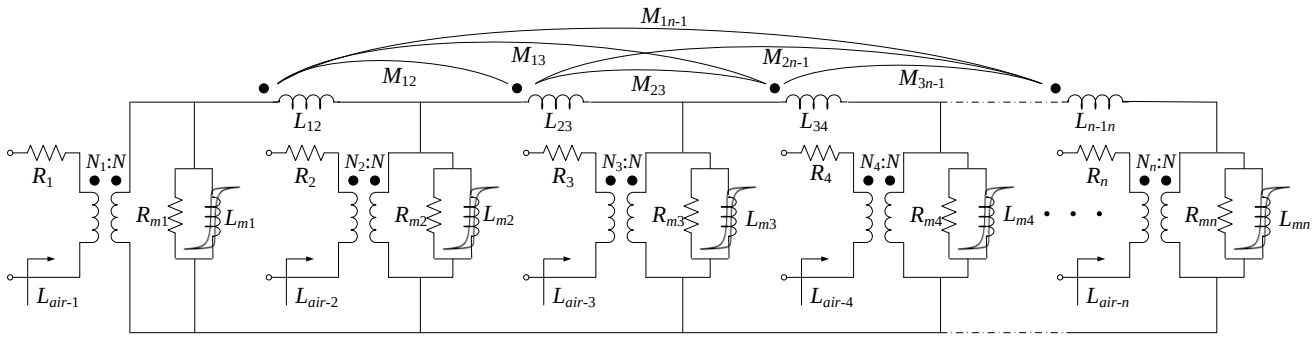

Fig. 5. Reversible multi-winding transformer model including resistances and ideal transformers; $L_{air\text{-}1}$, $L_{air\text{-}2}$, … $L_{air\text{-}n}$ are the saturation inductances of the windings for the modification of the terminal response of the model for the high saturation region.

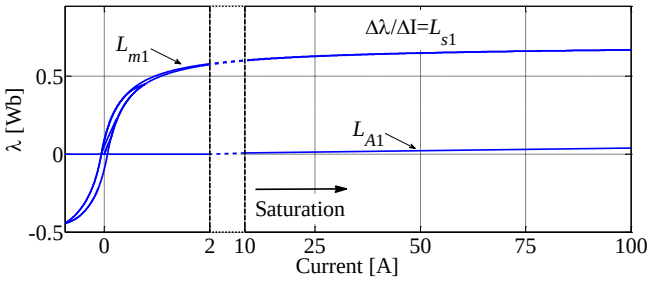

Fig. 4. Magnetizing characteristic of the branch L_{m1} for a 1 kVA 120 V shell-type transformer.

To accurately represent the above mentioned phenomenon, the non-linear air inductances (inductances L_{A1} to L_{A2n-1} in Fig. 2) are represented with two slopes; zero in normal operating regions, and a constant slope in high saturation. Fig. 4 illustrates the magnetizing characteristics of the inductor L_{m1} and the air inductance L_{A1}. In this figure, L_{s1} represents the inductance of the linear part (in deep saturation) of the magnetizing curve. The series inductances L_{A1} and L_{m1}; L_{A2}, L_{A3}, and L_{m2} …; and L_{A2n-2}, L_{A2n-1}, and L_{mn} could be merged into single inductors. For example, according to the characteristics of L_{A1} shown in Fig. 4, only the high saturation slope of L_{m1} changes to L_1= L_{A1}+ L_{s1}, where L_1 is the modified slope of L_{m1} in the high saturation region. Similarly, L_n represents the deep saturation slope of the magnetizing inductor L_{mn} in the model. Then, the winding resistances, core losses, and ideal transformers are added to the circuit of Fig. 2; see in Fig. 5 the final model.

The principal advantage of this model, which differentiates it from the model of [8], is the computation of the deep saturation inductances of the magnetizing inductors (L_{mn}). Note that according to the equivalent circuits of Figs. 2 and 5, a hysteretic magnetizing inductor is connected in parallel with the terminals of each winding. These n inductors are frequently called magnetizing or non-linear branches in this paper. The existence of the n branches provides adequate degrees of freedom to correctly characterize the different equivalent inductance values from the terminals in the saturation region.

As noted above, the electromagnetic behavior of the core and air is different under normal operating condition than in deep saturation. Therefore, magnetizing branches are modeled in two steps: First the non-linear behavior of the iron core in the non-saturated region, below the knee point, is considered including hysteresis; second, the linear behavior of the iron core in deep saturation is added. The guidelines for the calculation of the unknown parameters of the model are described in the following subsections.

A. Magnetizing Branches: Hysteresis Curve

In an open circuited transformer excited with rated voltage, the iron core operates below the knee point, where the value of the magnetizing inductance is substantially larger than the leakage inductances. Hence, the leakage inductances together with its mutual couplings are negligible in comparison with the magnetizing inductances. Note that, during the standardized open circuit test with nominal voltage excitation, the magnetic flux is concentrated in the iron core. Therefore, similar hysteresis curve and magnetizing parameters (R_m and L_m) are obtained from measurements on the different windings. This has been demonstrated experimentally by measuring almost the same magnetizing current in all windings when excited with rated voltage, within measuring accuracy.

In the normal operating region, the measured λ_m-i_m characteristic could be distributed between the n magnetizing branches considering the leg/yoke geometrical proportions. Because the leakage inductances do not exist, the nonlinear branches of Fig. 2 are effectively in parallel. Note that, it is possible to estimate the design details, such as dimensions of the iron core and windings with the method of [15]. Nevertheless, for simplicity, it is assumed that the transformer window is square. Thus, the length of the legs is the same as the length of the yokes. Also, it is assumed that the distances between the neighboring windings are the same. Hence, the leakage fluxes leave the yoke at points located at 1/n, 2/n, …, (n-1)/n of the length of the yoke (see nodes n_1, n_2, ..n_{n-1} in Fig. 2). Therefore, the limbs are physically divided into n-2 regions which result in L_{m2}= L_{m3}=…=L_{mn-1}. Besides, L_{m1}=L_{mn}, because normally the width of the center leg is twice the width of the side legs and the length of the flux paths are the same (distance between nodes n_1, n'_1, and n_{n-1}, n'_{n-1} in Fig. 2). Finally, for the n-winding transformer, the method of [9] is extended as follows:

$$L_{m1} = L_{mn} = \frac{4nL_m}{n+2}, \quad L_{m2} = L_{m3} = \cdots = L_{mn-1} = 2nL_m \qquad (1)$$

where L_m is the magnetizing inductance measured from any winding. Hence, the λ-i characteristics of each branch are obtained with the following expressions:

$$\begin{aligned} &\lambda_{m1}(k) = \lambda_{m2}(k) = \cdots = \lambda_{mn}(k) = \lambda_m(k) \\ &i_{m1}(k) = i_{mn}(k) = \frac{(n+2)i_m(k)}{4n} \\ &i_{m2}(k) = i_{m3}(k) = \cdots = i_{mn-1}(k) = \frac{i_m(k)}{2n} \end{aligned} \qquad (2)$$

where λ_{mi}-i_{mi} is the magnetizing curve of the i^{th} nonlinear branch and k is the k^{th} point of the data. Trapezoidal rule of integration is applied to compute λ_m from the measured terminal voltage obtained from the open circuit tests. Note that current i_m is measured in the primary (low voltage) winding and the induced voltage is captured at the open circuited secondary (high voltage) winding.

B. Magnetizing Branches: Deep Saturation Region

The magnetic circuit of an open circuited transformer consists of several parallel branches connected to a *mmf* (see Fig. 3). The circuit can be simplified (by series/parallel combinations) resulting in a single nonlinear reluctance with hysteretic characteristic for normal conditions and linear behavior in deep saturation. The dual electrical representation of this model is a single hysteretic branch. Therefore, the simplest dual representation of a transformer model in the open circuit condition is a single hysteretic inductor in series with the terminal resistance of the corresponding winding. This could be seen in Fig. 6 (a)

and (b) for the first and the second windings of a two-winding transformer.

Note that, the leakage inductances do not have a physical existence in open circuit conditions (because there is no leakage flux when only one winding is energized). However, to simulate the normal operating conditions, a model requires of the representation of the leakage flux between the two windings (when at least two windings are energized). To have a unique model in both open and short circuit conditions, the leakage components need to be added to the circuits according to Fig. 6 (c). However, the addition of the leakage inductance affects the behavior of the open circuit condition of the model of Fig. 6 especially in the deep saturation region.

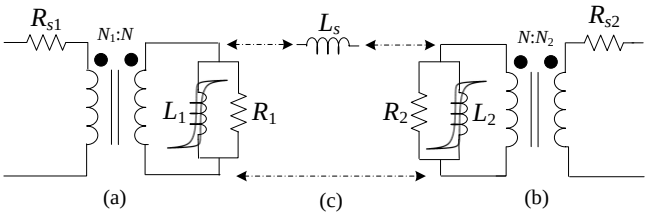

Fig. 6. Infrastructure of a duality-derived π model for a 2- winding transformer; (a) the simplest dual representation of the 1st winding for all open circuit conditions; (b) the simplest dual representation of the 2nd winding for all open circuit conditions; (c) addition of the leakage inductance to consider the contribution of the leakage flux during the short circuit and normal loaded conditions. The joint connection of L_s, L_1 and L_2 affects the open circuit behavior of the transformer especially in deep saturation.

Fig. 7. Equivalent circuits for the calculation of the saturation inductances for a three-winding transformer; simplified circuit seen from (a) the 1st winding, (b) the 2nd winding, (c) the 3rd winding.

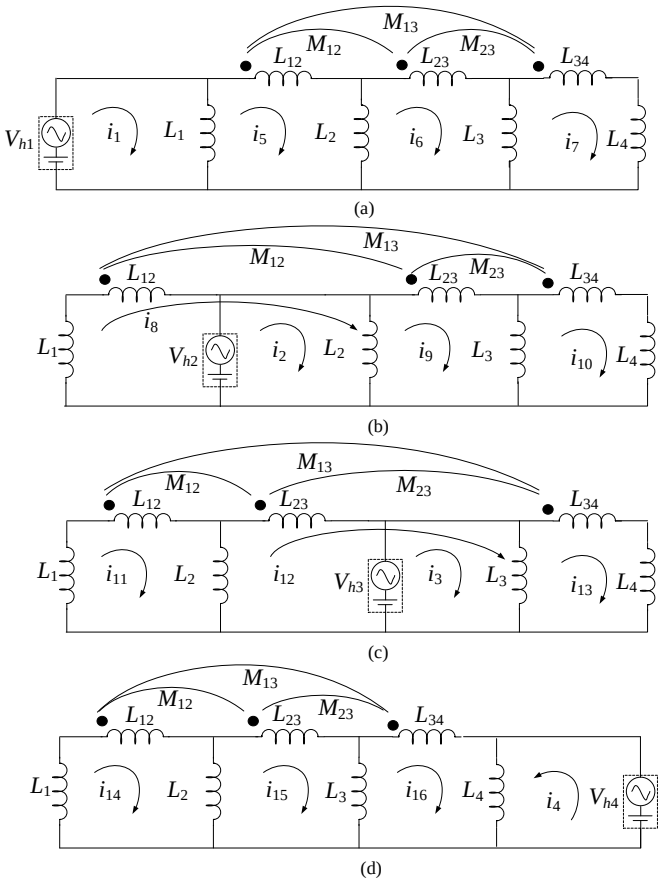

Fig. 8. Equivalent circuits for the calculation of the saturation inductances seen from the four terminals of the four-winding transformer; simplified circuit seen from (a) the 1st winding, (b) the 2nd winding, (c) the 3rd winding, (d) the 4th winding.

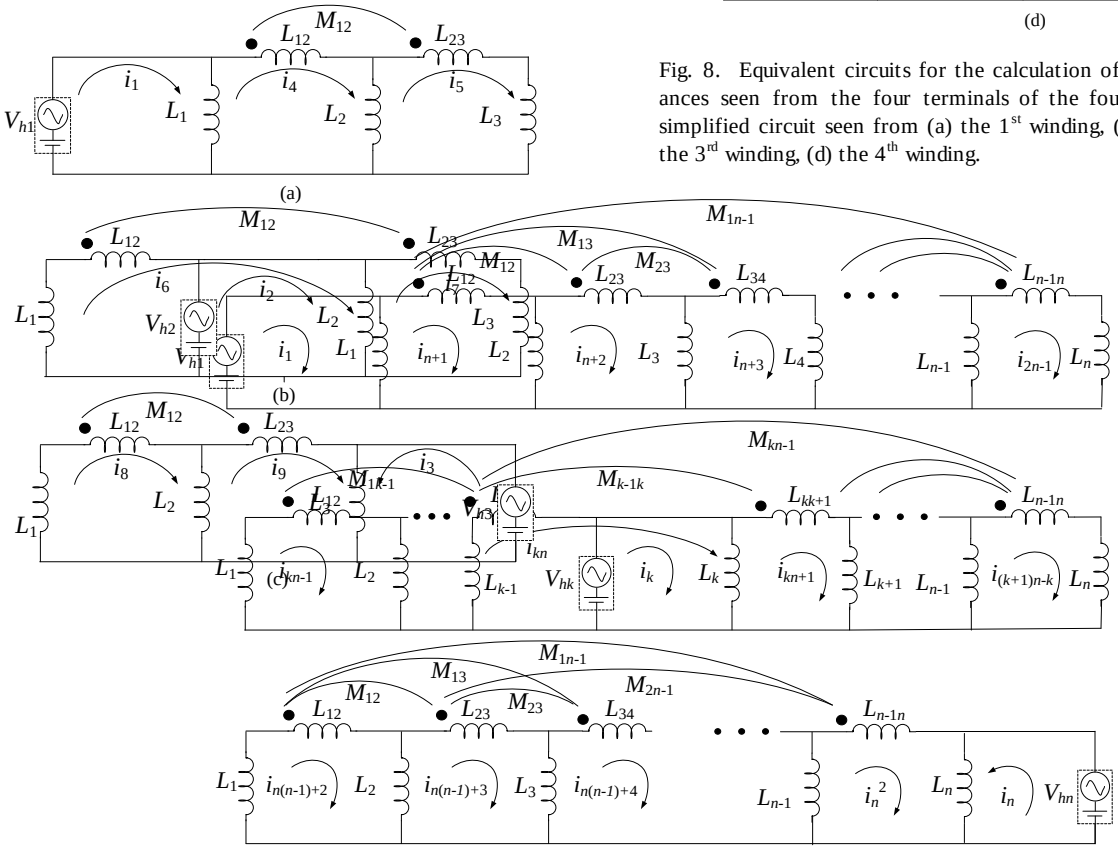

Fig. 9. Simplified equivalent circuits seen from the n terminals of the n-winding transformer for the calculation of the saturation inductances.

The leakage inductance is negligible when transformers operate below the knee point in the open circuit condition. This is so because the magnetizing inductances are much larger than the leakage inductance. For higher excitations, however, the slope of the magnetizing curves decays to the values of the deep saturation inductances L_1, L_2,…, and L_n, which are of the same order of magnitude than the leakage inductances. Under these conditions, the effect of the leakage inductance in the equivalent circuit cannot be neglected, considering the fact that leakage inductances are requisites for normal operation and are a part of the model (see Figs. 2 and 5). This causes a mismatch between the terminal measurements and the behavior of the model of [8] in the deep saturation region. To overcome this drawback, general formulas are proposed to precisely calculate L_1, L_2, …, and L_n.

1) Derivation of the System Equations:

To retrofit the terminal behavior of the model in deep saturation, L_1, L_2, …, L_n need to be calculated correctly. Fig. 7 illustrates the equivalent circuits seen from different terminals of a three winding transformer. Note that, in each case the secondary and tertiary windings are open circuited and the damping components are removed for the analysis since only saturation inductances are measured. The primary winding is excited with a hybrid *ac/dc* voltage source to drive the transformer into deep saturation as recommended in [12]. The modeling technique is based on terminal measurements, therefore, the topology of the model is consistent for transformers with or without tank, magnetic tank shunts, belts, etc. However, the deep saturation inductance measurements are affected in the presence of these transformer parts, which change the values of L_1, L_2, …, L_n. The term "air-core inductance" [12] can only be used for an air coil or a transformer without core and tank. Therefore, in this paper, it is substituted with "saturation inductance" as in [16]. As the result of the *ac/dc* excitation, all three magnetizing branches operate in the linear saturated region. Therefore, these branches are represented with the corresponding constant slope part of the deep saturation region (L_1, L_2, and L_3). Fig. 8 illustrates the equivalent circuits seen from the terminals of a four-winding transformer in deep-saturation. Similar circuits are derived for the *n*-winding transformer as shown in Fig. 9.

The first step is to obtain the equivalent inductances seen from the terminals of the model ($L_{air\text{-}1}$, $L_{air\text{-}2}$,…, $L_{air\text{-}n}$) with respect to the variables L_1, L_2, …, L_n. The judicious selection of the meshes, including direction and numbering, as illustrated in Figs. 7 to 9, is essential to obtain simplified equations suitable for generalization. These mesh equations are written for the fundamental components of the voltage and current, where V_i is the fundamental component of the hybrid voltage source V_{hi}, as follows:

$$j\omega[K]_{n^2\times n^2}[I]_{n^2\times 1}=[V]_{n^2\times 1} \quad , \quad [K]=\begin{bmatrix} A & B \\ B^T & D \end{bmatrix} \tag{3}$$

The current and voltage vectors are as follows:

$$[I]=\begin{bmatrix} i_1, i_2, i_3, \ldots i_{n^2} \end{bmatrix}^T \quad , \quad [V]=[v_1, v_2, \ldots v_n, 0, 0, \ldots 0]^T \tag{4}$$

The $A_{n\times n}$ matrix for the three-, four-, and *n*-winding transformers are written as follows:

$$\begin{aligned} [A]_{3\times 3} &= diag[L_1 \quad L_2 \quad L_3] \\ [A]_{4\times 4} &= diag[L_1 \quad L_2 \quad L_3 \quad L_4] \\ [A]_{n\times n} &= diag[L_1 \quad L_2 \quad \ldots \quad L_{n-1} \quad L_n] \end{aligned} \tag{5}$$

The elements of $B_{n\times n(n\text{-}1)}$ for the three-winding transformer are zeros except for the following components:

$$B_{11}=-L_1 \, , B_{36}=L_3 \, , B_{23}=L_2 , B_{24}=-L_2 \tag{6}$$

For the four-winding transformer, the following elements of *B* are nonzero:

$$\begin{aligned} &B_{11}=-L_1, B_{4,12}=L_4, B_{24}=L_2, B_{25}=-L_2 \\ &B_{38}=L_3, \; B_{39}=-L_3 \end{aligned} \tag{7}$$

The nonzero elements of the *B* matrix for the *n*-winding transformer are as follows:

$$\begin{aligned} &B_{11}=-L_1, B_{n,(n-1)n}=L_n \\ &B_{i,(i-1)n}=L_i, B_{i,(i-1)n+1}=-L_i, \quad i=2,3,\cdots n-1 \end{aligned} \tag{8}$$

The *D* matrix is written as follows:

$$[D_a]_{(n-1)\times(n-1)}=\begin{bmatrix} L_1+L_2+L_{12} & M_{12}-L_2 & M_{13} & \ldots & M_{1n-2} & M_{1n-1} \\ M_{12}-L_2 & L_2+L_3+L_{23} & M_{23}-L_3 & M_{24} & M_{2n-2} & M_{2n-1} \\ M_{13} & M_{23}-L_3 & L_3+L_4+L_{34} & M_{34}-L_4 & M_{3n-2} & M_{3n-1} \\ \vdots & M_{24} & M_{34}-L_4 & \ddots & & \vdots \\ M_{1n-2} & & & & L_{n-2}+L_{n-1}+L_{n-2,n-1} & M_{n-2,n-1}-L_{n-1} \\ M_{1n-1} & M_{2n-1} & M_{3n-1} & \ldots & M_{n-2,n-1}-L_{n-1} & L_{n-1}+L_n+L_{n-1,n} \end{bmatrix} \tag{12}$$

$$f_1(L_1,L_2,L_3)=L_1-\left[L_1^2\left(L_2+L_3+L_{23}\right)\right]/\left[\left(L_1+L_2+L_{12}\right)\left(L_2+L_3+L_{23}\right)-\left(M_{12}-L_2\right)^2\right]-L_{air-1}=0 \tag{15}$$

$$f_2(L_1,L_2,L_3)=\left[L_2\left(L_1+L_{12}\right)\left(L_3+L_{23}\right)-L_2M_{12}^2\right]/\left[\left(L_1+L_2+L_{12}\right)\left(L_2+L_3+L_{23}\right)-\left(M_{12}-L_2\right)^2\right]-L_{air-2}=0 \tag{16}$$

$$f_3(L_1,L_2,L_3)=L_3-\left[L_3^2\left(L_1+L_2+L_{12}\right)\right]/\left[\left(L_1+L_2+L_{12}\right)\left(L_2+L_3+L_{23}\right)-\left(M_{12}-L_2\right)^2\right]-L_{air-3}=0 \tag{17}$$

$$[D]_{(n-1)^2\times(n-1)^2}=\begin{bmatrix}[D_a] & & & \\ & [D_a] & & \\ & & \ddots & \\ & & & [D_a]\end{bmatrix} \quad (9)$$

where, D_a for the three-winding transformer is:

$$[D_a]_{2\times2}=\begin{bmatrix}L_1+L_2+L_{12} & M_{12}-L_2\\ M_{12}-L_2 & L_2+L_3+L_{23}\end{bmatrix} \quad (10)$$

For the four-winding transformer D_a is:

$$[D_a]_{3\times3}=\begin{bmatrix}L_1+L_2+L_{12} & M_{12}-L_2 & M_{13}\\ M_{12}-L_2 & L_2+L_3+L_{23} & M_{23}-L_3\\ M_{13} & M_{23}-L_3 & L_3+L_4+L_{34}\end{bmatrix} \quad (11)$$

and for the *n*-winding transformer the D_a matrix is given in (12) shown at the bottom of the page.

2) Solution of the System Equations:

The air core inductances ($L_{air\text{-}1}$, $L_{air\text{-}2}$,…$L_{air\text{-}n}$) seen from each winding are calculated from the following expressions (see Figs. 7, 8 and 9):

$$L_{air-1}=\frac{v_1}{j\omega i_1},\quad L_{air-2}=\frac{v_2}{j\omega i_2},\quad \ldots L_{air-n}=\frac{v_n}{j\omega i_n} \quad (13)$$

Equation (13) can be substituted into (3). Note that, unknowns i_{n+1}, i_{n+2}, …, i_n [2] in (3) do not need to be computed. Therefore, Kron reduction [17] is used to eliminate those variables and the system order decreases from n^2 to n:

$$K_{new}=A-B\times D^{-1}\times B^T$$
$$I_{new}=[i_1,i_2,\ldots i_n]^T\quad,\quad V_{new}=[v_1,v_2,\ldots v_n]^T \quad (14)$$

The result of this step is a system of n nonlinear equations with n unknowns L_1, L_2, …, L_n. Equations (15) to (17), at the bottom of the previous page, are the resultant equations for a three-winding transformer. Note that, $L_{air\text{-}1}$, $L_{air\text{-}2}$, …, $L_{air\text{-}n}$ are known parameters which are experimentally measured with a hybrid *ac*/*dc* source method as proposed in [12]. Some alternative methods to measure high saturation behavior of transformers could be found in [18]-[21].

To solve the system of non-linear algebraic equations, the trust-region-reflective algorithm is applied using the embedded Matlab function 'lsqnonlin'. This function minimizes the set of non-linear equations with least square data-fitting as follows:

$$\min\left\|f(L_1,L_2,L_3\ldots L_n)\right\|_2^2=\min\begin{pmatrix}f_1(L_1,L_2,L_3\ldots L_n)^2\\ +f_2(L_1,L_2,L_3\ldots L_n)^2\\ \vdots\\ +f_n(L_1,L_2,L_3\ldots L_n)^2\end{pmatrix} \quad (18)$$

The parameters are initialized with the saturation inductance values: $L_1(0)=L_{air\text{-}1}$, $L_2(0)=L_{air\text{-}2}$, $L_3(0)=L_{air\text{-}3}$, …, $L_n(0)=L_{air\text{-}n}$. Finally, the characteristics of the *n* magnetizing branches computed by (2) are extended from the last point to infinity using L_1, L_2,…, L_n as constant slopes.

C. Leakage Inductances

The leakage inductances are calculated as in reference [8] using the standard short circuit tests performed on each pair of windings independently [22]. The self inductances are:

$$L_{i,i+1}=Ls_{i,i+1},\qquad i=1,2,\ldots n-1 \quad (19)$$

where $Ls_{i,i+1}$ is the measured leakage inductance between windings i, and i+1, and $L_{si,i}$ =0 [8]. Consequently, the mutual inductances M_{ij} are calculated with the following expression:

$$M_{ij}=\frac{Ls_{i,j+1}+Ls_{i+1,j}-Ls_{i,j}-Ls_{i+1,j+1}}{2} \quad (20)$$

Expressions (19) and (20) have been validated experimentally in [10] for transformers of 96 and 360 MVA. The results are identical to the BCTRAN model proposed in [1].

D. Core Losses

Constant resistors R_{m1}, R_{m2}, …, R_{mn} are added to consider the iron core losses [23]. The method applied in [9] is extended for the *n*-winding transformers. The following equations are obtained with the same assumptions presented in Section II. A (above):

$$R_{m1}=R_{mn}=\frac{n^2R_m}{2},\quad R_{m2}=R_{m3}=\cdots=R_{mn-1}=\frac{n^2R_m}{n+2} \quad (21)$$

where R_m is the equivalent resistance computed from the standard open circuit measurements to represent the iron-core losses.

III. Model Validation

Reversible models for three- and four-winding transformers are developed and validated in this section. The models are implemented for a 1-kVA, 120 V, 4-winding isolation transformer. The complete data, such as iron core dimensions, leakage inductances between different windings, saturation inductances and resistances of different windings, etc. are available in [14]. The reversible model is compared with the conventional model (called nonreversible model) and measurements for validations in different transient conditions.

In the nonreversible model, all parameters are derived according to the guidelines presented in previous sections except the nonlinear branches. In this model, the magnetizing characteristics are extended without the corrections provided in Section II-B. The saturation inductance of the innermost winding is used to adjust the model parameters which give the correct transient behavior of the innermost winding. Note that the same winding resistances are used in both models. Therefore, the performance differences are only due to the use of the wrong saturation inductances in the traditional model.

A. Three-Winding Model

The model for the three-winding transformer is obtained from the first three windings of the four-winding transformer under study. The 4th winding is left disconnected.

1) Inrush Currents:

The transformer is energized through a switch that closes when the voltage of the sinusoidal source is crossing zero. The

transformer is demagnetized before each experiment. Fig. 10 illustrates the accuracy of the reversible model in comparison to the nonreversible model. In this case, the nonreversible model overestimates the inrush currents by 21.5%, and 22.9%, for the second and the third windings, respectively. The comparison of the results for inrush currents are presented in Table I. The differences between the reversible model results and measurements are about 5%.

2) Ferroresonance:

For ferroresonance experiments, a 44 μF series capacitance is connected between the source and the transformer terminal. The transformer is completely demagnetized and the capacitor is discharged before each measurement. The simulation results are compared to measurements in Table II. One can observe that the simulation results are in good agreement with the laboratory measurements. The same tests are performed for the 22 μF and 66 μF capacitors, and satisfactory results with errors less than 5% are achieved. EMTP simulations show that the nonreversible model is also correct for the calculation of ferroresonance. The overall differences between the reversible and nonreversible models are less than 2%.

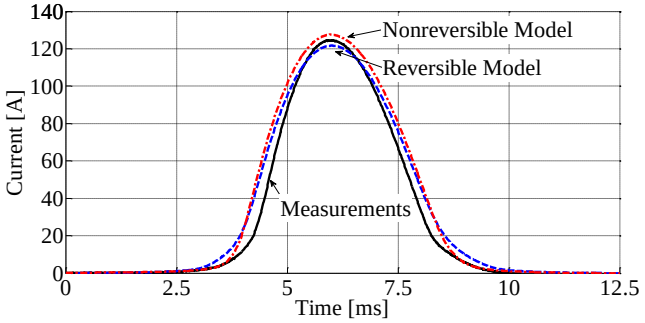

(a)

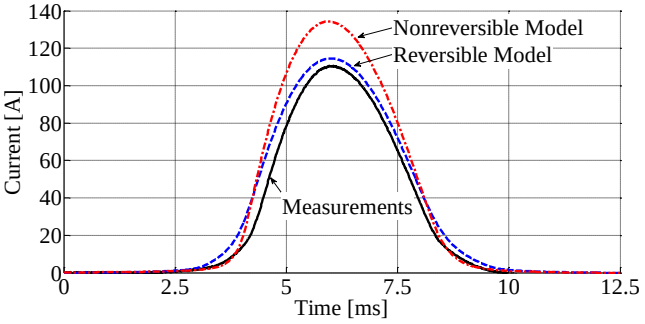

(b)

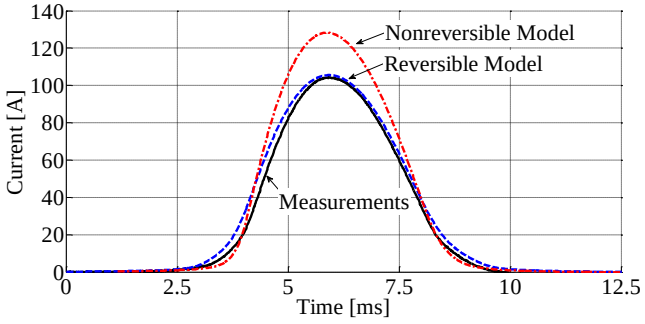

(c)

Fig. 10. First peak of inrush currents to validate the three-winding model; (a) Innermost winding, (b) Inner winding, (c) Outer winding.

3) Geomagnetic Induced Currents:

Geomagnetic induced currents cause a *dc* potential on the surface of the earth. Therefore, during GIC, the transformer neutral is biased with a *dc* voltage [24]. This condition is simulated in the laboratory and EMTP with a hybrid *dc*/*ac* excitation. The hybrid voltage source includes a *dc* generator in series with an *ac* source. The *dc* voltage could be controlled with the field excitation of the generator. The hybrid source is connected to the primary terminal of the transformer while the secondary terminal is open circuit. The schematic diagram of the laboratory setup is presented in Fig. 11. The switch is always closed in this experiment.

Simulations results for the nonreversible and the reversible models are compared versus measurements in Table III. One can see a good agreement between the reversible model and measurements. The nonreversible model shows relative errors of 8%, and 18.8% with respect to the measurements.

4) GIC + Energization

One of the extreme cases of inrush currents could occur when the transformer is energized on zero crossing of the voltage while the neutral of transformer is biased by geomagnetic induced currents. This phenomenon is simulated with both the nonreversible and the reversible models (see Fig. 11 for the simulated circuit). The results are compared for the three-winding transformer model. The nonreversible model predicts the inrush currents with 16.3%, and 20.5% errors for the inner, and outer windings, when compared to the reversible model. Fig. 12 shows the simulation results for the outer winding. These results show the significance of the reversible model for extreme cases with higher degrees of saturation.

TABLE I
COMPARISON OF INRUSH CURRENT PEAK VALUES FOR THE THREE-WINDING TRANSFORMER

Winding	Meas. [A]	Nonrev. [A]	Diff. (%)	Rev. [A]	Diff. (%)
1st	124.4	127.6	2.6	121.7	2.1
2nd	110.6	134.4	21.5	114.5	3.5
3rd	104.5	128.4	22.9	105.6	1.0

TABLE II
MAXIMUM TEMPORARY OVERVOLTAGE MEASURED AND SIMULATED FOR THE THREE-WINDINGS TRANSFORMER AND A 44 μF CAPACITOR [V]

Winding	Meas. [V]	Nonrev. [V]	Diff. (%)	Rev. [V]	Diff. (%)
1st	226.5	213.9	5.6	216.1	4.6
2nd	226.4	212.2	6.3	216.4	4.4
3rd	223.5	214.7	3.9	216.5	3.1

TABLE III
COMPARISON OF GEOMAGNETIC INDUCED CURRENTS PEAK VALUES FOR THE THREE-WINDINGS TRANSFORMER

Winding	V_{dc} [V]	Meas. [A]	Nonrev. [A]	Diff. (%)	Rev. [A]	Diff. (%)
1st	4.09	46.4	47.4	2.1	44	5.1
2nd	3.59	39.9	43.4	8.0	37.7	5.5
3rd	4.74	44.8	51.3	18.7	44.5	0.7

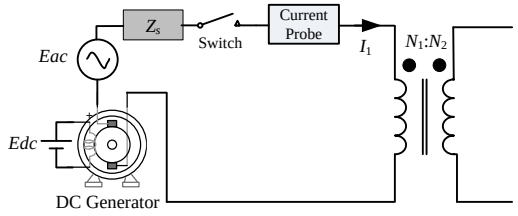

Fig. 11. Laboratory test setup for the geomagnetic induced currents.

B. Four Winding Model

The reversible model is validated for the four-winding transformer under inrush current, ferroresonance, and GIC. The results are compared to the nonreversible model and measurements in Tables IV to VI. The great agreement between the results of simulations for the reversible model and laboratory measurements for all of the windings demonstrates the effectivity of the reversible model (all differences are under 5%). On the other hand, the nonreversible model does not properly represent the behavior of all four windings simultaneously. The errors range from a few percent and up to 24%.

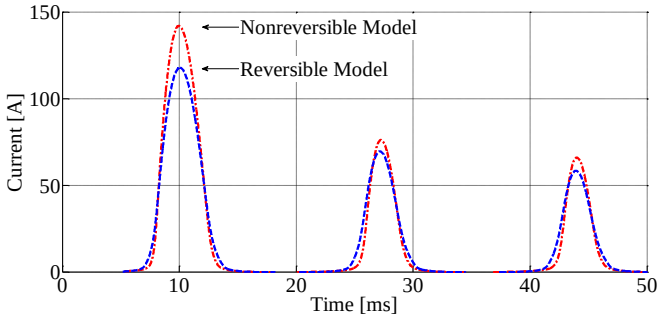

Fig. 12. Inrush current when transformer coils are drawing geomagnetic induced currents. Note that due to the lack of space only the behavior of the outer winding is depicted.

TABLE IV
COMPARISON OF INRUSH CURRENT PEAK VALUES FOR THE FOUR-WINDING TRANSFORMER

Winding	Meas. [A]	Nonrev. [A]	Diff. (%)	Rev. [A]	Diff. (%)
1st	124.4	123.1	1.0	121.2	2.6
2nd	110.6	131.8	19.2	111.7	1.0
3rd	104.5	127.8	22.3	100.2	4.1
4th	94.6	117.4	24.1	93.8	0.8

TABLE V
MAXIMUM TEMPORARY OVERVOLTAGE MEASURED AND SIMULATED FOR THE FOUR-WINDINGS TRANSFORMER AND A 44 μF CAPACITOR [V]

Winding	Meas.	Nonrev.	Diff. (%)	Rev.	Diff. (%)
1st	226.5	214.3	5.4	216.9	4.2
2nd	226.4	214.2	5.4	216.1	4.5
3rd	223.5	214.3	4.1	215.7	3.5
4th	221.9	213.4	3.8	214.4	3.4

TABLE VI
COMPARISON OF GEOMAGNETIC INDUCED CURRENTS PEAK VALUES FOR THE FOUR-WINDINGS TRANSFORMER

Winding	V_{dc} [V]	Meas. [A]	Nonrev. [A]	Diff. (%)	Rev. [A]	Diff. (%)
1st	4.09	46.4	46.2	0.4	47.3	1.9
2nd	3.59	39.9	42.4	6.3	40.3	1.0
3rd	4.74	44.8	50.2	12.0	46.1	2.9
4th	4.72	42.6	47.3	11.0	43.8	2.8

IV. CONCLUSIONS

The model of references [8] and [9] has been retrofitted to produce a reversible model for multi-winding transformers. Analytical formulae have been derived to calculate the required parameters from terminal tests. The model can be easily implemented in EMTP-type programs for *n*-winding transformers since all components are available in their library. The model has been validated by comparing measurements and simulations for three- and four-winding transformers for inrush currents, ferroresonance, and geomagnetic induced currents.

The results show the necessity of the proposed improvement to compute transients involving deep saturation. The model is physically sound and very simple to implement without access to the construction geometry and material information of the transformer. All model parameters can be computed from terminal tests.

V. REFERENCES

[1] V. Brandwajn, H. W. Dommel, and I. I. Dommel, "Matrix Representation of Three-Phase N-winding Transformers for Steady-State and Transient Studies," *IEEE Trans Power App. Syst.*, vol. PAS-101, no. 6, pp. 1369–1378, Jun. 1982.

[2] V. A. Niemela, G. R. Skutt, A. M. Urling, Y. Chang, T. G. Wilson, H. A. Owen, and R. C. Wong, "Calculating the Short-Circuit Impedances of a Multiwinding Transformer From its Geometry," in *Proc. IEEE Power Electron. Spec. Conf.*, 1989, pp. 607-617.

[3] H. Mohseni, "Multi-Winding Multi-Phase Transformer Model with Saturable Core," *IEEE Trans. Power Del.*, vol. 6, pp. 166–173, Jan. 1991.

[4] A. Schellmanns, K. Berrouche, and J. Keradec, "Multiwinding Transformers: A Successive Refinement Method to Characterize a General Equivalent Circuit," *IEEE Trans. Inst. Meas.*, vol. 47, pp. 1316–1321, Oct. 1998.

[5] R. W. Erickson and D. Maksimovic, "A Multi-Winding Magnetics Model Having Directly Measurable Parameters," in *Proc. IEEE Power Electron. Spec. Conf.*, 1998, pp. 1472-1478.

[6] J. Wang, A. F. Witulski, J. L. Vollin, T. K. Phelps, and G. I. Gardwell, "Derivation, Calculation and Measurement of Parameters for a Multi-Winding Transformer Electrical Model," in *Proc. IEEE Applied Power Electron. Conf. and Exp.*, 1999, pp. 220-226.

[7] J. M. Lopera, M. J. Prieto, A. M. Pernia, and F. Nuno, "A Multiwinding Modeling Method for High Frequency Transformers and Inductors," *IEEE Trans. Power Electron.*, vol. 18, pp. 896–906, May. 2003.

[8] C. Álvarez-Mariño, F. de León, and X. M. López-Fernández, "Equivalent Circuit for the Leakage Inductance of Multi-Winding Transformers: Unification of Terminal and Duality Models," *IEEE Trans. Power Del.*, vol. 27, pp. 353-361, Jan. 2012.

[9] F. de León and J. A. Martinez, "Dual Three-winding Transformer Equivalent Circuit Matching Leakage Measurements," *IEEE Trans. Power Del.*, vol. 24, pp. 160–168, Jan. 2009.

[10] M. Lambert, M. Martínez-Duró, J. Mahseredjian, F. de León, and F. Sirois, "Transformer Leakage Flux Models for Electromagnetic Transients: Critical Review and Validation of a New Model," accepted for publication in the *IEEE Trans. Power Del.*

[11] C. M. Arturi, "Transient Simulation and Analysis of a Three-Phase Five-Limb Step-Up Transformer Following and Out-of-Phase Synchronization," *IEEE Trans. Power Del.*, vol. 6, pp. 196–207, Jan. 1991.

[12] F. de León, S. Jazebi, and A. Farazmand, "Accurate Measurement of the Air-Core Inductance of Iron-Core Transformers with a Non-Ideal Low-Power Rectifier," *IEEE Trans. Power Del.*, vol. 29, pp. 294-296, Feb. 2014.

[13] S. E. Zirka, Y. I. Moroz, C. M. Arturi, N. Chiesa, and H. K. Høidalen, "Topology-Correct Reversible Transformer Model," *IEEE Trans. Power Del.*, vol. 27, pp. 2037–2045, Oct. 2012.

[14] S. Jazebi, F. de León, A. Farazamand, and D. Deswal, "Dual Reversible Transformer Model for the Calculation of Low-Frequency Transients," *IEEE Trans. Power Del.*, vol. 28, pp. 2509-2517, Oct. 2013.

[15] S. D. Mitchell and J. S. Welsh, "Initial Parameter Estimates and Constraints to Support Gray Box Modeling of Power Transformers," *IEEE Trans. Power Del.*, vol. 28, pp. 2411-2418, Oct. 2013.
[16] M. Lambert, J. Mahseredjian, Electromagnetic Transient-Type Transformer Models for Geomagnetically-Induced Current (GIC) Studies. EPRI, Palo Alto, CA: 2013, 3002000832.
[17] G. Kron, Tensor Analysis of Networks. Wiley, 1939.
[18] E. P. Dick and W. Watson, "Transformer models for transient studies based on field measurements," *IEEE Trans Power App. Syst.*, vol. PAS-100, no. 1, pp. 409–418, Jan. 1981.
[19] C. G. A. Koreman, "Determination of the magnetizing characteristic of three-phase transformers in field tests", *IEEE Trans. Power Del.*, vol. 4, pp. 1779–1785, Jul. 1989.
[20] S. Abdulsalam, W. Xu, W. L. A. Neves, and X. Liu, "Estimation of transformer saturation characteristics from inrush current waveforms", *IEEE Trans. Power Del.*, vol. 21, no. 1, pp. 170–177, Jan. 2006.
[21] S. Calabro, F. Coppadoro, and S. Crepaz, "The measurement of the magnetizing characteristics of large power transformers and reactors through D.C. excitation," *IEEE Trans. Power Del.*, vol. PWRD-1, no. 4, pp. 224–234, Oct. 1986.
[22] *IEEE Standard Test Code for Dry-Type Distribution and Power Transformers, Recognized as an American National Standard (ANSI)*, IEEE Standard C57.12.91-1995, 1995.
[23] Slow Transients Task Force of the IEEE. Modeling and Analysis of System Transients Using Digital Programs Working Group " Modeling and Analysis Guidelines for Slow Transients--Part III: The Study of Ferroresonance," *IEEE Trans. Power Del.*, vol. 15, pp. 255–265, Jan. 2000.
[24] R. A. Walling and A. H. Khan, "Characteristics of Transformer Exciting Current During Geomagnetic Disturbances," *IEEE Trans. Power Del.*, vol. 6, pp. 1707-1714, Oct. 1991.